arXiv:2105.03607v4 [math.DS] 21 Mar 2023

MEAN SUBTRACTION AND MODE SELECTION IN DYNAMIC MODE DECOMPOSITION

GOWTHAM S SEENIVASAHARAGAVAN*, MILAN KORDA†, HASSAN ARBABI ‡, AND IGOR MEZIĆ§

Abstract. Koopman mode analysis has provided a framework for analysis of nonlinear phenomena across a plethora of fields. Its numerical implementation via Dynamic Mode Decomposition (DMD) has been extensively deployed and improved upon over the last decade. We address the problems of mean subtraction and DMD mode selection in the context of finite dimensional Koopman invariant subspaces.

Preprocessing of data by subtraction of the temporal mean of a time series has been a point of contention in companion matrix-based DMD. This stems from the potential of said preprocessing to render DMD equivalent to temporal DFT. We prove that this equivalence is impossible in linearly consistent data, when the order of the DMD-based representation of the dynamics exceeds the dimension of the system. Therefore, this parity of DMD and DFT can be indicative of an inadequacy of data, in the sense that the number of snapshots taken is not enough to represent the true dynamics of the system.

We then rigorously justify the practice of pruning DMD eigen-values based on the norm of the respective modes. Once a minimum number of time delays has been taken, DMD eigen-values corresponding to DMD modes with low norm are shown to be spurious, and hence must be discarded. When dealing with mean-subtracted data, the above criterion for detecting synthetic eigen-values can be applied if DMD is preceded by time delay embedding.

Key words. Koopman operator, Mean subtraction, Dynamic Mode Decomposition, Spurious eigen-values

AMS subject classifications. 37M10, 37N10, 47N20

1. Introduction.

The balance of simplicity and generalizability is essential for the utility of a learning algorithm. In addition, temporal relationships must be accounted for when the object being modelled is a dynamical system. The Koopman operator [17] provides a principled and rigorous approach to constructing balanced and temporally aware models [24, 22]. The spectral objects of this infinite-dimensional linear operator lead to generalizable linear models of non-linear dynamics. Consequently, algorithms for computing these spectral quantities, particularly the so-called Dynamic Mode Decomposition (DMD) [28, 30, 35], have been the focus of sustained research.

Procedurally, DMD is simply a linear fit followed by an eigen-decomposition. Hence, it has been applied to data from a plethora of natural and engineered phenomena; see for example the survey [8]. In parallel, theoretical investigations have probed the effect of time delays, choice of observables and convergence to Koopman spectral objects - see [18] as well as the reviews [31] and [25] for a detailed discussion. This work continues the conversation on the pragmatic issue of removing the temporal mean of a time series, and its theoretical implications for DMD.

The infinite-time average, when it exists, is the leading term of the Koopman mode decomposition [22]. Its removal brings focus on the temporally varying parts of the process, and has been adopted in a diverse set of analyses [6, 27, 29, 4]. Nonetheless, in practice, this step may render Companion DMD [28] equivalent to a temporal

*Department of Mechanical Engineering, University of California Santa Barbara
†Methods and Algorithms for Control, LAAS-CNRS
‡Department of Mechanical Engineering, Massachusetts Institute of Technology
§Department of Mechanical Engineering, University of California Santa Barbara

Discrete Fourier Transform (DFT) [9]. The negative consequences include misrepresentation of dissipative dynamics and a bijection between the trajectory length and DMD spectrum.

The relationship between mean-subtracted DMD and DFT is substantially clarified in a more recent work by Hirsch and co-workers [14]. Although their primary contribution is an *alternative* to temporal mean removal that is shown to be equivalent to including an affine term in DMD, they also study the original pre-processing step in itself. First, they point out that [9] only provides a *sufficient* condition for the equivalence of mean-subtracted DMD and DFT. Then, they prove that this condition is not satisfied when there is linear consistency of data (i.e. the requirement that data be connected by a linear mapping), an underlying Koopman invariant subspace and more samples than its dimension (termed over-sampling here). Finally, they provide numerical evidence that suggests that linear consistency and over-sampling can actually negate DMD-DFT equivalence, i.e., be a sufficient condition for non-equivalence.

Our primary contribution is a *necessary and sufficient condition* for the equivalence of mean-subtracted DMD and DFT. Using this geometric condition, we generate counterexamples that disprove the converse of the sufficient condition in [9] and consequently the flawed discussion in [14]. We, then, formally show that linear consistency[1] and over-sampling prevent the equivalence of mean-subtracted DMD and DFT. By the contrapositive, DMD-DFT equivalence can be used to decide if more data is needed to construct an accurate DMD model. Under the stronger condition of Koopman invariant observables, we also show the converse: DMD-DFT equivalence can result from paucity of data.

We then study the practice of mode-selection in DMD. This post-processing step is used to address numerical artifacts arising from the imperfect tuning of DMD model order. In the companion matrix formulation, the order or capacity of the DMD model is the length of the training trajectory. The minimum order required for generalizability is the dimension of the underlying Koopman invariant subspace. Since this dimension is unknown in practice, the safest option is to keep it as large as possible [19].

A setback with this approach is the deluge of DMD eigen-values to contend with. A common choice is to neglect those corresponding to DMD modes with very small norm [28, 33, 2, 20, 11, 10]. We formally validate this choice when the observables lie in a finite dimensional Koopman invariant subspace, and extend its applicability to mean-subtracted data.

We prove that DMD eigen-values corresponding to DMD modes with non-zero norm comprise the Koopman spectrum. Therefore, DMD eigen-values whose DMD modes have negligible norm may be discarded. This strategy of pruning the DMD spectrum can also be used with mean-subtracted data, provided the data is sufficiently delay embedded before performing DMD. These results rely upon linear consistency and access to enough data. While the former can be met with time delays, the latter can be partially addressed purely from data using the characterization of DMD-DFT equivalence developed in this work.

This paper is organized as follows: Section 2 details the notation adopted in this work. Section 3 introduces the Koopman operator and Dynamic Mode Decomposition before reviewing the effect of mean subtraction in subsection 3.3. In particular, subsection 3.4 contextualizes existing literature in the setting of finite dimensional Koopman invariant subspaces. Drawing on these, Section 4 explores the relationship

[1] An appropriate number of time delays [7, 1] can ensure linear consistency.

between mean subtracted DMD and DFT, resulting in an a posteriori check that alerts to data insufficiency. Section 5 justifies DMD mode norm as a criterion for filtering DMD eigen-values and, then, extends it to mean-subtracted data. Section 6 sees the numerical verification of all major results on (mainly) linear time invariant systems (LTIs), the Van der Pol oscillator and the lid-driven cavity at various flow regimes. It also features a minor detour into the efficacy of mode-norm based filtering, in the presence of output noise. Section 7 summarizes the findings and points out relevant questions that remain unanswered.

2. Notation. The notation is mostly standard for our primary objects of interest: (finite) sets, vectors and matrices. The elements of an object are written with subscripts that always start at 1. The operation $\#(\cdot)$ returns the number of elements in the argument, as illustrated below. Sets are denoted with upper-case letters and are enclosed by curly braces. For example,

$$L \;:=\; \{\lambda_i\}_{i=1}^{r} \;=\; \{\lambda_1, \lambda_2, \cdots, \lambda_r\} \;\implies\; \#(L) = r.$$

Vectors are typically in $\mathbb{C}^m$, labelled with bold-faced lower-case letters and represented as columns:

$$\mathbf{v} \;=\; [v_i]_{i=1}^{m} \;=\; \begin{bmatrix} v_1 \\ v_2 \\ \vdots \\ v_m \end{bmatrix} \;\implies\; \#(\mathbf{v}) = m.$$

The symbol $\mathbf{e}_i$ denotes the i-th standard basis vector. By $\mathbf{gp}_{n+1}[\lambda]$, we denote the vector whose elements are the first $n+1$ terms of the geometric sequence beginning at 1 with ratio λ.

$$\mathbf{gp}_{n+1}[\lambda] := [\lambda^{i-1}]_{i=1}^{n+1} = [1, \lambda, \lambda^2, \ldots, \lambda^n]^T.$$

Constant vectors (those with only one unique coefficient) are represented by their value in boldface and dimension as a subscript.

$$\mathbf{1}_m = [1]_{i=1}^{m}.$$

Matrices are in $\mathbb{C}^{m\times n}$, denoted by bold-faced upper-case letters and written as ordered sets of columns.

$$\mathbf{A} = [\mathbf{a}_j]_{j=1}^{n} = [a_{ij}]_{i,j=1}^{m,n} = \begin{bmatrix} | & | & & | \\ \mathbf{a}_1 & \mathbf{a}_2 & \cdots & \mathbf{a}_n \\ | & | & & | \end{bmatrix}.$$

The (Hermitian) transpose of $\mathbf{A}$ is written as $(\mathbf{A}^H)$ $\mathbf{A}^T$. The letter $\mathbf{I}$ is reserved for the identity matrix.

$$\mathbf{I}_n \;=\; [\mathbf{e}_j]_{j=1}^{n} \;=:\; [\delta_{ij}]_{i,j=1}^{n}.$$

Constant matrices are written similar to their vector counterparts:

$$\mathbf{0}_{m\times n} = [\mathbf{0}_m]_{j=1}^{n} = [0]_{i,j=1}^{m,n}.$$

The expression $\mathbf{T}[\mathbf{c}]$ represents the companion matrix with 1 on the first sub-diagonal and $\mathbf{c}$ as the last column.

$$\mathbf{c} \in \mathbb{C}^n \implies \mathbf{T}[\mathbf{c}] = \begin{bmatrix} & & & c_1 \\ 1 & & & c_2 \\ & 1 & & c_3 \\ & & \ddots & \vdots \\ & & 1 & c_n \end{bmatrix}.$$

Sub-spaces are written in script. For instance, $\mathcal{R}(\mathbf{Z})$ and $\mathcal{N}(\mathbf{Z})$ denote the column-space and null-space of $\mathbf{Z}$ respectively. Orthogonal projectors play a crucial role in this work. Under the standard inner product on $\mathbb{C}^m$, $\mathcal{P}_{\mathcal{W}}$ denotes the orthogonal projector onto the subspace $\mathcal{W}$. If we let $\mathbf{A}^\dagger$ denote the Moore-Penrose pseudo-inverse of $\mathbf{A}$, we get:

$$\mathcal{P}_{\mathcal{R}(\mathbf{A})} = \mathbf{A}\mathbf{A}^\dagger, \quad \mathcal{P}_{\mathcal{N}(\mathbf{A}^H)} = \mathbf{I} - \mathbf{A}\mathbf{A}^\dagger.$$

3. Preliminaries. We provide an overview of the ideas needed to understand and build upon existing work regarding mean-subtraction and DMD. We begin with a brief introduction to the Koopman operator (subsection 3.1) and its approximation via Dynamic Mode Decomposition (subsection 3.2). This permits a high level discussion of the effect of mean-subtraction in DMD and the relevant gaps in literature that are addressed in this work (subsection 3.3). To facilitate a more detailed exposition, we then introduce finite dimensional Koopman invariant subspaces (subsection 3.4), and the notions of linear consistency and well-posedness (subsection 3.5). Subsequently, we recap the most relevant theoretical contribution from [14], highlight its shortcomings and thus set the stage for their resolution (subsection 3.6).

3.1. The Koopman operator. Consider an autonomous discrete time dynamical system in $\mathbb{R}^p$.

$$\boldsymbol{v}^+ = \Gamma(\boldsymbol{v}),\ \boldsymbol{v} \in \mathbb{R}^p. \tag{3.1}$$

The map Γ can be used to define a Koopman operator, U, that acts on functions on the state-space: [17, 24]

$$\begin{aligned} &U : \mathcal{H} \to \mathcal{H} \\ &U \circ \psi := \psi \circ \Gamma. \end{aligned} \tag{3.2}$$

where $\mathcal{H}$ is a function space that is closed under the action of U.

The Koopman operator is linear and infinite-dimensional. Its' spectral objects can provide significant insight into the dynamics of (3.1) [22]. A most pertinent property is that linearity allows the eigen-functions[2] of U to describe the evolution of any function in their span. For any eigenfunction ϕ_j of U, we have

$$(U \circ \phi_j)(\boldsymbol{v}) = \phi_j(\Gamma(\boldsymbol{v})) = \lambda_j \phi_j(\boldsymbol{v}).$$

Therefore, for any $f = \sum_j c_j \phi_j$, we get by linearity of U

$$(U \circ f)(\boldsymbol{v}) = (U \circ \sum_j c_j \phi_j)(\boldsymbol{v}) = \sum_j c_j \lambda_j \phi_j(\boldsymbol{v}).$$

[2]We assume that the choice of $\mathcal{H}$ is such that non-trivial eigen-functions exist.

Consequently, f may be forecast over multiple time steps, say d, by simply raising the eigen-values to the power d.

$$f(\Gamma^d(\boldsymbol{v})) = (U^d \circ f)(\boldsymbol{v}) = (U^d \circ \sum_j c_j \phi_j)(\boldsymbol{v}) = \sum_j c_j \lambda_j^d \phi_j(\boldsymbol{v}).$$

This expansion, dubbed the Koopman mode decomposition (KMD), explains temporal observations of a potentially *nonlinear* process (3.1) in terms of *intrinsic* exponentials. Unsurprisingly, many algorithms have been designed to approximate this spectral expansion, with DMD being the most prominent.

3.2. Dynamic Mode Decomposition (DMD). Dynamic Mode Decomposition [28, 35] constructs a finite section of the Koopman operator [23], with respect to a specified set of observables (called the dictionary). Suppose we have m observables of interest $\{\psi_i\}_{i=1}^m$ in our dictionary. Using these functions, we define the m-dimensional vector $\boldsymbol{\psi} := [\psi_i]_{i=1}^m$. The inputs to DMD are two matrices $\mathbf{X}$ and $\mathbf{Y} \in \mathbb{C}^{m \times n}$ obtained by sampling $\boldsymbol{\psi}$ and $U\boldsymbol{\psi}$ respectively on a finite set of n states $\{\boldsymbol{v}_j\}_{j=1}^n$.

$$\mathbf{X} := [\boldsymbol{\psi}(\boldsymbol{v}_j)]_{j=1}^n, \quad \mathbf{Y} := [U\boldsymbol{\psi}(\boldsymbol{v}_j)]_{j=1}^n = [\boldsymbol{\psi}(\Gamma(\boldsymbol{v}_j))]_{j=1}^n. \tag{3.3}$$

The finite-dimensional linear map that best represents the transition from $\mathbf{X}$ to $\mathbf{Y}$ is the DMD matrix denoted as $\mathbf{A}_{\text{Exact}}$:

$$\mathbf{A}_{\text{Exact}} := \min_{\mathbf{A}} \|\mathbf{A}\mathbf{X} - \mathbf{Y}\|_F^2. \tag{3.4}$$

The above objective first appeared in [33] and was called Exact DMD.

Remark 3.1. We would like to emphasize that the linear map being sought approximates the evolution of observables of the state and not the state itself. This distinction was not widely appreciated until the work of Williams and co-workers [35] where the definition of $\mathbf{X}$ and $\mathbf{Y}$, as given in (3.3), was made explicit. Furthermore, they termed the regression in (3.4) as Extended DMD (EDMD), in the scenario where one has the freedom to choose $\boldsymbol{\psi}$. This is in contrast to situations where one must make do with only the observables that are accessible, as is often the case in experimental settings. Since this manuscript is better aligned with the latter limited-observable scenario, we will refer to (3.4) as Exact DMD.

When the samples are successive iterates along the same orbit, i.e.

$$\forall\ j, \quad \boldsymbol{v}_{j+1} = \Gamma(\boldsymbol{v}_j),$$

a more concise representation of U is made possible by the temporal structure. This can be seen by first collecting the $n+1$ time sequential observations into the matrix $\mathbf{Z} \in \mathbb{C}^{m \times (n+1)}$:

$$\mathbf{z}_j = \boldsymbol{\psi}(\boldsymbol{v}_j), \quad j \in [1, n+1]. \tag{3.5}$$

The matrices $\mathbf{X}$ and $\mathbf{Y}$ are now sub-matrices of $\mathbf{Z}$ formed by dropping its last and first column respectively.

$$\mathbf{Z} = \begin{bmatrix} \mathbf{X} & | & \mathbf{z}_{n+1} \end{bmatrix} = \begin{bmatrix} \mathbf{z}_1 & | & \mathbf{Y} \end{bmatrix}.$$

Companion DMD [28] attempts to find the n-dimensional invariant subspace that best approximates the time series $\mathbf{Z}$ and is defined thus:

$$\begin{aligned}\mathbf{c}^*[\mathbf{Z}] &:= \begin{cases} \arg\min_{\mathbf{c}} \quad \|\mathbf{c}\|_2 & \mathbf{z}_{n+1} \in \mathcal{R}(\mathbf{X}) \\ \text{subject to } \mathbf{X}\mathbf{c} \;=\; \mathbf{z}_{n+1} & \\ \\ \arg\min_{\mathbf{c}} \quad \|\mathbf{X}\mathbf{c} - \mathbf{z}_{n+1}\|_2 & \text{Otherwise} \end{cases} \\ &= \mathbf{X}^\dagger \mathbf{z}_{n+1}. \end{aligned} \tag{3.6}$$

We let $\mathbf{T}^* \in \mathbb{C}^{n\times n}$ denote the companion matrix associated to $\mathbf{c}^*[\mathbf{Z}]$, i.e.,

$$\mathbf{T}^* := \mathbf{T}(\mathbf{c}^*[\mathbf{Z}]).$$

The size of $\mathbf{T}^*$ or, equivalently, the number of columns in $\mathbf{X}$ is a measure of the complexity of the DMD model, motivating the following definition:

$$\text{Companion-order}[\mathbf{Z}] := \#[\text{Columns in } \mathbf{Z}] - 1 \;=\; n. \tag{3.7}$$

The spectral decomposition of $\mathbf{T}^*$ can be used to approximate the Koopman mode decomposition of $\mathbf{Z}$. Suppose $\mathbf{T}^*$ has distinct eigen-values, i.e. $\sigma(\mathbf{T}^*) = \{\lambda_i^*\}_{i=1}^n$. Then, $\mathbf{T}^*$ is diagonalizable [16] and its spectral decomposition reads thus:

$$\mathbf{T}^* = \mathbf{V}^*\mathbf{\Lambda}^*(\mathbf{V}^*)^{-1}.$$

The columns of $\mathbf{V}^*$ are the eigen-vectors of $\mathbf{T}^*$. The matrix $\mathbf{\Lambda}^*$ is diagonal and $(\mathbf{V}^*)^{-1}$ is a Vandermonde matrix as described below:

$$\mathbf{\Lambda}^* \;=\; \begin{bmatrix} \lambda_1^* & & & \\ & \lambda_2^* & & \\ & & \ddots & \\ & & & \lambda_n^* \end{bmatrix}, \; (\mathbf{V}^*)^{-1} \;=\; \begin{bmatrix} 1 & \lambda_1^* & (\lambda_1^*)^2 & \dots & (\lambda_1^*)^{n-1} \\ 1 & \lambda_2^* & (\lambda_2^*)^2 & \dots & (\lambda_2^*)^{n-1} \\ \vdots & \vdots & \vdots & \ddots & \vdots \\ 1 & \lambda_n^* & (\lambda_n^*)^2 & \dots & (\lambda_n^*)^{n-1} \end{bmatrix}. \tag{3.8}$$

The modal decomposition of $\mathbf{Z}$ is obtained from the residue, $\mathbf{r}^*$, of the least squares problem in (3.6):

$$\mathbf{r}^* := \mathbf{z}_{n+1} - \mathbf{X}\mathbf{c}^*[\mathbf{Z}].$$

This vector lets us connect $\mathbf{X}$ and $\mathbf{Y}$ through the companion matrix $\mathbf{T}^*$.

$$\mathbf{Y} = \mathbf{X}\mathbf{T}^* + \mathbf{r}^*\mathbf{e}_n^H.$$

Using the spectral decomposition of $\mathbf{T}^*$ and defining $\mathbf{D}^* := \mathbf{X}\mathbf{V}^*$, we obtain:

$$\mathbf{Y} \;=\; \mathbf{X}\mathbf{V}^*\mathbf{\Lambda}^*(\mathbf{V}^*)^{-1} + \mathbf{r}^*\mathbf{e}_n^H \;=\; \mathbf{D}^*\mathbf{\Lambda}^*(\mathbf{V}^*)^{-1} + \mathbf{r}^*\mathbf{e}_n^H. \tag{3.9}$$

The j-th column of $\mathbf{D}^*$ is termed the DMD mode corresponding to the DMD eigen-value λ_j^*. Writing every column of the matrix equation (3.9) separately gives the following expansion:

$$\begin{aligned} \mathbf{z}_i &= \sum_{j=1}^n \mathbf{d}_j^*(\lambda_j^*)^{i-1}, \quad (\mathbf{r}^*)^H\mathbf{z}_i = 0 \qquad i = 1, \cdots n \\ \mathbf{z}_{n+1} &= \sum_{j=1}^n \mathbf{d}_j^*(\lambda_j^*)^n + \mathbf{r}^*. \end{aligned} \tag{3.10}$$

Comparing the Koopman mode expansion [22] and (3.10) suggests that the DMD mode $\mathbf{d}_j^* = \mathbf{X}\mathbf{v}_j^*$ may approximate the Koopman mode corresponding to λ_j^*. Further discussion on this approximation can be found in [23].

In contrast, approximating the Koopman modes via Exact DMD (3.4) involves an additional linear regression. One considers the unit right eigen-vectors of A_{Exact} and tries to scale each eigen-vector so as to best enable a spectral expansion, like (3.10), in terms of the pertinent eigen-values. These scale factors are termed "DMD amplitudes"[3]. In the discussion following Corollary 5.7, we will find that their magnitudes match the norms of the appropriate Companion DMD modes, under some conditions.

3.3. Effect of mean subtraction. Mean subtraction is a useful pre-processing step when the time series, $\mathbf{Z}$, is generated by the solution to a PDE with Dirichlet boundary conditions (BCs) [9]. It ensures that DMD based predictions using mean-subtracted data respect the BCs. This section summarizes relevant work on the potential drawbacks of doing this and efforts at resolution.

Let $\boldsymbol{\mu}$ be the temporal mean of the time series.

$$\boldsymbol{\mu} = \frac{1}{n+1}\sum_{i=1}^{n+1} \mathbf{z}_i = \frac{1}{n+1}\,\mathbf{Z}\;\mathbf{gp}_{n+1}[1]. \tag{3.11}$$

Removing the mean from each snapshot gives mean-subtracted versions of $\mathbf{Z}$ and $\mathbf{X}$:

$$\mathbf{Z}_{\text{ms}} := [\mathbf{z}_j - \boldsymbol{\mu}]_{j=1}^{n+1}, \quad \mathbf{X}_{\text{ms}} := [\mathbf{z}_j - \boldsymbol{\mu}]_{j=1}^{n}. \tag{3.12}$$

Suppose $\mathbf{y}_{\text{ms}}$ is defined to be the last column of $\mathbf{Z}_{\text{ms}}$ i.e. $\mathbf{y}_{\text{ms}} := \mathbf{z}_{n+1} - \mu$. Then, Companion DMD on the mean subtracted data would then read:

$$\begin{aligned} \mathbf{c}_{\text{ms}}[\mathbf{Z}] &:= \mathbf{c}^*[\mathbf{Z}_{\text{ms}}] \\ &= \arg\min_{\mathbf{c}} \quad \|\mathbf{c}\|_2 \\ &\quad \text{subject to } \mathbf{X}_{\text{ms}}\mathbf{c} \;=\; \mathbf{y}_{\text{ms}} \\ &= \mathbf{X}_{\text{ms}}^{\dagger}\;\mathbf{y}_{\text{ms}}. \end{aligned} \tag{3.13}$$

We emphasize that the formulation above is obtained from (3.6) by replacing $\mathbf{X}$ with $\mathbf{X}_{\text{ms}}$ and $\mathbf{z}_{n+1}$ with $\mathbf{y}_{\text{ms}}$. Since $\mathbf{y}_{\text{ms}}$ is always in $\mathcal{R}(\mathbf{X}_{\text{ms}})$, equation (3.13) only considers the first branch. The redundant second branch reads,

$$\arg\min_{\mathbf{c}} \; \|\mathbf{X}_{\text{ms}}\mathbf{c} - \mathbf{y}_{\text{ms}}\|_2, \tag{3.14}$$

and possesses multiple optima attaining the minimum value of 0. In fact, the optimal set is the affine subspace : $-\mathbf{1}_n + \mathcal{N}(\mathbf{X}_{\text{ms}})$. Two specific optima play a central role in the subsequent discussion. The first is $-\mathbf{1}_n$ which follows directly from the definition of the temporal mean (3.11). The second is $\mathbf{c}_{\text{ms}}[\mathbf{Z}]$ which is the optimum that is closest to the origin viz. the minimum norm solution. When $\mathbf{X}_{\text{ms}}$ has linearly independent columns, these two optima coincide.

LEMMA 3.2. *[9] If $\mathbf{X}_{\text{ms}}$ has full column rank, then $-\mathbf{1}_n$ is the unique optimum of (3.14). Consequently,*

$$\mathbf{c}_{\text{ms}}[\mathbf{Z}] = -\mathbf{1}_n.$$

There are three concerning aspects of this result:

[3] See sections 1.3 and 8.1.3 of [19] for a more detailed exposition.

1. Broad applicability: The requirement of linearly independent columns in $\mathbf{X}_{\text{ms}}$ is met when $\mathbf{Z}$ has full column rank, which is often the case when the snapshots are slices of the solution to a PDE.
2. Content independence: The vector $\mathbf{c}_{\text{ms}}[\mathbf{Z}]$ depends only on n, and has no regard for the information contained in $\mathbf{Z}_{\text{ms}}$
3. Spectral confinement: DMD eigen-values are restricted to be the $(n+1)$th roots of unity, modulo 1. As a result, the analog of (3.9) (or equivalently (3.10)) generated from the spectral decomposition of $\mathbf{T}[\mathbf{c}_{\text{ms}}[\mathbf{Z}]]$ will coincide with the Fourier decomposition of $\mathbf{Z}$.

In light of Lemma 3.2, it is important to note the distinction between the following two statements:

$$\text{Statement 1: } \mathbf{c}_{\text{ms}}[\mathbf{Z}] \;=\; -\mathbf{1}_n.$$
$$\text{Statement 2: } -\mathbf{1}_n \text{ is the unique optimum of (3.14).}$$

We will refer to Statement 1 as spectral equivalence and Statement 2 as complete equivalence of mean-subtracted DMD and DFT. By Lemma 3.2, complete equivalence implies spectral equivalence. However, at this juncture, we have no guarantee that the converse holds. Addressing this knowledge gap necessitates finding situations when complete equivalence does not occur. To this end, we primarily work with the weaker notion of spectral equivalence. Therefore, the term "equivalence" will henceforth serve as shorthand for spectral equivalence and will be denoted as $\boldsymbol{\mu}\text{DMD}[\mathbf{Z}] \equiv \text{DFT}$.

Definition 3.3. *We say that mean-subtracted DMD on the time series data* $\mathbf{Z}$ *is equivalent to DFT if* $\mathbf{c}_{\text{ms}}[\mathbf{Z}] = -\mathbf{1}_n$.

$$\boldsymbol{\mu}DMD[\mathbf{Z}] \equiv DFT \iff \mathbf{c}_{\text{ms}}[\mathbf{Z}] = -\mathbf{1}_n$$

The discovery of this equivalence evoked a range of responses. Some consciously steered clear of this pre-processing step [21], while a few willingly embraced it as a way to ensure that DMD eigen-values are on the unit circle [32, 5]. We highlight two contributions that significantly shaped our study:

1. Hirsch and co-workers [14] provide a clear exposition of the work by Chen et.al.[9] and derive sufficient conditions for $\mathbf{X}_{\text{ms}}$ to be rank defective. Although this greatly improves our understanding, the story is still incomplete. One cannot infer non-equivalence of mean-subtracted DMD and DFT, from the rank deficiency of $\mathbf{X}_{\text{ms}}$.
   We derive a necessary and sufficient condition (Theorem 4.1) for this equivalence that is weaker than asking for linear independence of the columns of $\mathbf{X}_{\text{ms}}$. This condition is used in Theorem 4.2 to generate a rich collection of time series data[4] that simultaneously exhibit DMD-DFT equivalence and linear dependence of the columns of $\mathbf{X}_{\text{ms}}$. Subsequently, our result helps elucidate the effect of model order on nearness to temporal DFT (see Theorem 4.3 and Corollary 4.4).
2. Avila & Mezić [4] recover physically meaningful patterns from highway traffic data using Koopman mode analysis. Their analysis is based on Hankel DMD [1] of mean-subtracted data matrices. This corresponds to delay embedding the mean-removed data before the DMD regression in (3.4).
   In Corollary 5.11, we show that this strategy (time delays after mean removal) recovers the true spectrum, in the related context of Companion DMD.

[4] We informally refer to a matrix as "time series data" if its rows lie in the row-space of a Vandermonde matrix i.e. it possesses a decomposition analogous to (3.17).

In order to formally substantiate our claims, we assume that there is a finite dimensional invariant subspace of U that contain every element of $\boldsymbol{\psi}$.

3.4. Finite dimensional Koopman invariant subspaces. Any function in the span of a finite number of Koopman eigen-functions can be forecast easily. A simple linear model will do, with its complexity bounded by the number of independent eigen-functions or equivalently the dimensions of the invariant subspace. This potential for generalizable linear forecasts of nonlinear dynamics has drawn extensive attention to find Koopman invariant subspaces containing desirable observables like the coordinates. For our purposes, it will be sufficient to assume the existence of such a spectral object.

Let the vector of m observables, $\boldsymbol{\psi}$, lie in a r-dimensional subspace $\mathcal{V}$ that is invariant under the action of the Koopman operator U. In addition, suppose the restriction of the Koopman operator to this subspace, denoted as $U|_{\mathcal{V}}$, has r-distinct eigenvalue-eigenfunction pairs: $\{(\lambda_j, \phi_j)\}_{j=1}^r$. Then, we may infer two quantitative relationships:

1. The subspace $\mathcal{V}$ is simply the span of the eigen-functions $\{\phi_j\}_{j=1}^r$. Let $\boldsymbol{\phi} := [\phi_j]_{j=1}^r$ be the vector formed by collecting all r eigen-functions. Then, the first assumption on $\boldsymbol{\psi}$ is tantamount to the existence of a matrix $\tilde{\mathbf{C}} \in \mathbb{C}^{m\times r}$ such that $\boldsymbol{\psi} = \tilde{\mathbf{C}}\boldsymbol{\phi}$.
2. The representation of $U|_{\mathcal{V}}$ in terms of the eigen-functions is a diagonal matrix $\boldsymbol{\Lambda} \in \mathbb{C}^{r\times r}$:
$$\boldsymbol{\Lambda} \;:=\; \begin{bmatrix} \lambda_1 & & & \\ & \lambda_2 & & \\ & & \ddots & \\ & & & \lambda_r \end{bmatrix}.$$
As such, the spectrum of $\boldsymbol{\Lambda}$ coincides with the spectrum of $U|_{\mathcal{V}}$. This set, henceforth denoted as $\sigma(\boldsymbol{\Lambda})$, equals $\{\lambda_j\}_{j=1}^r$.

Compiling the above findings, we obtain a concise description of the evolution of $\boldsymbol{\psi}$:

$$\begin{aligned} \boldsymbol{\phi}^+ &:= U\boldsymbol{\phi} = \boldsymbol{\Lambda}\boldsymbol{\phi} \\ \boldsymbol{\psi} &= \tilde{\mathbf{C}}\boldsymbol{\phi}. \end{aligned} \tag{3.15}$$

Consequently, the time series $\mathbf{Z}$ may be interpreted as the output of a linear system whose "state" is made up of the values of the eigen-functions at the actual state.

Without loss of generality, we assume that every column of $\tilde{\mathbf{C}}$ is non-zero. We define $\mathbf{C}$ as the column scaling of $\tilde{\mathbf{C}}$ by the eigen-coordinates of $\boldsymbol{\upsilon}_1$.

$$\operatorname{diag}[\boldsymbol{\phi}(\boldsymbol{\upsilon}_1)] \;:=\; \begin{bmatrix} \phi_1(\boldsymbol{\upsilon}_1) & & & \\ & \phi_2(\boldsymbol{\upsilon}_1) & & \\ & & \ddots & \\ & & & \phi_r(\boldsymbol{\upsilon}_1) \end{bmatrix}, \quad \mathbf{C} \;:=\; \tilde{\mathbf{C}}\operatorname{diag}[\boldsymbol{\phi}(\boldsymbol{\upsilon}_1)]. \tag{3.16}$$

We also construct a Vandermonde matrix $\boldsymbol{\Theta} \in \mathbb{C}^{r\times(n+1)}$ whose nodes are the Koopman eigen-values:

$$\boldsymbol{\Theta} := \begin{bmatrix} 1 & \lambda_1 & \lambda_1^2 & \dots & \lambda_1^n \\ 1 & \lambda_2 & \lambda_2^2 & \dots & \lambda_2^n \\ \vdots & \vdots & \vdots & \ddots & \vdots \\ 1 & \lambda_r & \lambda_r^2 & \dots & \lambda_r^n \end{bmatrix}.$$

The motivation for defining $\mathbf{C}$ and $\mathbf{\Theta}$ is that the time series $\mathbf{Z}$ can be written as their product[5]:

$$\mathbf{Z} = \mathbf{C}\mathbf{\Theta}. \tag{3.17}$$

Since the Vandermonde matrix $\mathbf{\Theta}$ is seen in many derived quantities, it will be convenient to define $\mathbf{\Theta}_j$ as $\mathbf{\Theta}$ without the last j columns.

$$\mathbf{\Theta}_j := \begin{bmatrix} 1 & \lambda_1 & \lambda_1^2 & \dots & \lambda_1^{n-j} \\ 1 & \lambda_2 & \lambda_2^2 & \dots & \lambda_2^{n-j} \\ \vdots & \vdots & \vdots & \ddots & \vdots \\ 1 & \lambda_r & \lambda_r^2 & \dots & \lambda_r^{n-j} \end{bmatrix} \implies \mathbf{\Theta}_0 = \mathbf{\Theta}. \tag{3.18}$$

As a result, the matrices $\mathbf{X}$ and $\mathbf{Y}$ may also be written similar to $\mathbf{Z}$ in (3.17).

$$\begin{aligned} \mathbf{X} = [\mathbf{z}_j]_{j=1}^{n} &= \mathbf{C}\mathbf{\Theta}_1. \\ \mathbf{Y} = [\mathbf{z}_i]_{i=2}^{n+1} &= \mathbf{C}\mathbf{\Lambda}\mathbf{\Theta}_1. \end{aligned} \tag{3.19}$$

3.5. Promoting generalizability in DMD models. The utility of any data-driven model, including DMD, depends on its performance with test data. This generalizability can be ensured in Exact DMD [33] via two conditions: well-posedness and linear consistency. We port these conditions to the companion matrix formulation and, later in Proposition 5.3, show that they guarantee generalizability once more.

Well-posedness deals with the complexity of the training data, and the ability of the DMD model to capture said richness.

DEFINITION 3.4. *Well-posedness [14] of Companion DMD*

$$\text{(3.6) } \textit{is well posed} \iff n \geq r \textit{ and } \forall\, i,\ \phi_i(\boldsymbol{\upsilon}_1) \neq 0.$$

$$\text{(3.6) } \textit{is strictly well posed} \iff n \geq r+1 \textit{ and } \forall\, i,\ \phi_i(\boldsymbol{\upsilon}_1) \neq 0.$$

Well-posedness ensures generalizability by requiring the training data exhibit all possible Koopman modes. Additionally, this condition requires that the Companion DMD model have sufficient capacity to represent the observables in all their complexity.

While well-posedness sorts out the ingredients required by DMD, linear consistency demands that the regression itself be perfect.

DEFINITION 3.5. *Linear consistency [33]*

$$(\mathbf{X}, \mathbf{Y}) \textit{ is linearly consistent} \iff \exists\ \mathbf{A} \textit{ such that } \mathbf{A}\mathbf{X} = \mathbf{Y}.$$

Although numerically verifiable, linear consistency may not lead to good generalization, especially when the number of snapshots is low. This shortcoming can be addressed if the image of every observable, $U \circ \psi_i$, lies in the span of the dictionary $\boldsymbol{\psi}$.

DEFINITION 3.6. *Koopman invariance of $\boldsymbol{\psi}$*

$$\boldsymbol{\psi} \textit{ is Koopman invariant} \iff \exists\ \mathbf{A} \textit{ such that } U \circ \boldsymbol{\psi} = \mathbf{A}\boldsymbol{\psi}.$$

In other words, Koopman invariance of $\boldsymbol{\psi}$ means linear consistency along any trajectory. More importantly, these notions coincide when the DMD problem is well-posed.

[5] Details in Appendix A.1

PROPOSITION 3.7. *Suppose the DMD problem is well-posed. Then,*

$$(\mathbf{X}, \mathbf{Y}) \textit{ is linear consistent} \iff \boldsymbol{\psi} \textit{ is Koopman invariant.}$$

Proof. Refer Appendix A.3 ∎

At this juncture, it is reasonable to question the utility of linear consistency in the companion matrix formulation since it seems to deal with the alternative approach of Exact DMD. Indeed, this is a subtle point that cannot be readily appreciated without the proofs that follow. The essence of the story is that Koopman invariance of $\boldsymbol{\psi}$ ensures that the spectral estimates from Companion-DMD are not contaminated by "imperfections" in $\boldsymbol{\psi}$.

Taking time delays is a simple and pragmatic way of bestowing Koopman invariance upon $\boldsymbol{\psi}$. Hence, this notion of invariance featured prominently in the development of Higher Order DMD[20]: a variant of DMD that meticulously uses time delayed observables for forecasting. Owing to the spatio-temporal nature of the systems that were studied, Koopman invariance of $\boldsymbol{\psi}$ was written in terms of "spatial" and "spectral" complexities.

DEFINITION 3.8. *Spectral and spatial complexities [20]*
Suppose $\forall i,\ \phi_i(\boldsymbol{\upsilon}_1) \neq 0$.

$$\textit{Spectral complexity } [\mathbf{Z}] \ := \ r, \quad \textit{Spatial complexity } [\mathbf{Z}] \ := \ \dim(\mathcal{R}(\tilde{\mathbf{C}})).$$

These conditions are related by the following proposition:

PROPOSITION 3.9. *Suppose* $\forall i,\ \phi_i(\boldsymbol{\upsilon}_1) \neq 0$. *Then, the following are equivalent:*
1. *Spectral complexity* $[\mathbf{Z}]$ = *Spatial complexity* $[\mathbf{Z}]$.
2. *The matrix* $\tilde{\mathbf{C}}$ *has full column rank.*
3. *The set of observables comprising* $\boldsymbol{\psi}$ *is Koopman invariant.*

Proof. Refer Appendix A.3 ∎

Henceforth, we will refer to the above conditions using the phrase "Koopman invariant $\boldsymbol{\psi}$". If the DMD problem (3.6) is well-posed, then Proposition 3.7 says that the three conditions listed in Proposition 3.9 may also be described by the conventional phrase of "linear consistency".

3.6. State of the art in mean-subtracted DMD. In the setting of (3.15), the contribution of [14] that forms the starting point of our work reads thus:

THEOREM 3.10. *Suppose the following hold:*
1. *Companion DMD problem (3.6) is well-posed.*
2. *The matrix pair* $(\mathbf{X}, \mathbf{Y})$ *is linearly consistent.*
3. $0 \notin \sigma(\boldsymbol{\Lambda})$.
4. $1 \in \sigma(\boldsymbol{\Lambda})$.
5. *The product* $\mathbf{X}\mathbf{1}_n \neq \mathbf{0}_m$.

Then, $\mathbf{X}_{\text{ms}}$ *does not have full column rank.*

To paraphrase, if DMD is well-posed and uses linearly consistent data with a non-zero mean and stationary mode, then $\mathbf{X}_{\text{ms}}$ does not have full column rank. Alas, Theorem 3.10, in conjunction with Lemma 3.2, falls short of producing a necessary condition for $\boldsymbol{\mu}$DMD$[\mathbf{Z}] \equiv$ DFT. This shortcoming is clarified in Theorem 4.2, using a stronger characterization of DMD-DFT equivalence (Theorem 4.1). Nonetheless, Theorem 3.10 points us in the correct direction to search for a necessary condition. An associated numerical experiment (Figure 4a in [14]) suggests that well-posedness,

linear consistency and non-zero mean may prevent $\boldsymbol{\mu}$DMD$[\mathbf{Z}] \equiv$ DFT. We formally prove a refined version of this implicit conjecture in Theorem 4.3. For the convenience of the reader, we summarize the assumptions that will be taken for granted in the sequel.

$$\begin{aligned} &\text{The time series } \mathbf{Z} \text{ is generated by (3.15) as given in (3.17).} \\ &\text{Koopman eigen-values are distinct.} \\ &\forall\, i,\ \phi_i(\boldsymbol{v}_1) \neq 0. \end{aligned} \tag{3.20}$$

4. Exploring the what and where of DMD-DFT equivalence. We begin by developing a necessary and sufficient condition for the equivalence of mean-subtracted DMD and DFT. Building on this result, we then study the relationship between mean-subtracted DMD and temporal DFT as a function of Companion-order$[\mathbf{Z}]$. This variable quantifies the capacity of the DMD model represented by $\mathbf{c}^*$ and, by (3.7), can be used interchangeably with n. We find that the occurrence of DMD-DFT equivalence is, for all practical purposes, dictated by the model capacity and the dimension of the underlying Koopman invariant subspace. Finally, we demonstrate that the requirements for the above results -linearly consistent data, and to a lesser extent, a Koopman invariant set of observables in $\boldsymbol{\psi}$ - can be met in practice using time delay embedding.

4.1. A geometric characterization of DMD-DFT equivalence.

THEOREM 4.1. *Mean subtracted DMD of* $\mathbf{Z}$ *is equivalent to temporal DFT if and only if the constant vector is orthogonal to* $\mathcal{N}(\mathbf{X}_{\text{ms}})$*, that is,*

$$\boldsymbol{\mu}DMD[\mathbf{Z}] \equiv DFT \iff \mathcal{P}_{\mathcal{N}(\mathbf{X}_{\text{ms}})}\mathbf{1}_n = 0.$$

Proof. Refer Appendix B.1 ∎

Thus, DMD-DFT equivalence is ensured when the constant vector has no projection onto $\mathcal{N}(\mathbf{X}_{\text{ms}})$ - A less stringent requirement than asking for a full column rank $\mathbf{X}_{\text{ms}}$[6]. This relaxation guides us towards situations where $\boldsymbol{\mu}$DMD$[\mathbf{Z}] \equiv$ DFT, despite $\mathbf{X}_{\text{ms}}$ having linearly dependent columns.

THEOREM 4.2. *Suppose* 1 *is not a Koopman eigenvalue i.e.* $1 \notin \sigma(\boldsymbol{\Lambda})$*. In addition, let* $n \in [2, r]$*. Also, denote the last column of* $\boldsymbol{\Theta}_1$ *as* $\mathbf{l}$*. Define the vector* $\mathbf{l}^\perp$ *as the projection of* $\mathbf{l}$ *that is orthogonal to the span of the first* $n-1$ *columns of* $\boldsymbol{\Theta}_1$*.*

$$\mathbf{l} := \begin{bmatrix} \lambda_1^{n-1} \\ \lambda_2^{n-1} \\ \vdots \\ \lambda_r^{n-1} \end{bmatrix}, \quad \mathbf{l}^\perp := \mathcal{P}_{\mathcal{N}(\boldsymbol{\Theta}_2^H)}\mathbf{l}.$$

Here, $\boldsymbol{\Theta}_2$ *denotes the sub-matrix formed by the first* $n-1$ *columns of* $\boldsymbol{\Theta}$*. Let* $\tilde{\mathbf{C}}$*, and hence the observables* $\boldsymbol{\psi}$*, be chosen as follows:*

$$\tilde{\mathbf{C}}_0 := (\mathbf{l}^\perp)^H(\boldsymbol{\Lambda} - \mathbf{I})^{-1}, \quad \tilde{\mathbf{C}} = \tilde{\mathbf{C}}_0 \begin{bmatrix} \phi_1(\boldsymbol{v}_1) & & & \\ & \phi_2(\boldsymbol{v}_1) & & \\ & & \ddots & \\ & & & \phi_r(\boldsymbol{v}_1) \end{bmatrix}^{-1}.$$

[6] Lemma 3.2 can be obtained from Theorem 4.1 by noting that $\mathcal{N}(\mathbf{X}_{\text{ms}}) = 0$ when $\mathbf{X}_{\text{ms}}$ has full column rank.

Then, mean-subtracted DMD is equivalent to temporal DFT even though $\mathbf{X}_{\text{ms}}$ *has linearly dependent columns.*

Proof. Refer Appendix B.2 ∎

Therefore, rank defectiveness of $\mathbf{X}_{\text{ms}}$ does not preclude DMD-DFT equivalence for the time series $\mathbf{Z}$. It is worth noting that linear inconsistency of $(\mathbf{X}, \mathbf{Y})$ and limited data are key ingredients in Theorem 4.2. Pursuing this line of thought, we find that the parameter regime where both conditions fail is devoid of DMD-DFT equivalence (Theorem 4.3).

4.2. Charting the domain of DMD-DFT equivalence. We probe the effect of Companion-order[$\mathbf{Z}$] i.e. n on DMD-DFT equivalence for the time series $\mathbf{Z}$. To this end, we partition the set of possible model orders into three regimes as described below:

1. Under-sampled ($n < r$): The model represented by $\mathbf{c}^*$ has insufficient capacity to precisely describe the system (3.15).
2. Just-sampled ($n = r$): The DMD model has the exact capacity needed to completely capture Koopman spectrum $\sigma(\mathbf{\Lambda})$.
3. Over-sampled ($n > r$): The capacity of the DMD model is more than sufficient to represent all r Koopman eigen-values.

We begin with the data-rich regime ($n > r$) where linear consistency prevents DMD-DFT equivalence.

THEOREM 4.3. *Mean-subtracted DMD is not a temporal DFT when data is linearly consistent and over-sampled.*

$$(\mathbf{X}, \mathbf{Y}) \text{ is linearly consistent } \& \; n \geq r+1 \implies \mathbf{c}_{\text{ms}}[\mathbf{Z}] \neq -\mathbf{1}_n.$$

Proof. Refer Appendix B.4 ∎

Thus, Theorem 3.10 can be extended by mildly strengthening the well-posedness, retaining linear consistency and dropping all other requirements. The contrapositive is of practical interest: Equivalence of mean-subtracted DMD and DFT may indicate a need to acquire more data for a reliable analysis. Scrutinizing the other data regimes gives the following result:

COROLLARY 4.4. *Suppose* $\boldsymbol{\psi}$ *is Koopman invariant. Then, the following hold in the just and under-sampled regimes:*

1. *When* $n = r$*, mean-subtracted DMD is equivalent to temporal DFT if and only if* 1 *is not a Koopman eigenvalue.*

$$\text{When } n = r, \; \boldsymbol{\mu}DMD[\mathbf{Z}] \equiv DFT \iff 1 \notin \sigma(\mathbf{\Lambda}).$$

2. *When* $n < r$ *i.e. the system is under-sampled, mean-subtracted DMD is equivalent to temporal DFT.*

$$n < r \implies \boldsymbol{\mu}DMD[\mathbf{Z}] \equiv DFT.$$

Proof. Refer Appendix B.5 ∎

The above result is a marginally diminished version of the true state of affairs. We actually have complete equivalence of DMD and DFT i.e. temporal DFT is the unique modal decomposition (of $\mathbf{Z}_{\text{ms}}$) whose error in predicting $\mathbf{y}_{\text{ms}}$ is orthogonal to the span of $\mathbf{X}_{\text{ms}}$.

Thus, we have a complete understanding of DMD-DFT equivalence, as defined in Definition 3.3, when the observables are Koopman invariant. Barring the pragmatically negligible case of just-sampling ($n = r$), under-sampling is necessary and sufficient for the equivalence of DMD and DFT.

4.3. DMD-DFT equivalence and delay embedding. Linear consistency of $(\mathbf{X}, \mathbf{Y})$ or more generally the Koopman invariance of $\boldsymbol{\psi}$ has been vital to our study of DMD-DFT equivalence. While this may not always hold, a simple remedy is to time delay the data $r-1$ times, assuming one has enough snapshots at hand.

4.3.1. Koopman invariance via time delays. Let $\mathbf{Z}_{\mathrm{d-delayed}}$ be the matrix obtained by taking d time delays of the original data matrix $\mathbf{Z}$.

$$\mathbf{Z}_{\mathrm{d-delayed}} := \begin{bmatrix} \mathbf{z}_1 & \mathbf{z}_2 & \cdots & \mathbf{z}_{n+1-d} \\ \mathbf{z}_2 & \mathbf{z}_3 & \cdots & \mathbf{z}_{n+2-d} \\ \vdots & \vdots & \ddots & \vdots \\ \mathbf{z}_{1+d} & \mathbf{z}_{2+d} & \cdots & \mathbf{z}_{n+1} \end{bmatrix}.$$

This matrix may be generated by $n+1-d$ sequential observations of (3.1) through an enlarged dictionary $\boldsymbol{\psi}_{\mathrm{d-delayed}}$. To see this, we first define $\tilde{\mathbf{C}}_{\mathrm{d-delayed}}$ and $\mathbf{C}_{\mathrm{d-delayed}}$ in analogy with $\tilde{\mathbf{C}}$ and $\mathbf{C}$.

$$\tilde{\mathbf{C}}_{\mathrm{d-delayed}} := \begin{bmatrix} \tilde{\mathbf{C}} \\ \tilde{\mathbf{C}}\boldsymbol{\Lambda} \\ \vdots \\ \tilde{\mathbf{C}}\boldsymbol{\Lambda}^d \end{bmatrix}, \quad \mathbf{C}_{\mathrm{d-delayed}} := \begin{bmatrix} \mathbf{C} \\ \mathbf{C}\boldsymbol{\Lambda} \\ \vdots \\ \mathbf{C}\boldsymbol{\Lambda}^d \end{bmatrix}.$$

Using the definition of $\boldsymbol{\Theta}_d$ in (3.18), we find:

$$\mathbf{Z}_{\mathrm{d-delayed}} = \mathbf{C}_{\mathrm{d-delayed}}\boldsymbol{\Theta}_d.$$

Moreover, (3.16) tells us how to connect $\mathbf{C}_{\mathrm{d-delayed}}$ and $\tilde{\mathbf{C}}_{\mathrm{d-delayed}}$:

$$\mathbf{C}_{\mathrm{d-delayed}} = \tilde{\mathbf{C}}_{\mathrm{d-delayed}} \begin{bmatrix} \phi_1(\boldsymbol{v}_1) & & & \\ & \phi_2(\boldsymbol{v}_1) & & \\ & & \ddots & \\ & & & \phi_r(\boldsymbol{v}_1) \end{bmatrix}.$$

In light of the derivation in Appendix A.1 that gives (3.17), the arguments above suggest that $\tilde{\mathbf{C}}_{\mathrm{d-delayed}}$ is the representation of $\boldsymbol{\psi}_{\mathrm{d-delayed}}$ in the eigen-basis $\boldsymbol{\phi}$:

$$\boldsymbol{\psi}_{\mathrm{d-delayed}} = \tilde{\mathbf{C}}_{\mathrm{d-delayed}}\boldsymbol{\phi}.$$

A classical argument from systems theory tells us that $r-1$ delays suffice to make $\boldsymbol{\psi}_{\mathrm{d-delayed}}$ Koopman invariant.

COROLLARY 4.5. *Suppose the set of observables $\boldsymbol{\psi}$ lies in a r-dimensional Koopman invariant subspace. Then, $\boldsymbol{\psi}$ can be enlarged into a Koopman invariant collection of observables if at least $r-1$ time delays are taken.*

$$d \geq r-1 \implies \boldsymbol{\psi}_{\mathrm{d-delayed}} \text{ is Koopman invariant.}$$

Proof. By Proposition 3.9, it suffices to show that $\tilde{\mathbf{C}}_{\mathrm{d-delayed}}$ has full column rank. The right eigen-vectors of $\mathbf{\Lambda}$ are the standard basis vectors and no column of $\tilde{\mathbf{C}}$ is 0. Hence, by the Eigenvector test for Observability [13], $(\mathbf{\Lambda}, \tilde{\mathbf{C}})$ is an observable pair. Since $\tilde{\mathbf{C}}_{\mathrm{d-delayed}}$ is the observability Grammian of $(\mathbf{\Lambda}, \tilde{\mathbf{C}})$, it has full column rank. ∎

Although $r-1$ delays are suggested, $\boldsymbol{\psi}$ may generate a Koopman invariant dictionary with fewer delays. Specifically, vector valued observables (i.e. $m > 1$) may generate a full column rank $\tilde{\mathbf{C}}_{\mathrm{d-delayed}}$ for $d < r-1$, as described in Lemma C of [20] and refined in Theorem 2 of [26]. In contrast, a scalar valued observable needs an absolute minimum of $r-1$ delays. In the forthcoming analysis, for the sake of simplicity, we use the potentially conservative prescription in Corollary 4.5 to ensure Koopman invariance.

Remark 4.6. Working with finite data forces a tradeoff between the number of delays taken, and the order of the DMD model used. This is explicitly quantified with the following observation:

$$\text{Companion-order}[\mathbf{Z}_{\mathrm{d-delayed}}] \;=\; n-d. \tag{4.1}$$

Consequently, for a r-dimensional Koopman invariant subspace, one needs $n - d \geq r$. We shall see that when the number of delays meets the criterion in Corollary 4.5, the Koopman spectrum, $\sigma(\mathbf{\Lambda})$, will be a subset of the DMD spectrum, $\sigma(\mathbf{T}^*)$.

4.3.2. DMD-DFT equivalence under delay embedding. We conclude this section by compiling our findings on DMD-DFT equivalence in the language of time delays. This necessitates a revisit of mean-removal in the context of $\mathbf{Z}_{\mathrm{d-delayed}}$.

Let θ denote the Companion-order of $\mathbf{Z}_{\mathrm{d-delayed}}$ i.e. one less than the number of columns in $\mathbf{Z}_{\mathrm{d-delayed}}$.

$$\theta \;:=\; \text{Companion-order}[\mathbf{Z}_{\mathrm{d-delayed}}]. \tag{4.2}$$

Then, the temporal mean of $\mathbf{Z}_{\mathrm{d-delayed}}$ is defined thus:

$$\boldsymbol{\mu}_{\mathrm{d-delayed}} := \mathbf{Z}_{\mathrm{d-delayed}} \frac{\mathbf{1}_{\theta+1}}{\theta+1}.$$

The mean-subtracted version of $\mathbf{Z}_{\mathrm{d-delayed}}$ would, then, read:

$$(\mathbf{Z}_{\mathrm{d-delayed}})_{\mathrm{ms}} := \mathbf{Z}_{\mathrm{d-delayed}} - \boldsymbol{\mu}_{\mathrm{d-delayed}} \mathbf{1}_{\theta+1}^T. \tag{4.3}$$

Now, we define $(\mathbf{X}_{\mathrm{d-delayed}})_{\mathrm{ms}}$ as the sub-matrix corresponding to the first θ columns of $(\mathbf{Z}_{\mathrm{d-delayed}})_{\mathrm{ms}}$ and $(\mathbf{y}_{\mathrm{d-delayed}})_{\mathrm{ms}}$ as the column vector corresponding to the last column of $(\mathbf{Z}_{\mathrm{d-delayed}})_{\mathrm{ms}}$. This gives the following identity:

$$(\mathbf{Z}_{\mathrm{d-delayed}})_{\mathrm{ms}} = \left[(\mathbf{X}_{\mathrm{d-delayed}})_{\mathrm{ms}} \quad | \quad (\mathbf{y}_{\mathrm{d-delayed}})_{\mathrm{ms}} \right].$$

Consequently, we have:

$$\mathbf{c}_{\mathrm{ms}}[\mathbf{Z}_{\mathrm{d-delayed}}] = (\mathbf{X}_{\mathrm{d-delayed}})_{\mathrm{ms}}^{\dagger} (\mathbf{y}_{\mathrm{d-delayed}})_{\mathrm{ms}}.$$

By Definition 3.3, mean-subtracted DMD of $\mathbf{Z}_{\mathrm{d-delayed}}$ is equivalent to temporal DFT if and only if $\mathbf{c}_{\mathrm{ms}}[\mathbf{Z}_{\mathrm{d-delayed}}]$ doesn't equal $-\mathbf{1}_\theta$. In short,

$$\boldsymbol{\mu}\mathrm{DMD}[\mathbf{Z}_{\mathrm{d-delayed}}] \equiv \mathrm{DFT} \iff \mathbf{c}_{\mathrm{ms}}[\mathbf{Z}_{\mathrm{d-delayed}}] = -\mathbf{1}_\theta.$$

Using Theorem 4.1, we may re-write the above as follows:

$$\boldsymbol{\mu}\text{DMD}[\mathbf{Z}_{\text{d}-\text{delayed}}] \equiv \text{DFT} \iff \mathcal{P}_{\mathcal{N}((\mathbf{X}_{\text{d}-\text{delayed}})_{\text{ms}})}\mathbf{1}_\theta = \mathbf{0}.$$

Finally, we extend the notions of under, just and over-sampling to $\mathbf{Z}_{\text{d}-\text{delayed}}$ by using θ (defined in equation (4.2)) as the model order. Hence, under-sampling refers to $\theta < r$, just-sampling means $\theta = r$ and over-sampling denotes $\theta > r$.

We can now provide a more pragmatic version of Theorem 4.3 and Corollary 4.4 where time delays are used to meet the relatively abstract conditions of linear consistency and Koopman invariance.

COROLLARY 4.7. *Suppose the conditions in equation (3.20) are true. If at least $r-1$ time delays have been taken, i.e. $d \geq r-1$, then we have DMD-DFT equivalence for $\mathbf{Z}_{\text{d}-\text{delayed}}$ if and only if we are under-sampled or in the just-sampled regime without a Koopman eigenvalue at 1.*

$$\boldsymbol{\mu}DMD[\mathbf{Z}_{\text{d}-\text{delayed}}] \equiv DFT \iff (\theta < r) \; OR \; (\theta = r \;\&\; 1 \notin \sigma(\boldsymbol{\Lambda})).$$

To summarize, when Koopman invariant observables are used, oversampling is (practically) necessary and sufficient to preclude the equivalence of mean-subtracted DMD and DFT. The requisite Koopman invariance can be attained by delay embedding the snapshots.

5. Extracting invariant subspaces. The primary goal of this section is to show that Companion DMD on data that has been subject to mean subtraction followed by sufficient time delays can recover the Koopman eigen-values $\sigma(\boldsymbol{\Lambda})$. This is achieved through a preliminary analysis of Companion DMD on raw data i.e. without mean removal.

5.1. Spectral objects without mean-subtraction. We prove that the DMD eigen-values, $\sigma(\mathbf{T}^*)$, contain the true Koopman eigen-values, $\sigma(\boldsymbol{\Lambda})$, if we have linearly consistent data of sufficient length ($n \geq r$). Furthermore, the corresponding Koopman modes are the only non-zero DMD modes. We begin by motivating our venture from a generalizability perspective.

5.1.1. Generalizability of DMD. Generalizability is the primary motivation behind our desire to approximate the Koopman eigen-values through the DMD spectrum. In order to quantify this notion in the companion matrix formulation (3.6), we consider the test matrix $\mathbf{Z}({\boldsymbol{v_1}}^{\text{test}}) \in \mathbb{C}^{m\times(n+1)}$. The columns of this matrix comprise the time series generated by observing the trajectory beginning at ${\boldsymbol{v_1}}^{\text{test}}$ through the observables $\boldsymbol{\psi}$.

$$\mathbf{z}_j({\boldsymbol{v_1}}^{\text{test}}) = \boldsymbol{\psi}(\Gamma^{j-1}({\boldsymbol{v_1}}^{\text{test}})), \quad j \in [1, n+1]. \tag{5.1}$$

Suppose $\mathbf{X}({\boldsymbol{v_1}}^{\text{test}})$ is the sub-matrix of $\mathbf{Z}({\boldsymbol{v_1}}^{\text{test}})$ corresponding to the first n columns and $\mathbf{y}({\boldsymbol{v_1}}^{\text{test}})$ is the last column of $\mathbf{Z}({\boldsymbol{v_1}}^{\text{test}})$. Then, generalizability associated with Companion DMD may be defined thus:

DEFINITION 5.1. *The DMD model corresponding to $\mathbf{c}^*$ is said to be generalizable if it can perfectly predict the observables in $\boldsymbol{\psi}$ along any trajectory.*

$$\forall \; {\boldsymbol{v_1}}^{\text{test}}, \; \mathbf{X}({\boldsymbol{v_1}}^{\text{test}}) \; \mathbf{c}^* = \mathbf{y}({\boldsymbol{v_1}}^{\text{test}}).$$

We show that perfect predictions are possible if and only if the DMD eigen-values contain the Koopman eigen-values.

LEMMA 5.2. *Suppose the assumptions listed in (3.20) are true. The DMD model corresponding to* $\mathbf{c}^*$ *is generalizable if and only if the spectrum of* $\mathbf{T}^*$ *i.e. the DMD eigen-values contain the Koopman spectrum.*

$$\forall\ \boldsymbol{v_1}^{\text{test}},\ \mathbf{X}(\boldsymbol{v_1}^{\text{test}})\ \mathbf{c}^*\ =\ \mathbf{y}(\boldsymbol{v_1}^{\text{test}})\ \iff\ \sigma(\mathbf{T}^*) \supset \sigma(\mathbf{\Lambda}).$$

Proof. Refer Appendix C. ∎

As mentioned earlier, generalizability has been studied in the context of the Exact DMD formulation given in (3.4). In particular, Theorem 4.5 of [14] says that well-posedness and linear consistency together guarantee the generalizability of the model represented by A_{Exact}.

We show that the same duo are sufficient for generalizability in the companion matrix formulation. We build upon an existence result due to [26] that is unduly restricted to roots of unity. We remove this restriction to allow for arbitrary and distinct eigen-values:

PROPOSITION 5.3. *Suppose (3.20) holds. Then, the feasible set of the DMD minimization in (3.6) contains a generalizable model if and only if the problem is well-posed.*

$$n \geq r\ \iff\ \exists\ \mathbf{c}\ \textit{such that}\ \forall\ \boldsymbol{v}_1,\ \mathbf{X}(\boldsymbol{v}_1)\ \mathbf{c}\ =\ y(\boldsymbol{v}_1).$$

In addition, if $(\mathbf{X}, \mathbf{Y})$ *is linearly consistent and* $n = r$*, then the generalizable model is unique.*

Proof. Same as Theorem 1 in [26]. The sequence of arguments there applies equally well to the case of arbitrary and distinct eigen-values. ∎

Thus, well-posedness guarantees that a subset of the models permitted in (3.6) will be generalizable. We would like this subset to contain the DMD model given by $\mathbf{c}^*$. It so happens that linear consistency suffices for the DMD model to acquire generalizability.

Once we obtain a generalizable DMD model, it is natural to ask what part of it confers generalizability. According to Lemma 5.2, this is tantamount to extracting Koopman eigen-values from the DMD spectrum. Mode-norm based pruning offers a simple and data-driven solution to this question: The DMD eigen-values whose DMD modes have non-zero norm are the Koopman eigen-values.

5.1.2. Identifying Koopman eigen-values via the DMD mode norm. We start by defining the set of "DMD eigen-values with non-trivial DMD modes":

$$\sigma_{\text{nontriv}}[\mathbf{Z}, \mathbf{c}^*] := \{\lambda \in \sigma(\mathbf{T}[\mathbf{c}^*]) |\ \exists\, \mathbf{v}_\lambda \text{ such that } \mathbf{T}[\mathbf{c}^*]\mathbf{v}_\lambda = \lambda \mathbf{v}_\lambda\ \&\ \mathbf{X}\mathbf{v}_\lambda \neq 0\}. \tag{5.2}$$

By explicitly acknowledging the dependence of $\mathbf{c}^*$, we can use this construction to prove mode-norm based pruning in a relatively general setting. This is then specialized to cases with and without mean subtraction.

THEOREM 5.4. *Consider any matrix* $\check{\mathbf{C}} \in \mathbb{C}^{m \times r}$*. Let* $\check{\mathbf{Z}} \in \mathbb{C}^{m \times (n+1)}$ *be the time series generated from* $\check{\mathbf{C}}$ *as follows:*

$$\check{\mathbf{Z}} := \check{\mathbf{C}}\mathbf{\Theta}.$$

Suppose $\check{\mathbf{c}}^*$ *is the optimal solution to the Companion DMD objective (3.6) for the time series* $\check{\mathbf{Z}}$ *and* $\check{\mathbf{T}}^*$ *the associated companion matrix.*

$$\check{\mathbf{c}}^* := \mathbf{c}^*[\check{\mathbf{Z}}], \quad \check{\mathbf{T}}^* := \mathbf{T}[\check{\mathbf{c}}^*].$$

If $\check{\mathbf{C}}$ *has linearly independent columns and* $n \geq r$*, then the Koopman spectrum is made of DMD eigen-values whose modes have non-zero norm.*

$$\check{\mathbf{C}} \textit{ is full column rank} \quad \& \quad n \geq r \implies \sigma_{\text{nontriv}}[\check{\mathbf{Z}}, \check{\mathbf{c}}^*] = \sigma(\mathbf{\Lambda}).$$

Proof. Refer Appendix C. ∎

In order to study $\mathbf{Z}$, equation (3.17) suggests that the matrix $\mathbf{C}$ (or equivalently $\tilde{\mathbf{C}}$) presume the role of $\check{\mathbf{C}}$ in Theorem 5.4. Acknowledging that Companion-order$[\mathbf{Z}] = n$, we have the following result, entirely in terms of the data matrices $\mathbf{Z}$, $\mathbf{X}$ and $\mathbf{Y}$:

COROLLARY 5.5. *Well-posedness and linear consistency guarantee identification of Koopman eigen-values.*

$$(\mathbf{X}, \mathbf{Y}) \textit{ is linearly consistent } \& \textit{ Companion-order}[\mathbf{Z}] \geq r \implies \sigma_{\text{nontriv}}[\mathbf{Z}, \mathbf{c}^*(\mathbf{Z})] = \sigma(\mathbf{\Lambda}).$$

Proof. By Propositions 3.7 and 3.9, linear consistency of $(\mathbf{X}, \mathbf{Y})$ is equivalent to $\tilde{\mathbf{C}}$ having full column rank since the problem is well-posed. Equation (3.20) tells us that $\mathbf{C}$ has full column rank too. Apply Theorem 5.4 with $\check{\mathbf{C}} \to \mathbf{C}$. ∎

Therefore, when $(\mathbf{X}, \mathbf{Y})$ is linearly consistent and the DMD regression (3.6) is well-posed, Companion DMD can coherently extract $\sigma(\mathbf{\Lambda})$ via the mode-norm. Hence, the model given by $\mathbf{c}^*$ is generalizable.

Remark 5.6. We can now connect DMD mode norms to DMD amplitudes. When the conditions in Corollary 5.5 are met, we have:

$$\mathbf{X}^\dagger = \mathbf{\Theta}_1^\dagger \mathbf{C}^\dagger.$$

This gives $\mathbf{A}_{\text{Exact}} = \mathbf{C}\ \mathbf{\Lambda}\ \mathbf{C}^\dagger$. Moreover, its compact version viz. $\mathbf{A}_{\text{SVD}}$ (see [30]) is similar to $\mathbf{U}_{\mathbf{C}}^H \mathbf{A}_{\text{Exact}} \mathbf{U}_{\mathbf{C}}$, where $\mathbf{U}_{\mathbf{C}}$ is the left singular matrix of $\mathbf{C}$. Thus, the eigen-values of both DMD matrices [7] contain the Koopman eigen-values, which can be singled out by their non-zero DMD amplitudes. In particular, the absolute value of each non-zero amplitude equals the norm of the respective Companion DMD mode.

5.1.3. Enabling mode-norm based pruning using time delays. The requirement of linear consistency in Corollary 5.5 can be met by taking enough delays, as shown in Corollary 4.5. Consequently, a trajectory of length $2r$ is sufficient to characterize an r-dimensional Koopman invariant subspace. We formally compile this finding:

COROLLARY 5.7. *Suppose* $\mathbf{Z}$ *meets the requirements in* (3.20)*. If a minimum of* $r-1$ *time delays are taken and a DMD model of order (as defined in* (4.2)*) at least* r *is constructed, then the DMD eigen-values corresponding to DMD modes with non-zero norm comprise the Koopman spectrum.*

$$d \geq r-1 \ \& \ \theta \geq r \implies \sigma_{\text{nontriv}}[\mathbf{Z}_{\text{d-delayed}}, \mathbf{c}^*[\mathbf{Z}_{\text{d-delayed}}]] = \sigma(\mathbf{\Lambda}).$$

Proof. Consider the sub-matrices of $\mathbf{Z}_{\text{d-delayed}}$ required to test for linear consistency:

$$\mathbf{X}_{\text{d-delayed}} := \mathbf{C}_{\text{d-delayed}} \mathbf{\Theta}_{d+1}, \quad \mathbf{Y}_{\text{d-delayed}} := \mathbf{C}_{\text{d-delayed}} \mathbf{\Lambda} \mathbf{\Theta}_{d+1}.$$

[7] $\mathbf{A}_{\text{Exact}}$ can only have 0 as its trivial eigenvalue, while $\mathbf{A}_{\text{SVD}}$ has none.

According to Corollary 4.5, $d \geq r-1$ ensures that $(\mathbf{X}_{\text{d-delayed}}, \mathbf{Y}_{\text{d-delayed}})$ is linearly consistent. We are given that Companion-order$[\mathbf{Z}_{\text{d-delayed}}] \geq r$. Hence, by Corollary 5.5, all Koopman eigen-values are recovered and distinguished by non-zero DMD mode norm. ∎

Therefore, the Koopman spectrum can be extracted whenever we have sufficient samples of a time series satisfying (3.20). Even if its observables are different from $\boldsymbol{\psi}$, the mean-subtracted time series (B.5) meets this criterion and hence is amenable to Corollary 5.7.

5.2. Spectral objects with mean-subtraction. We demonstrate that time delays help recover Koopman eigen-values from mean subtracted data by recognizing the Vandermonde matrix implicit in $\mathbf{Z}_{\text{ms}}$ and then applying Corollary 5.7. Recall from (B.5) that the row-space of $\mathbf{Z}_{\text{ms}}$ lies within that of the modified Vandermonde matrix $\boldsymbol{\Theta}_{\text{ms}}$:

$$\mathbf{Z}_{\text{ms}} = \mathbf{C}_{\text{ms}}\boldsymbol{\Theta}_{\text{ms}}.$$

We would like to compute the Koopman spectrum, to the extent possible, from the mean-subtracted time series $\mathbf{Z}_{\text{ms}}$. If we sufficiently delay embed the mean-removed data and then perform DMD, by Corollary 5.7, mode-norm based pruning will recover all the nodes of $\boldsymbol{\Theta}_{\text{ms}}$. According to the equation (B.5), every Koopman eigenvalue that does not equal 1 will be a node of $\boldsymbol{\Theta}_{\text{ms}}$. Hence, the DMD eigen-values with non-zero DMD modes will subsume most of the Koopman spectrum. The fate of the eigenvalue at 1 is more nuanced and understanding it requires a closer look at the efficacy of mean removal (subsection 5.2.1) and time-delayed versions of $\mathbf{Z}_{\text{ms}}$ (subsection 5.2.2).

5.2.1. On the effectiveness of mean-removal. The purpose of mean subtraction is to remove the row corresponding to the eigenvalue 1 from $\boldsymbol{\Theta}$. Hence, its efficacy may be graded by the presence or absence of 1 among the nodes of $\boldsymbol{\Theta}_{\text{ms}}$.

DEFINITION 5.8. *We say that mean subtraction is successful if there is no row of* $\boldsymbol{\Theta}_{\text{ms}}$ *corresponding to* $\mathbf{1}_{n+1}^T$.

If our observables are Koopman invariant, the outcome of mean subtraction solely depends on the Koopman spectrum $\sigma(\boldsymbol{\Lambda})$ and the length of the trajectory $(n+1)$. In other words, when $\tilde{C}$ has full column rank, the success or failure of mean removal is entirely determined by the Vandermonde matrix $\boldsymbol{\Theta}$. We formally state our claim in the two theorems that follow:

THEOREM 5.9. *Suppose* $\boldsymbol{\psi}$ *is a Koopman invariant set of observables. Let* p^* *be the smallest natural number such that every Koopman eigen-value is a* p^**-th root of unity.*

$$\forall\ \lambda \in \sigma(\boldsymbol{\Lambda}),\ \lambda^{p^*} = 1$$
$$\forall\ 1 \leq q < p^*,\ \exists\ \lambda \in \sigma(\boldsymbol{\Lambda})\ \textit{such that}\ \lambda^q \neq 1.$$

Then, mean subtraction succeeds on the time series data $\mathbf{Z}$ *if and only if the trajectory length (the number of columns) is a multiple of* p^*.

$$\textit{Mean subtraction succeeds on } \mathbf{Z} \iff (n+1) \mod p^* = 0.$$

Proof. Refer Appendix D. ∎

THEOREM 5.10. *Suppose* $\boldsymbol{\psi}$ *is a Koopman invariant set of observables. If the Koopman eigen-values are not roots of unity for some common natural number* q*, then mean subtraction fails irrespective of the length of the trajectory.*

$$\forall\ q \in \mathbb{N},\ \exists\ \lambda \in \sigma(\boldsymbol{\Lambda})\ \textit{such that}\ \lambda^q \neq 1 \implies \forall\ n \in \mathbb{N},\ \textit{mean subtraction fails.}$$

Proof. Refer Appendix D. ∎

To summarize, mean subtraction succeeds for the time series $\mathbf{Z}$ if and only if the Koopman eigen-values are the roots of unity for some common natural number, and the trajectory length $(n+1)$ is a multiple of the smallest such natural number. For example, suppose $\boldsymbol{\psi}$ is Koopman invariant and $\sigma(\boldsymbol{\Lambda}) = \{-1, 1, i, -i\}$. Then, by Theorem 5.9, mean subtraction succeeds whenever $(n+1)$ is a multiple of 4. However, if $\sigma(\boldsymbol{\Lambda}) = \{-\frac{1}{2}, 1, i, -i\}$ or $\sigma(\boldsymbol{\Lambda}) = \{-1, 1, i, e^{\mathrm{i}\frac{2\pi}{\sqrt{2}}}\}$, then mean subtraction always fails according to Theorem 5.10. This is because both scenarios have an eigenvalue ($-\frac{1}{2}$ in the former and $e^{\mathrm{i}\frac{2\pi}{\sqrt{2}}}$ in the latter) that can never be a root of unity.

5.2.2. Delay embedding of mean-removed time series. Let $(\mathbf{Z}_{\mathrm{ms}})_{\mathrm{d-delayed}}$ denote the matrix obtained from $\mathbf{Z}_{\mathrm{ms}}$ by taking d time-delays.

$$(\mathbf{Z}_{\mathrm{ms}})_{\mathrm{d-delayed}} := \begin{bmatrix} \mathbf{z}_1 - \boldsymbol{\mu} & \mathbf{z}_2 - \boldsymbol{\mu} & \dots & \mathbf{z}_{n+1-d} - \boldsymbol{\mu} \\ \mathbf{z}_2 - \boldsymbol{\mu} & \mathbf{z}_3 - \boldsymbol{\mu} & \dots & \mathbf{z}_{n+2-d} - \boldsymbol{\mu} \\ \vdots & \vdots & \ddots & \vdots \\ \mathbf{z}_{1+d} - \boldsymbol{\mu} & \mathbf{z}_{2+d} - \boldsymbol{\mu} & \dots & \mathbf{z}_{n+1} - \boldsymbol{\mu} \end{bmatrix}. \tag{5.3}$$

Observe that the matrix $(\mathbf{Z}_{\mathrm{ms}})_{\mathrm{d-delayed}}$ subtly differs from the seemingly related matrix $(\mathbf{Z}_{\mathrm{d-delayed}})_{\mathrm{ms}}$. By (5.3), the former is obtained by removing the temporal mean $\boldsymbol{\mu}$ from $\mathbf{Z}$ and then taking d time delays. However, the latter is constructed according to (4.3) by taking d time-delays and then removing a different temporal mean $\boldsymbol{\mu}_{\mathrm{d-delayed}}$. In other words, mean subtraction precedes delay embedding for $(\mathbf{Z}_{\mathrm{ms}})_{\mathrm{d-delayed}}$ while the order is flipped for $(\mathbf{Z}_{\mathrm{d-delayed}})_{\mathrm{ms}}$.

Despite this difference, both matrices have the same number of columns. This stems from their common embedding dimension and the fact that mean removal doesn't alter the size of a matrix. Consequently, if we define the order of the DMD model constructed with $(\mathbf{Z}_{\mathrm{ms}})_{\mathrm{d-delayed}}$ as

$$\theta_{\mathrm{ms}} \;:=\; \text{Companion-order}[(\mathbf{Z}_{\mathrm{ms}})_{\mathrm{d-delayed}}], \tag{5.4}$$

then, we have the following identity:

$$\theta_{\mathrm{ms}} \;=\; \theta. \tag{5.5}$$

In the sequel, we use these two symbols interchangeably, as appropriate for the context.

5.2.3. DMD of mean-subtracted data under time delays. We formally prove our claim on recovering the Koopman spectrum, excluding 1, from mean-removed data.

Corollary 5.11. *Suppose we perform Companion DMD on delayed versions of the mean-subtracted data matrix $\mathbf{Z}_{\mathrm{ms}}$, as defined in (5.3). If the number of time-delays and model order exceed a minimum value determined entirely by r, then the DMD eigen-values corresponding to non-zero modes contain the Koopman spectrum, sans* 1. *The pruned DMD spectrum will also contain* 1 *if and only if mean subtraction fails, as described in Definition 5.8.*

1. *If $1 \notin \sigma(\boldsymbol{\Lambda})$, then $d \;\geq\; r$ and $\theta_{\mathrm{ms}} \;\geq\; r+1$ ensure that:*

$$\sigma_{\mathrm{nontriv}}\left[(\mathbf{Z}_{\mathrm{ms}})_{\mathrm{d-delayed}}, \mathbf{c}^*\left[(\mathbf{Z}_{\mathrm{ms}})_{\mathrm{d-delayed}}\right]\right] = \begin{cases} \sigma(\boldsymbol{\Lambda}) \cap \{1\}^C & \textit{Mean subtraction succeeds} \\ \sigma(\boldsymbol{\Lambda}) \cup \{1\} & \textit{Otherwise} \end{cases}$$

2. *If* $1 \in \sigma(\mathbf{\Lambda})$*, then a similar spectral result holds. The minimum requirements on time delays and Companion-order drop by 1. Yet, the pruned DMD spectrum* $\sigma_{\text{nontriv}}\left[(\mathbf{Z}_{\text{ms}})_{\text{d}-\text{delayed}}, \mathbf{c}^*\left[(\mathbf{Z}_{\text{ms}})_{\text{d}-\text{delayed}}\right]\right]$ *remains unaltered.*

Proof. Suppose $1 \notin \sigma(\mathbf{\Lambda})$. Then, $\mathbf{\Theta}_{\text{ms}}$ has utmost $r+1$ rows, regardless of the efficiency of mean subtraction. Hence, when $\mathbf{Z}_{\text{ms}}$ is delayed at least r times and the Companion-order of the delayed matrix is at least $r+1$, by Corollary 5.7, we can identify the Koopman spectrum using the DMD mode norm. The same line of reasoning when $1 \in \sigma(\mathbf{\Lambda})$ puts the minimum requirements one lower than in its absence. ∎

Therefore, a DMD eigenvalue with non-zero mode norm is a bona fide Koopman eigenvalue, unless it is 1 itself. The DMD eigen-values thus filtered will contain the Koopman spectrum modulo 1.

Remark 5.12. Once again, the performance of Exact and SVD-based DMD can be compared with the companion matrix approach. When the requirements of Corollary 5.11 hold,

$$\mathbf{A}_{\text{Exact,ms}} = (\mathbf{C}_{\text{ms}})_{\text{d}-\text{delayed}} \mathbf{\Lambda}_{\text{ms}} (\mathbf{C}_{\text{ms}})^{\dagger}_{\text{d}-\text{delayed}},$$

where $\mathbf{\Lambda}_{\text{ms}}$ is the diagonal matrix made of the nodes of $\mathbf{\Theta}_{\text{ms}}$. The matrix $\mathbf{A}_{\text{SVD,ms}}$ is the compression of $\mathbf{A}_{\text{Exact,ms}}$ onto the range of $(\mathbf{C}_{\text{ms}})_{\text{d}-\text{delayed}}$. Thus, the DMD eigenvalues[8] corresponding to non-zero DMD amplitudes are the diagonal entries of $\mathbf{\Lambda}_{\text{ms}}$. These are the Koopman eigen-values, $\sigma(\mathbf{\Lambda})$, without or with 1 when mean subtraction works or fails respectively.

Consequently, Hankel DMD on mean-subtracted data followed by DMD amplitude based pruning will produce meaningful Koopman spectral objects. Hence, the approach adopted in [4] stands vindicated.

In conclusion, the Koopman spectrum can be estimated from mean-subtracted data by delay embedding it before DMD. The resulting DMD eigen-values with non-zero DMD mode norm form a super-set of the Koopman spectrum sans 1 i.e. $\sigma(\mathbf{\Lambda}) \cap \{1\}^c$. If there is a pruned DMD eigenvalue that doesn't belong to $\sigma(\mathbf{\Lambda}) \cap \{1\}^c$, it can only be 1. Unfortunately, it is not easy to figure out the authenticity of 1 purely from data. On the bright side, this spectral corruption is mild and more importantly predictable after sufficient time delays.

6. Numerical experiments. We study[9] numerically observable consequences of the transient predictions in Corollary 4.7 & the spectral guarantees in Corollaries 5.7 and 5.11. The abstractness of these results concerning DMD-DFT equivalence and mode-norm based pruning necessitates their translation to concrete computational tasks.

For instance[10], validating Corollary 4.7 requires that we assess its predictions about the presence or absence of DMD-DFT equivalence, over an appropriate range of model orders. Similarly, we need to check if the DMD modes with non-zero norm pick out the Koopman eigen-values as predicted by Corollaries 5.7 and 5.11. Observe that the associated predictions involve equality of vectors for DMD-DFT equivalence and of finite sets in mode-norm pruning. Alas, it is difficult to observe equalities in computations that use finite precision arithmetic.

[8] Trivial eigen-values are non-existent in $\mathbf{A}_{\text{SVD,ms}}$ and effectively so (i.e. 0) in $\mathbf{A}_{\text{Exact,ms}}$.

[9] All code used in this analysis can found at https://github.com/gowtham-ss-ragavan/msub_mdselect_dmd.git

[10] Assume that the required conditions, notably those listed in equation (3.20), are met.

To this end, we re-phrase the relevant results in a numerically tangible fashion using two real-valued indicators, named "Relative distance to DFT" and "KMD-Quality", that take values between 0 and 1. The former measures the deviation from the vector equality that signals DMD-DFT equivalence. The latter grades the performance of mode-norm based filtering of DMD eigen-values. Consequently, we are able to systematically test the chief theoretical findings of this manuscript.

We test the major results on a variety of dynamical systems of increasing complexity. We primarily work with linear-time invariant (LTI) systems since their Koopman spectra are well-known and the conditions required, like those in (3.20), can be met. We also validate our theory using the Van der Pol oscillator and the lid-driven cavity from [3]. In contrast to the LTI systems, we have no guarantee of meeting the required conditions in (3.20) nor do we possess complete knowledge of the associated Koopman spectra. Hence, we restrict our attention to Corollary 4.7 and use its contrapositive to speculate the dimension of the underlying Koopman invariant subspace.

Once a dynamical system is chosen, we pick an appropriate range of Companion-orders and $\#[delays]$ in which the theorems are to be examined. For each choice of model-order (θ) and delay embedding dimension (d), we compute "Relative distance to DFT" and "KMD-Quality" over an ensemble of trajectories and dictionaries.

To see this in detail, suppose $\theta_{\max}$ is the maximal Companion-order and $d_{\max}$ the largest number of time delays to be taken. Consider the trajectory of length $\theta_{\max}+d_{\max}+1$ beginning at $\boldsymbol{v}_1$ and observed through the vector of m observables $\boldsymbol{\psi}$. The length of the trajectory has been chosen so that we can compute the two numerical indicators for every pair (θ, d) in the entire parameter range. For the choice of (θ, d), the time series matrix $\mathbf{Z}$ reads thus:

$$\mathbf{Z} = \begin{bmatrix} \boldsymbol{\psi}(\boldsymbol{v}_1) & \boldsymbol{\psi}(\Gamma(\boldsymbol{v}_1)) & \dots & \boldsymbol{\psi}(\Gamma^{\theta+d}(\boldsymbol{v}_1)) \end{bmatrix}. \tag{6.1}$$

To paraphrase, $\mathbf{Z}$ corresponds to sampling $\boldsymbol{\psi}$ on the first $\theta+d+1$ elements of the trajectory. Subsequently, we construct the DMD models required to test the results being studied. Each corollary requires a different model, and this is detailed in Table 6.1.

TABLE 6.1
Theoretical results paired with the DMD model required for their numerical scrutiny.

Theory to test	DMD model required
Corollary 4.7	$\mathbf{c}_{\mathrm{ms}}[\mathbf{Z}_{\mathrm{d-delayed}}]$
Corollary 5.7	$\mathbf{c}^{*}\,[\mathbf{Z}_{\mathrm{d-delayed}}]$
Corollary 5.11	$\mathbf{c}^{*}\,[(\mathbf{Z}_{\mathrm{ms}})_{\mathrm{d-delayed}}]$

Once DMD regression[11] produces $\mathbf{c}^{*}$ and $\mathbf{c}_{\mathrm{ms}}$, it is then straightforward to compute "KMD-Quality" and "Relative distance to DFT" respectively. We then iterate this calculation over every pair (θ, d) in the parameter regime of interest. Finally, we also repeat this parametric sweep, at a higher level, over many trajectories[12]. Consequently, we can study the statistics of "Relative distance to DFT" and "KMD-Quality" for every pair of Companion-order (θ) and $\#[delays]$ (d) being tested. This is facilitated by box-whisker plots of these two indicators with respect to Companion-order.

In the two sub-sections that follow, we begin by defining the numerical indicator of concern to the theorem being tested. Then, for each of the systems listed above, we

[11] A relative threshold of 10^{-8} is used in all pseudo-inverse computations.
[12] We also switch the dictionary for each trajectory for an added level of randomness.

compute the indicator for over a range of model orders and time delays. The second sub-section, which tests mode-norm based pruning of the DMD spectrum, concludes with a short study on the effect of observation noise upon the spectral guarantees of Corollary 5.7.

6.1. (Non)-equivalence of DMD and DFT. The root-mean-squared error between $\mathbf{c}_{\text{ms}}[\mathbf{Z}_{\text{d-delayed}}]$ and $-\mathbf{1}_\theta$ can measure the deviation of mean-subtracted DMD from DFT.

$$\textbf{Relative distance to DFT } [\mathbf{Z}_{\text{d-delayed}}] := \frac{\|\mathbf{c}_{\text{ms}}[\mathbf{Z}_{\text{d-delayed}}] + \mathbf{1}_\theta\|}{\sqrt{\theta}} \tag{6.2}$$

This numerical quantity takes values from 0 to 1. 0 indicates DMD-DFT equivalence, while the rest point to its absence. We begin our numerical exploration with dynamical systems where the conditions listed in equation (3.20) are known to hold.

6.1.1. Systems with a known invariant subspace. Consider the linear time invariant systems resulting from the following simplifications to equations (3.1) and (3.15):

$$\Gamma_i(\boldsymbol{\upsilon}) = \boldsymbol{\Lambda}_i\boldsymbol{\upsilon}, \quad \boldsymbol{\phi}_i(\boldsymbol{\upsilon}) = \boldsymbol{\upsilon}, \quad \boldsymbol{\psi}_i = \tilde{\mathbf{C}}_i\boldsymbol{\phi}_i, \quad i = 1a, 1b, 3. \tag{6.3}$$

where $\tilde{\mathbf{C}}_i$ are arbitrarily chosen row vectors with non-zero entries and $\boldsymbol{\Lambda}_i$ are diagonal matrices. In other words, the state $\boldsymbol{\upsilon}$ is updated by simply scaling each component as described by $\boldsymbol{\Lambda}_i$. This makes every component of the state into an eigen-function. The observables $\boldsymbol{\psi}_i$ are obtained by a linear transformation of the state. Spectral details of the three systems can be found in Table 6.2. All three are neutrally stable, but 1 is an eigenvalue only of LTI_{1a}.

TABLE 6.2
eigen-values of the LTI systems in (6.3).

Name	LTI_{1a}	LTI_{1b}	LTI_3
$\sigma(\boldsymbol{\Lambda})$	$\{\mathrm{e}^{\mathrm{i}\frac{2j\pi}{7}}\}_{j=1}^{7}$	All 7 on the unit circle	$\lvert\lambda_i\rvert = 1,\ i = 1,2,3,4$ $\{\lvert\lambda_5\rvert, \lvert\lambda_6\rvert, \lvert\lambda_7\rvert\} = 0.97, 0.93, 0.87$

Since every entry of $\tilde{\mathbf{C}}_i$ is non-zero, $r = 7$ for all three LTIs. Assuming that at-least 6 time delays are taken, Corollary 4.7 makes the following predictions: LTI_{1a} has a Koopman eigenvalue at 1. So, the relative distance to DFT will be insignificant when $\theta < 7$ and otherwise for $\theta \geq 7$. The same trend will hold for LTI_{1b} and LTI_3, with the boundary shifting from 7 to 8 due to the absence of 1 in their Koopman spectrum.

For the unitary systems LTI_{1a} and LTI_{1b}, the expected trend is clearly visible in sub-figures (a) and (b) of Figure 6.1. The relative distance to DFT is orders of magnitude larger when θ crosses the critical value. Moreover, the shadowing of this feature by the pertinent inter-quartile ranges (IQRs), denoted by boxes coloured according to the number of delays taken, suggests that the observation is independent of the choice of initial condition. The icing on the cake is that when $\theta = r = 7$, the effect of having $1 \in \sigma(\boldsymbol{\Lambda})$ is in concordance with Corollary 4.4. The system LTI_{1b}, which does not have a Koopman eigenvalue at 1, has low values of relative distance to DFT indicating DMD-DFT equivalence. To the contrary, LTI_{1a} exhibits a value that is orders of magnitude larger because its Koopman spectrum contains 1.

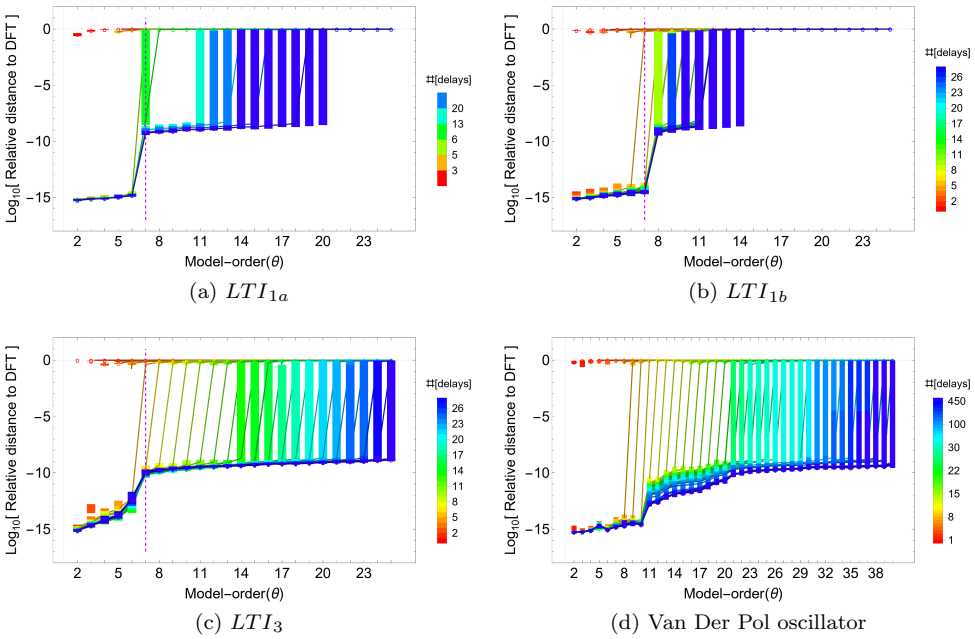


FIG. 6.1. *Box plots of the relative distance to DFT reveal its dependence on the model order* (θ) *and the number of time delays (Colour-coded). The magenta line indicates* r *(when it is known). When at least 6 time delays are taken,* $LTI_{1a}(LTI_{1b})$ *displays a plateau starting at a Companion-order of 7(8) as predicted by Corollary 4.7. Although this plateau begins earlier than expected (at* $\theta = 7$ *instead of* $\theta = 8$*) for* LTI_3*, the overall trend conforms to the theoretical prediction of Corollary 4.7. In contrast, we do not know the system order* (r) *for the observations from the Van der Pol oscillator. Nonetheless, panel (d) exhibits a step-like trend with sufficient time delays. The location of the jump may be indicative of an underlying 10 or 11 dimensional Koopman invariant subspace.*

The computations with LTI_3 are not in exact agreement with the theoretical claims, particularly when θ matches r. Recall that Corollary 4.7 predicts the same trend for LTI_3 and LTI_{1b} since neither has a Koopman eigenvalue at 1. In sub-figure (c) of Figure 6.1, we observe that DMD-DFT equivalence appears to hold for model orders less than 7 and is absent when θ exceeds 7. However, when θ is 7, we see non-equivalence of mean-subtracted DMD and DFT, in contrary to the theoretical prediction of equivalence. We believe that this is a numerical issue arising from the three stable Koopman eigen-values of this system (see Table 6.2) and the inherent fragility of statements concerning the just-sampled regime. As a precautionary measure, we exclude LTI_3 from the numerical validation of the mode-extraction theorems in subsection 6.2.

6.1.2. Systems with an unknown invariant subspace. We now analyse autonomous systems where we do not know, a priori, if our observables lie in a finite dimensional Koopman invariant subspace. This does not prevent us from repeating the computational study done for the LTI systems. Indeed, we will use the numerical results in conjunction with the contrapositive of Corollary 4.7 to provide a lower bound on the dimension of the Koopman invariant subspace containing our observables. The idea is that when at least $r-1$ delays are taken, a negation of the predictions made by Corollary 4.7 generically means that the data is not produced by observing an

r-dimensional Koopman invariant subspace, as described in (3.15).

In order to explain this, we note that if the predictions of Corollary 4.7 are inconsistent with a numerical study that has taken sufficient time delays, then equation (3.20) does not hold. The list of conditions in (3.20) may be re-phrased as follows:

1. The columns of $\mathbf{Z}$ are sequential observations of a finite dimensional Koopman invariant subspace.
2. This invariant subspace has distinct Koopman eigen-values.
3. The initial condition has a non-zero projection onto every eigen-space.

In practice, it is possible to drop the last two conditions. The second condition holds generically since the set of matrices that are not diagonalizable has zero measure. The third condition always holds if we choose to work with the smaller Koopman invariant subspace corresponding to the sum of eigen-spaces having a non-zero projection. This change of perspective is valid because the reduced subspace is equally capable of generating the training set $\mathbf{Z}$ through sequential observations. Therefore, the negation of equation (3.20) generically means that $\mathbf{Z}$ was not generated by a finite dimensional Koopman invariant subspace. We can now provide a more detailed description of the forthcoming numerical experiments.

For every dynamical system, we begin with the assumption that our observables lie in a finite dimensional Koopman invariant subspace. We also assume that we have an upper bound $r_{\max}$ on its dimension. This may be a theoretically informed cap or, if little is known about the system, simply the maximum Companion-order that is palatable from a modelling perspective. Suppose we take at least $r_{\max}-1$ time delays i.e. $d \geq r_{\max}-1$. Then, by Corollary 4.7, **Relative distance to DFT** $[\mathbf{Z}_{\mathrm{d-delayed}}]$ must behave like a step function with respect to Companion order (θ). It must be near zero for model order less than $r+1$ (r if 1 is a Koopman eigenvalue) and significantly higher for larger model orders. The absence of a step-like behaviour for model orders less than or equal to $r_{\max}+1$ would then mean that our observable lies in a Koopman invariant subspace of dimension greater than $r_{\max}$.

Consider the discrete time system (3.1) obtained by sampling the flow map of the Van der Pol oscillator at equi-spaced points in time. The differential equation generating the flow map reads:

$$\begin{aligned} \dot{v_1} &= v_2 \\ \dot{v_2} &= (1-v_1^2)v_2 - v_1. \end{aligned}$$

Recall that v_1 and v_2 are components of the state vector $\boldsymbol{v}$. We choose our observable as an arbitrary but known linear combination of the state:

$$\boldsymbol{\psi}[\boldsymbol{v}] := \tilde{\mathbf{C}}\boldsymbol{v}, \qquad \tilde{\mathbf{C}} \in \mathbb{C}^{1\times 2}.$$

Panel (d) of Figure 6.1 exhibits a step like behavior that is observed consistently when a minimum number of delays are taken. The jump in relative distance to DFT occurs between Companion-orders 10 and 11. Hence, the state observables *may* lie in a Koopman invariant subspace of dimension 10 or 11. Unfortunately, we cannot use Corollary 4.7 to turn this speculation into a guarantee.

We close this discussion with the lid-driven cavity over a range of Reynolds numbers (Re). As Re increases, the flow transitions from periodic to chaotic, passing through quasi-periodic and mixed behaviour [3]. Our observable is an arbitrarily chosen linear functional of an associated stream-function. The underlying Koopman invariant subspace and the corresponding $\tilde{\mathbf{C}}$ are unknown. As with the Van der Pol

oscillator, DMD-DFT transition, depicted in Figure 6.2, sheds some light on the size of the Koopman invariant subspace.

The qualitative change in dynamics over the range of Re considered is reflected in the relationship between relative distance to DFT and Companion-order. As the Reynolds number increases, we see that the step-like trend has its jump smeared out over a wider range of Companion-orders. The plateau begins at larger values of Companion-order before disappearing altogether. Hence, we *may* have a Koopman invariant subspace containing our observable in the first three cases. However, for $Re = 30,000$, we can go further and certify that our observable does not lie in a Koopman invariant subspace of dimension less than 25.

To get this guarantee, we first assume that there is a Koopman invariant subspace of maximal dimension $r_{\max} = 24$. The concomitant requirement of at least 23 delays is met by the study corresponding to the dark blue boxes in panel (d) of Figure 6.2. Hence, by Corollary 4.7, we would expect it to spike at least for a Companion-order of 25. In contrast to studies with a lower number of time delays, the trend shown by the dark blue boxes lacks a jump. Hence, the underlying Koopman invariant subspace cannot have a dimension less than 25.

Therefore, Corollary 4.7 can provide a data-driven lower bound on the dimension of the Koopman invariant subspace containing the observables $\boldsymbol{\psi}$. This is accomplished by taking a minimum number of time delays and looking for *discrepancies* with its predictions. Alas, one cannot use the confirmation of the same predictions to certify the existence of a finite dimensional Koopman invariant subspace.

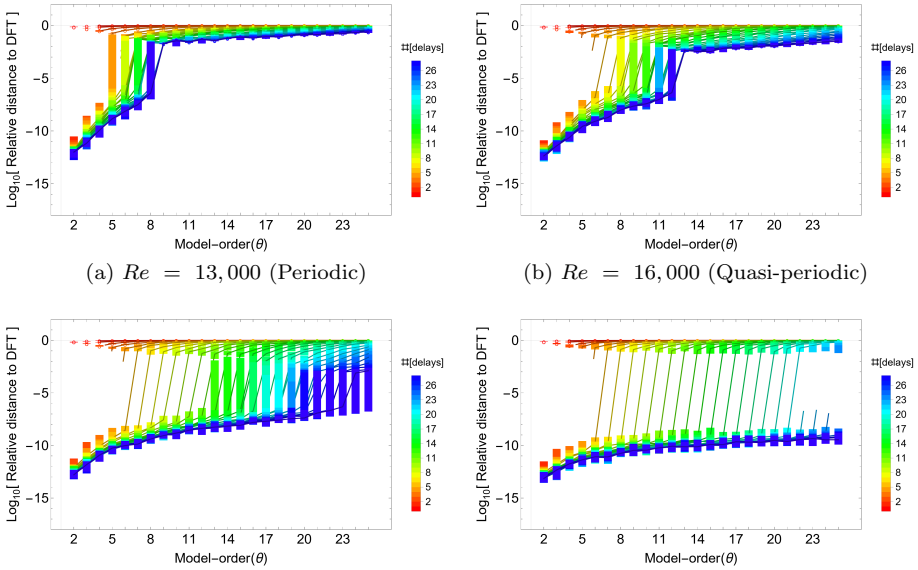
6.2. Pruning DMD eigen-values with the mode norm. Corollaries 5.7 and 5.11 justify using the DMD mode norm to recognize the Koopman eigen-values contained in the DMD spectrum. They provide conditions under which this pruning method identifies the Koopman spectrum from the DMD eigen-values. In both corollaries, successful identification is encoded by a set equality of the following format:

$$\sigma_{\text{nontriv}}(\tilde{\mathbf{Z}}, \mathbf{c}) = B. \tag{6.4}$$

Here, $\tilde{\mathbf{Z}}$ represents the data matrix derived from $\mathbf{Z}$ by taking some combination of time delays and mean subtraction, $\mathbf{c}$ denotes the appropriate DMD optimum and B is the target set derived from $\sigma(\mathbf{\Lambda})$. By equation (5.2), the term on the left is the set of all eigen-values of $\mathbf{T}[\mathbf{c}]$ whose corresponding DMD modes have non-zero norm. The quantity on the right (B) is the Koopman spectrum, $\sigma(\mathbf{\Lambda})$, for Corollary 5.7 and a minor modification of the same for Corollary 5.11.

The set equality discussed above can be numerically characterized using a quantity termed **KMD-Quality**. It is a real-valued function of $\tilde{\mathbf{Z}}, \mathbf{c}$ and B that takes values between 0 (disastrous) and 1 (perfection). The precise mathematical definition is complicated, and can be found in Appendix E. Nonetheless, it is possible to perform quantitative inference using only its two properties detailed below:

1. Spectral containment: KMD-Quality quantifies the perturbation required to make B a subset of the often larger set $\sigma(\mathbf{T}[\mathbf{c}])$. It provides an upper bound $(-\log_{10}[\text{KMD-Quality}])$ on the radius of the smallest disc that must be drawn about every element of $\sigma(\mathbf{T}[\mathbf{c}])$ to subsume B. In other words, the closed $(-\log_{10}[\text{KMD-Quality}])$-neighbourhood of $\sigma(\mathbf{T}[\mathbf{c}])$ contains the set B. For example, if KMD-Quality $= 0.1$, then B is contained within the set formed by the union of discs centered on each element of $\sigma(\mathbf{T}[\mathbf{c}])$ and of radius 1. On the other hand, KMD-Quality $= 0.8 \approx 10^{-0.1}$ means that every member of the target B is within a distance of 0.1 from the spectrum of $\mathbf{T}[\mathbf{c}]$. In the



(a) $Re = 13,000$ (Periodic) (b) $Re = 16,000$ (Quasi-periodic)

(c) $Re = 20,000$ (Mixed) (d) $Re = 30,000$ (Chaotic)

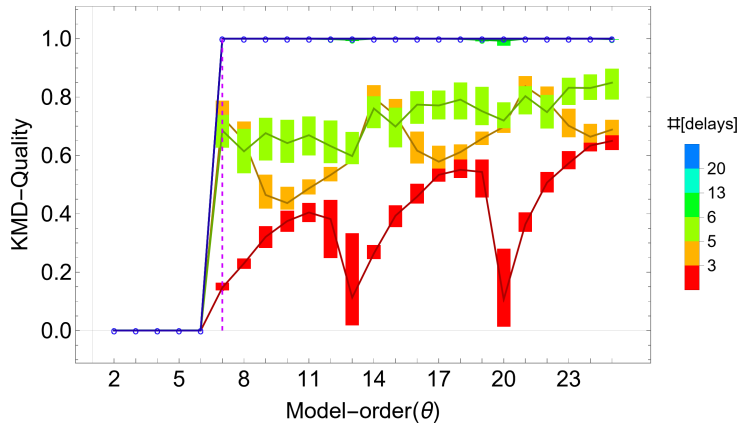
FIG. 6.2. *Box plots of the relative distance to DFT reflect the increasing complexity of the cavity flow and thus delineate qualitatively different flow regimes. The first three display jumps that are eventually robust to the number of delays (although the robustness wears down with increasing Re). According to Corollary 4.7, such a trend* may *be the result of observing finite-dimensional Koopman invariant subspaces of increasing dimension. The final plot is conspicuous in its lack of a discontinuity. By Corollary 4.7, we infer that the dimension of the underlying Koopman invariant subspace is at least 25. This observation agrees with the fact that the Koopman operator does not possess any eigen-functions when the underlying dynamics is chaotic.*

context of Corollaries 5.7 and 5.11, the latter is a more favorable situation because every member of the target set B (Koopman spectrum) has a better approximant in $\sigma(\mathbf{T}[\mathbf{c}])$ (DMD spectrum).

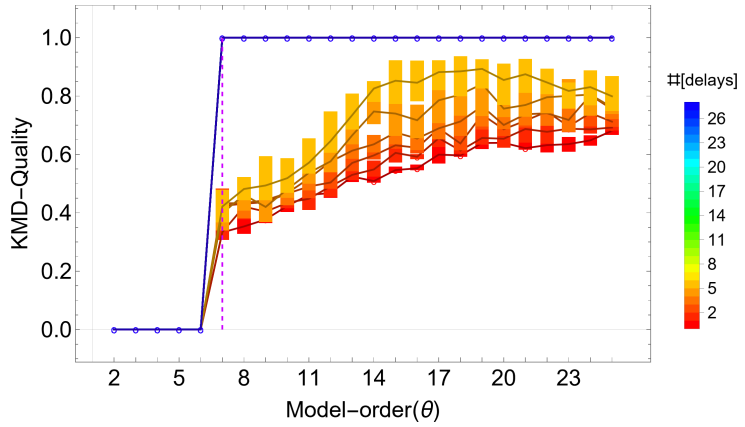
2. Index of non-triviality: KMD-Quality is a lower bound on the fractional contribution of the modes corresponding to B, to the square Frobenius norm of the DMD mode matrix. When B accounts for all the "non-zero" DMD modes, KMD-Quality touches 1. However, if B misses out on a mode of significance (read high norm), KMD-Quality plummets.

To summarize, KMD-Quality scores the numerical validity of equation (6.4) with a number between 0 (False) and 1 (True). Hence, a value close to 1 means that the predictions of Corollaries 5.7 and 5.11 are in agreement with the numerical study.

We test Corollary 5.7 and Corollary 5.11 in subsection 6.2.1 and subsection 6.2.2 respectively. Testing these mode-extraction theorems requires that the Koopman eigen-values be known beforehand. So, we restrict our study to the LTI systems described in equation (6.3) and Table 6.2. In addition, we exclude LTI_3 due to numerical issues and only use LTI_{1a} and LTI_{1b} as test-beds. We conclude our study of mode-norm based pruning with a brief investigation, in subsection 6.2.3, on the validity of Corollary 5.7 when data is contaminated with sensor noise.



(a) LTI_{1a}



(b) LTI_{1b}

FIG. 6.3. *We test the claim of Corollary 5.7 that DMD eigen-values with non-zero mode norm comprise the Koopman spectrum. The test systems (see figure captions) are linear time-invariant and the observable is just a linear combination of the state (see equation (6.3)). The quantity on the Y-axis, "KMD-Quality", takes on a value of 1 if and only if the above claim holds true. The inputs used to compute this indicator are listed in (6.5). In both the figures above, we see that KMD-Quality is 1 when at least 6 time delays are taken, and* $\theta \geq 7$. *This is in perfect agreement with the predictions of Corollary 5.7.*

6.2.1. DMD on data without mean-removal. In testing Corollary 5.7, for every choice of (θ, d), we compute KMD-Quality using the inputs:

$$\tilde{\mathbf{Z}} = (\mathbf{Z})_{\text{d-delayed}},\ B = \sigma(\mathbf{\Lambda}) \text{ and } \mathbf{c} = \mathbf{c}^* \left[(\mathbf{Z})_{\text{d-delayed}}\right]. \tag{6.5}$$

The system LTI_{1a} is studied for θ in the range 2 to 25, using time delays: 0, 3, 6, 13, 20 & 27. The first panel in Figure 6.3 shows the validity of Corollary 5.7 for this example. Recall from equation (6.3) that the observable deployed here is a linear combination of the 7-dimensional state with all coefficients non-zero. The scalar nature of the observable means that 6 time delays are *necessary* and sufficient to attain Koopman invariance. The scalar observable deployed here requires at least 6 time delays before Koopman invariance is attained. Deploying time delays less than 6 wrecks identification, even with a model whose capacity (read θ) is far greater than

the minimum requirement of 7. Even so, it is worth noting that this set of models, pertaining to time delays 0, 3 and 5, shows a promising positive trend on increasing the model order. Once the minimum number of delays and model order is met, mode norm can extract the Koopman spectrum reliably, as seen by the KMD-Quality plateauing at 1 with non-existent IQRs.

We test LTI_{1b} over the same set of Companion-orders, but for a larger set of time-delays ranging from 0 to 28. Corollary 5.7 suggests at least 6 time delays and a minimum Companion-order of 7 for generalizability. This prediction is numerically attested in panel (b) of Figure 6.3, by KMD-Quality levelling out at a value of 1 in the suggested parameter regime.

We close this section by testing Corollary 5.7 on all three LTI systems, when the number of time delays is *much larger* than the minimum requirement. In theory, all three plots must align for $\theta \geq 7$ and $\#[\text{delays}] \geq 6$ However, Figure 6.4 shows that the KMD-Quality plateau for LTI_3 recedes when we take delays more than 26, and appears to settle down around 0.6. An explanation for this fall is that the contribution of the three stable eigen-values diminishes for large delays, and is eventually truncated when we perform SVD with a fixed relative tolerance. The common thread of singular value truncation makes it unlikely that Exact or SVD-enhanced versions of DMD will surmount this shortcoming.

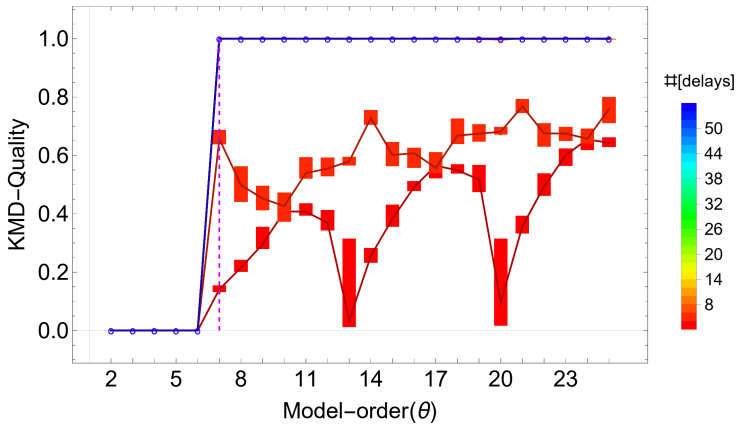
6.2.2. DMD on mean-removed data. Testing Corollary 5.11 is more involved than Corollary 5.7 for two reasons. Firstly, the target set can take two different values depending on the success or failure of mean removal. Secondly, the pertinent efficacy of mean removal, as defined in Definition 5.8, does not always possess an explicit dependence on the choice of model order (θ) and number of time delays (d).

We tackle the first intricacy by computing KMD-Quality for each of the two possibilities of B i.e. $\sigma(\mathbf{\Lambda}) \cap \{1\}^C$ and $\sigma(\mathbf{\Lambda}) \cup \{1\}$, at every choice of θ and d. The second complication is resolved by using Koopman invariant observables as they permit the use of Theorems 5.9 and 5.10 to predict the outcome of mean removal solely from the choice of model order and $\#[\text{delays}]$. For this reason, the matrices $\tilde{\mathbf{C}}$ differ from those deployed in any of the other sections in that they now possess full column rank as opposed to being rank-defective row vectors elsewhere.

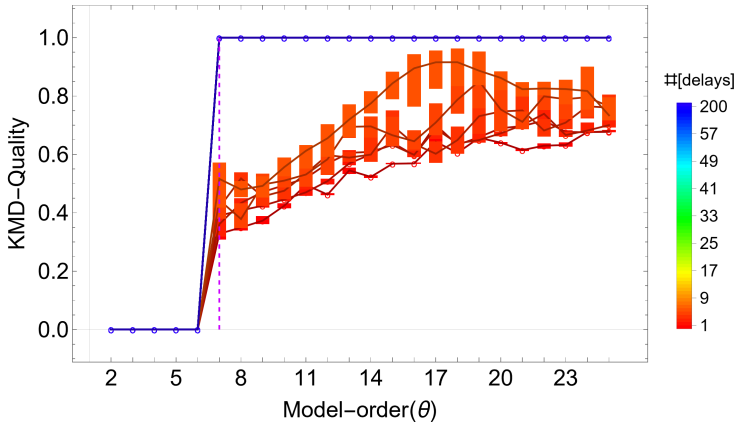
In LTI_{1a}, mean-subtraction succeeds if and only if θ_{ms} is a multiple of 7. To understand this, we first note that the Koopman spectrum comprises of all the 7-th roots of unity. As described in the preceding paragraph, we use Koopman invariant observables while testing Corollary 5.11. Therefore, by Theorem 5.9, mean subtraction will succeed if and only if the trajectory length is a multiple of 7. According to (6.1), the choice of d time-delays and a Companion-order of θ_{ms} (which is the same as θ by equation (5.5)) corresponds to a trajectory of length $\theta_{\text{ms}} + d + 1$. As such, for any given Companion-order (θ_{ms}), it is possible to take an appropriate number of time delays (d) so that $\theta_{\text{ms}} + d + 1$ is a multiple of 7 and, thereby, ensure that mean subtraction succeeds. By choosing time delays $6, 13, 20$ and 27, we ensure that mean subtraction only works when θ_{ms} is a multiple of 7 i.e. $7, 14, 21$ and 28.

We can now solidify our expectations for the tests concerning Corollary 5.11. If at least 6 delays are taken and $\theta_{\text{ms}} \geq 7$, the set of DMD eigen-values with non-zero DMD modes will be $\sigma(\Lambda) \cap \{1\}^C$ when θ_{ms} is a multiple of 7 and $\sigma(\Lambda) \cup \{1\}$ otherwise. We check this set equality by computing KMD-Quality for the two possible target sets separately with the following common inputs:

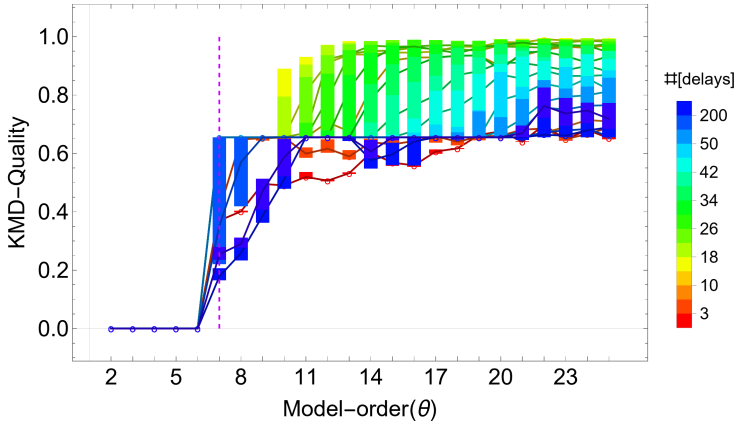
$$\tilde{\mathbf{Z}} \;=\; (\mathbf{Z}_{\text{ms}})_{\text{d-delayed}} \text{ and } \mathbf{c} \;=\; \mathbf{c}^* \left[(\mathbf{Z}_{\text{ms}})_{\text{d-delayed}}\right]. \tag{6.6}$$



(a) LTI_{1a}

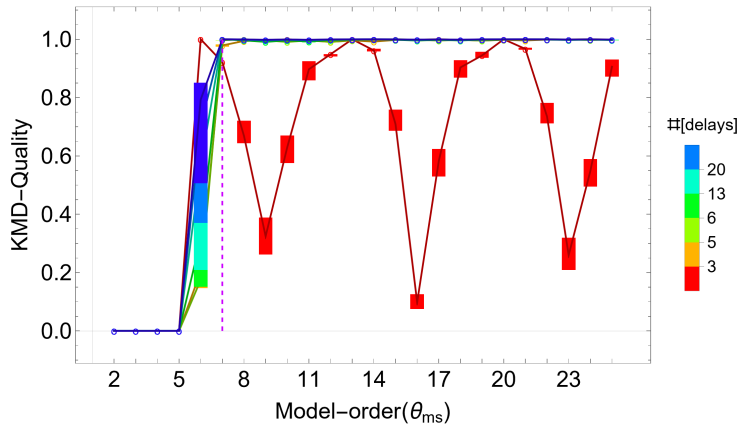


(b) LTI_{1b}

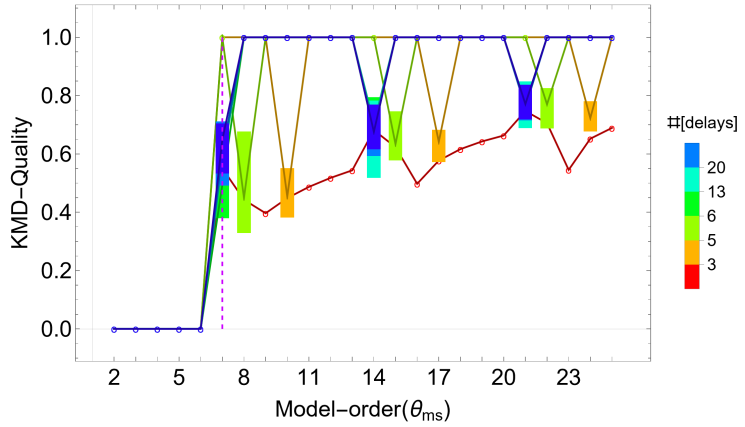


(c) LTI_3

FIG. 6.4. *We test the claim of Corollary 5.7 once more, using time delays that greatly exceed the minimum theoretical requirement (7 here). This should be harmless in theory and the numerical evidence concurs for the unitary systems LTI_{1a} and LTI_{1b}. However, LTI_3 has eigen-values within the unit disc whose contribution becomes insignificant when dealing with a large number of time delays. Thus, plateau of KMD-Quality seen in the first two systems is smoothed out in sub-figure(c). For larger time delays, especially beyond 26, the jump is spread over a growing range of model-orders and the plateau at 1 disappears.*



(a) $B = \sigma(\mathbf{\Lambda}) \cap \{1\}^C$

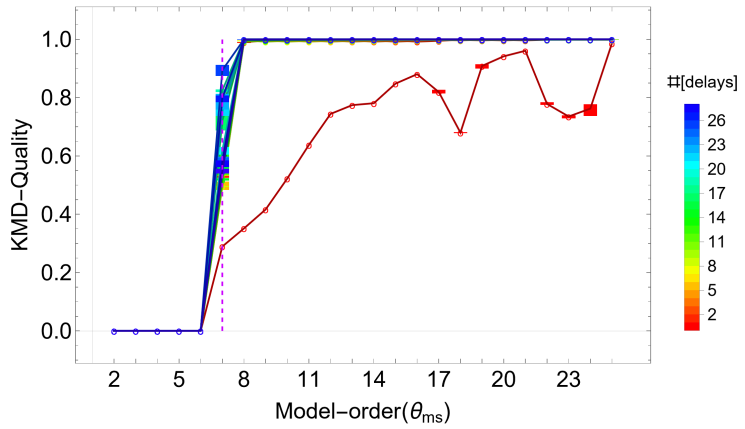


(b) $B = \sigma(\mathbf{\Lambda}) \cup \{1\}$

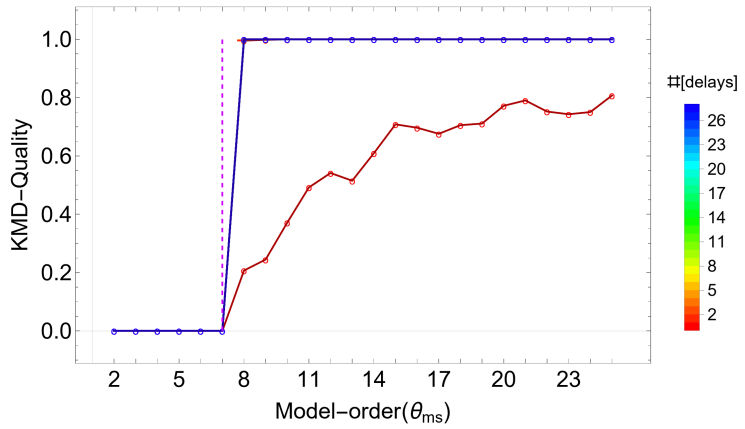
FIG. 6.5. *Identifying the Koopman eigen-values ($\sigma(\mathbf{\Lambda})$) of LTI_{1a} from mean removed data: We plot KMD-Quality along the Y-axis with common parameters listed in (6.6) and the target set B as specified above. KMD-Quality of 1 means that the set of all DMD eigen-values with non-zero DMD modes is the same as the target set B - the outcome that is considered successful identification. Corollary 5.11 predicts the trend of KMD-Quality when at-least 6 time delays are used and $\theta_{\text{ms}} \geq 7$. It says that KMD-Quality must be 1 if and only if θ_{ms} is a multiple of 7 in sub-figure (a). Sub-figure (b) is expected to display a complementary trend in that KMD-Quality must be 1 if and only if the model order is not a multiple of 7. While these predictions are true for panel (b), we see in panel (a) that KMD-Quality seem to be 1 even when θ_{ms} is not a multiple of 7. We reconcile this disagreement as follows: Although Corollary 5.11 predicts that KMD-Quality will not be 1 when θ_{ms} is not a multiple of 7, it doesn't preclude KMD-Quality from being arbitrarily close 1.*

In sub-figure (a) of Figure 6.5, the target set is $B = \sigma(\mathbf{\Lambda}) \cap \{1\}^C$. Therefore, Corollary 5.11 predicts that KMD-Quality will take on a value of 1 only for $\theta_{\text{ms}} = 7, 14, 21$ and 28. Similarly, in sub-figure (b), the target is $B = \sigma(\mathbf{\Lambda}) \cup \{1\}$. So, KMD-Quality is expected to be 1 only when $\theta_{\text{ms}} \geq 7$ and is not a multiple of 7.

While the predictions are spot on for sub-figure (b), they appear to have gone awry in sub-figure (a) where we find a plateau of KMD-Quality at 1, instead of peaks at $\theta_{\text{ms}} = 7, 14, 21$ and 28. A similar phenomenon is observed with LTI_{1b} (see sub-figure (a) of Figure 6.6) and, in the corresponding discussion, we attribute it to the *numerical success* of mean subtraction.



(a) Target $= \sigma(\mathbf{\Lambda}) \cap \{1\}^C$



(b) Target $= \sigma(\mathbf{\Lambda}) \cup \{1\}$

FIG. 6.6. *Identifying the Koopman eigen-values* ($\sigma(\mathbf{\Lambda})$) *of* LTI_{1b} *from mean removed data: Recall that KMD-Quality of 1 indicates successful identification of the target set, while lower values denote the contrary. In sub-figure (b), Corollary 5.11 guarantees that if at least 7 time delays are taken, KMD-Quality will level out at 1 beginning with a Companion-order of 8. From the second panel, we see that this prediction holds true. In sub-figure (a), it is expected that the plateau of KMD-Quality will not reach the maximal value of 1 due to an incomplete target set. However, as with* LTI_{1a}*, KMD-Quality effectively maxes out at 1 for panel (a) too. This apparent disagreement is a consequence of the fragility of the prediction "KMD-Quality* $\neq$ *1", in that such a statement doesn't prevent KMD-Quality from being very close to 1.*

LTI_{1b} is relatively uncomplicated since mean subtraction has a low probability of success in this scenario. Its eigen-values are chosen as 7 random points on the unit circle. Since it is unlikely for 7 randomly chosen points on the unit circle to be roots of unity for some common power (bounded by the maximal θ considered), we conclude from Theorem 5.10 that mean subtraction fails with high probability.

Since 1 is not a Koopman eigenvalue, Corollary 5.11 recommends at least 7 time delays and a minimum Companion-order of 8. This is supposed to produce pruned DMD eigen-values corresponding to $\sigma(\mathbf{\Lambda}) \cup \{1\}$. Hence, one would expect a KMD-Quality of 1 over the recommended regime in panel (b) of Figure 6.6, but not panel (a) whose target set omits $\lambda = 1$. We see that sub-figure (b) confirms the predictions

of Corollary 5.11 with a step-like behaviour once the minimal number of delays is met. Surprisingly, the plateau is replicated in sub-figure (a), even though the target set incorrectly excludes $\lambda = 1$.

This apparent disparity between theory and simulation in sub-figure (a) of Figures 6.5 and 6.6 can be reconciled by considering the fragility of the statement "KMD-Quality $\neq 1$". Since KMD-Quality can take any value in the interval $[0, 1]$, it can be arbitrarily close to unity without actually being 1. It so happens that the deviation from 1 is large enough to be visible in sub-figure (b) of Figure 6.5 in contrast to sub-figure (a) above it where the difference from unity simply manifests as a thicker line at 1.

We now attempt to rationalize the significantly smaller deviations from unity in sub-figure (a) of Figures 6.5 and 6.6. We first note note that the DMD spectrum contains $\sigma(\mathbf{\Lambda}) \cup \{1\}$ because KMD-Quality maxes out at 1 for panel (b) of both figures. By using the precise definition of this numerical indicator in (E.1), we find that KMD-Quality simplifies to be the ratio of the sum of squared target DMD mode norms to the total sum of squared DMD mode norms. Since this ratio is close to unity even when 1 is excluded from the target, it must be that the DMD mode corresponding to 1 has a small norm. By the definition of $\mathbf{C}_{\text{ms}}$ in (B.5), we can then infer that $\|\mathbf{c}_1 - \boldsymbol{\mu}\|$ ($\|\boldsymbol{\mu}\|$) is minuscule when $1 \in \sigma(\mathbf{\Lambda})$[13] ($1 \notin \sigma(\mathbf{\Lambda})$). The former situation corresponds to LTI_{1a} while LTI_{1b} is likely to fall in the latter owing to the stochastic provenance of its Koopman eigen-values.

Hence, mean subtraction appears to *numerically succeed* in removing the stationary mode from the time series $\mathbf{Z}$, despite theoretical results to the contrary (Theorems 5.9 and 5.10). We believe that neutral stability is crucial for this observation as it permits the sum $\mathbf{gp}_{n+1}[\lambda]^T \mathbf{1}_{n+1}$ to be bounded. Since the mean involves dividing this sum by $n + 1$, its magnitude diminishes for large values of n.

6.2.3. Mode-norm based filtering under output noise. We briefly investigate the efficacy of extracting Koopman eigen-values as described in Corollary 5.7, when the observations are contaminated with sensor noise. Consider the matrix $\mathbf{N} \in \mathbb{C}^{m \times (n+1)}$ whose columns are independent samples drawn from the same probability distribution. Suppose it corrupts our time series $\mathbf{Z}$ as follows:

$$\mathbf{Z}_{\text{noisy}} = \mathbf{Z} + \mathbf{N}.$$

The objective here is to extract the Koopman eigen-values $\sigma(\mathbf{\Lambda})$ when we are given $\mathbf{Z}_{\text{noisy}}$ instead of $\mathbf{Z}$.

Our approach is to filter out the noise and use the de-noised time series to perform Companion DMD. To this end, we adapt pre-processing strategies that have been developed in the setting of Exact DMD, to the companion matrix formulation. Although there are many places to draw from (see Section 3.1.2 in [8] and references therein), we focus on two approaches that jive with the theme of taking time delays.

1. Total-least squares (TLS) DMD: A DMD variant that accounts for error in both inputs and outputs, unlike the classical formulation that neglects input distortions [12]. The TLS version of Companion DMD, developed in accordance with the approach outlined in section 2.3 of [12], amounts to using a low-rank approximation (via the SVD) of $\mathbf{Z}_{\text{noisy}}$ as an estimate of $\mathbf{Z}$ in (3.6).
2. Noise-resistant DMD: A more recent work [34] with links to the stochastic Koopman operator. Its companion matrix version involves pre-multiplying

[13] $\mathbf{c}_1$ is the Koopman mode with eigenvalue 1.

$(\mathbf{Z}_{\text{noisy}})_{\text{d}-\text{delayed}}$ with a delayed matrix $\frac{1}{d+1} * (\mathbf{Z}_{\text{filter}})_{\text{d}-\text{delayed}}$. The columns of $\mathbf{Z}_{\text{filter}}$ are sequential observations along the same trajectory, that have no temporal overlaps with $\mathbf{Z}_{\text{noisy}}$ to ensure that the i.i.d. noise is averaged out during matrix multiplication.

Once again, our test cases are the unitary LTI systems, LTI_{1a} & LTI_{1b}. Sensor noise is drawn from the uniform distribution of 0 mean and standard deviation 5 (25) for LTI_{1a} (LTI_{1b}). We fix the rank of the approximant in TLS Companion DMD to be 7, the number of unique Koopman modes in $\mathbf{Z}$. The number of columns in $(\mathbf{Z}_{\text{filter}})_{\text{d}-\text{delayed}}$ is kept 14 to ensure linear consistency of the filtered data $\frac{1}{d+1} * ((\mathbf{Z}_{\text{filter}})_{\text{d}-\text{delayed}})^H (\mathbf{Z}_{\text{noisy}})_{\text{d}-\text{delayed}}$.

In Figure 6.7, TLS and noise-resistant Companion DMD exhibit step-like trends after sufficient time delays, thereby demonstrating their de-noising capabilities. The minimum number of time delays depends on the algorithm, but is always greater than the lower bound of $r - 1$ for the noiseless scenario. The performance in LTI_{1b} is more informative regarding the spread of KMD-Quality. It suggests that the fluctuations of KMD-Quality across different trajectories may be reduced by increasing the Companion-order along with time delays. Curiously, the same strategy helps Companion DMD on noisy data (Noisy Companion) perform reasonably well. This suggests that time delays somehow mute the adverse effects of noise.

7. Conclusions and Future Work. The relationship between mean subtracted DMD and temporal DFT has been clarified in the setting of finite dimensional Koopman invariant subspaces. When the observables drawn from such a subspace are themselves invariant under the action of the Koopman operator, non-equivalence is tantamount to data sufficiency. Taking as many time delays as the number of distinct Koopman modes suffices to attain the required invariance. Therefore, DMD-DFT equivalence vanishes when data is plentiful, and time-delayed. The contrapositive provides an ironic interlude to this venture: What was viewed a potential rot could actually be an indicator of sampling requirements.

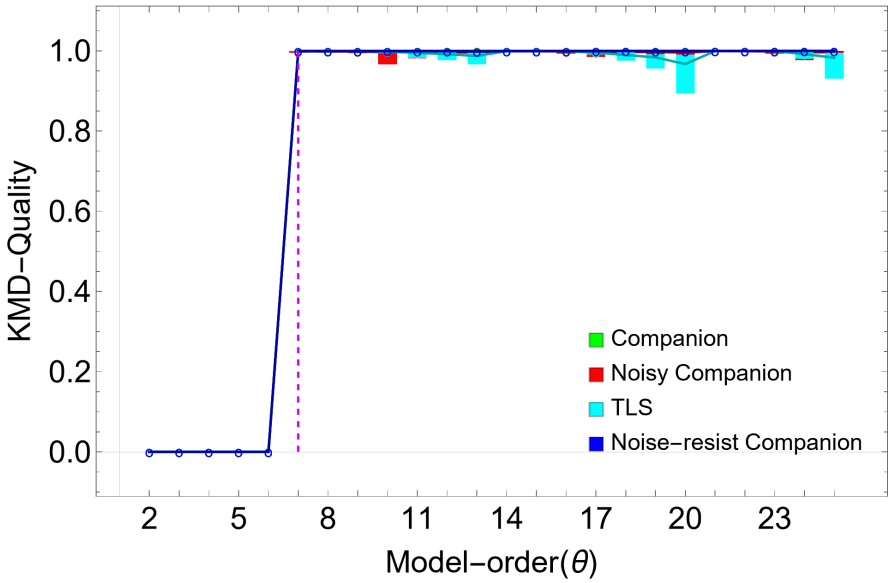
In the same setting, the practice of filtering DMD eigen-values based on the norm of the corresponding DMD modes has been rigorously justified. When data is linearly consistent and the DMD regression is well-posed, the DMD eigen-values thus pruned comprise the Koopman spectrum. A similar result holds under mean-subtraction, if a few time delays are taken before performing DMD.

Many aspects of this work are open for study. The departure from DMD-DFT equivalence appears to happen as two jumps with increasing time delays. The theory developed in this work predicts the first jump. Understanding the second jump and the robustness of the overall transition to noise will improve the reliability of DMD-DFT equivalence in inferring system order.

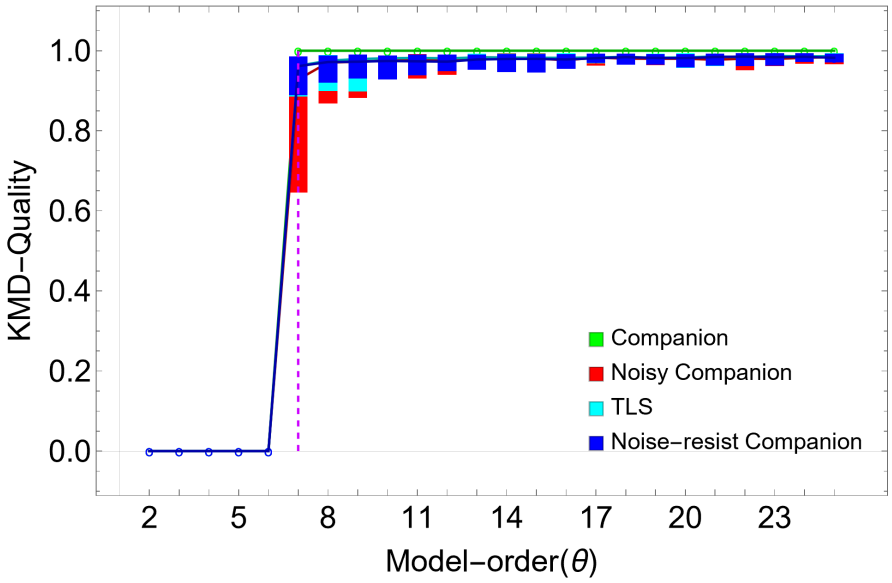
On a different note, transient dynamics seem to be lost when we take one too many time delays. This signals a need for devising algorithms that are sensitive to the senescence of off-attractor behaviour. Along the same vein, it would be useful to establish upper bounds on the number of time delays that can be safely taken, in relation to the underlying Koopman spectrum.

Acknowledgments. This work was supported by the Army Research Office (ARO-MURI W911NF-17-1-030) and the National Science Foundation (Grant no. 1935327).

REFERENCES



(a) LTI_{1a}: 200 delays, $\sigma = 5$



(b) LTI_{1b}: 20 delays, $\sigma = 25$

FIG. 6.7. *Contrasting the performance of different pre-processing strategies designed to combat the effect of sensor noise in Companion DMD: Noisy Companion (DMD on noisy data that has been time-delayed) performs fairly well when the model capacity (θ) exceeds the system order (7). TLS and noise-resistant versions of Companion DMD show KMD-Quality converging faster to 1, with lesser uncertainty. Hence, they possess superior de-noising capabilities in comparison to Noisy Companion. For $\theta \geq 7$, the KMD-Quality for all three algorithms doesn't quite reach 1 and has a non-zero spread. Both of these shortcomings can be brought down by taking more time delays.*

[1] H. Arbabi and I. Mezic, *Ergodic theory, dynamic mode decomposition, and computation of spectral properties of the koopman operator*, SIAM Journal on Applied Dynamical Systems, 16 (2017), pp. 2096–2126.
[2] H. Arbabi and I. Mezić, *Study of dynamics in post-transient flows using koopman mode decomposition*, Physical Review Fluids, 2 (2017), p. 124402.
[3] H. Arbabi and I. Mezic, *Spectral analysis of mixing in 2d high-reynolds flows*, arXiv preprint arXiv:1903.10044, (2019).
[4] A. Avila and I. Mezić, *Data-driven analysis and forecasting of highway traffic dynamics*, Nature communications, 11 (2020), pp. 1–16.
[5] M. D. Bohon, A. Orchini, R. Bluemner, C. O. Paschereit, and E. J. Gutmark, *Dynamic mode decomposition analysis of rotating detonation waves*, Shock Waves, (2020), pp. 1–13.
[6] B. W. Brunton, L. A. Johnson, J. G. Ojemann, and J. N. Kutz, *Extracting spatial–temporal coherent patterns in large-scale neural recordings using dynamic mode decomposition*, Journal of neuroscience methods, 258 (2016), pp. 1–15.
[7] S. L. Brunton, B. W. Brunton, J. L. Proctor, E. Kaiser, and J. N. Kutz, *Chaos as an intermittently forced linear system*, Nature communications, 8 (2017), pp. 1–9.
[8] S. L. Brunton, M. Budišić, E. Kaiser, and J. N. Kutz, *Modern koopman theory for dynamical systems*, arXiv preprint arXiv:2102.12086, (2021).
[9] K. K. Chen, J. H. Tu, and C. W. Rowley, *Variants of dynamic mode decomposition: Boundary condition, koopman, and fourier analyses*, Journal of Nonlinear Science, 22 (2012), pp. 887–915.
[10] Z. Drmac, I. Mezic, and R. Mohr, *Data driven koopman spectral analysis in vandermonde–cauchy form via the dft: Numerical method and theoretical insights*, SIAM Journal on Scientific Computing, 41 (2019), pp. A3118–A3151.
[11] D. A. Haggerty, M. J. Banks, P. C. Curtis, I. Mezić, and E. W. Hawkes, *Modeling, reduction, and control of a helically actuated inertial soft robotic arm via the koopman operator*, arXiv preprint arXiv:2011.07939, (2020).
[12] M. S. Hemati, C. W. Rowley, E. A. Deem, and L. N. Cattafesta, *De-biasing the dynamic mode decomposition for applied koopman spectral analysis of noisy datasets*, Theoretical and Computational Fluid Dynamics, 31 (2017), pp. 349–368.
[13] J. P. Hespanha, *Linear systems theory*, Princeton university press, 2018.
[14] S. M. Hirsh, K. D. Harris, J. N. Kutz, and B. W. Brunton, *Centering data improves the dynamic mode decomposition*, SIAM Journal on Applied Dynamical Systems, 19 (2020), pp. 1920–1955.
[15] M. A. Hitz and E. Kaltofen, *Efficient algorithms for computing the nearest polynomial with constrained roots*, in Proceedings of the 1998 international symposium on Symbolic and algebraic computation, 1998, pp. 236–243.
[16] R. A. Horn and C. R. Johnson, *Matrix analysis*, Cambridge university press, 2012.
[17] B. O. Koopman, *Hamiltonian systems and transformation in hilbert space*, Proceedings of the National Academy of Sciences of the United States of America, 17 (1931), p. 315.
[18] M. Korda and I. Mezić, *On convergence of extended dynamic mode decomposition to the koopman operator*, Journal of Nonlinear Science, 28 (2018), pp. 687–710.
[19] J. N. Kutz, S. L. Brunton, B. W. Brunton, and J. L. Proctor, *Dynamic mode decomposition: data-driven modeling of complex systems*, SIAM, 2016.
[20] S. Le Clainche and J. M. Vega, *Higher order dynamic mode decomposition*, SIAM Journal on Applied Dynamical Systems, 16 (2017), pp. 882–925.
[21] S. B. Leask and V. G. McDonell, *On the physical interpretation of proper orthogonal decomposition and dynamic mode decomposition for liquid injection*, arXiv preprint arXiv:1909.07576, (2019).
[22] I. Mezić, *Spectral properties of dynamical systems, model reduction and decompositions*, Nonlinear Dynamics, 41 (2005), pp. 309–325.
[23] I. Mezic, *On numerical approximations of the koopman operator*, arXiv preprint arXiv:2009.05883, (2020).
[24] I. Mezić and A. Banaszuk, *Comparison of systems with complex behavior*, Physica D: Nonlinear Phenomena, 197 (2004), pp. 101–133.
[25] S. E. Otto and C. W. Rowley, *Koopman operators for estimation and control of dynamical systems*, Annual Review of Control, Robotics, and Autonomous Systems, 4 (2021), pp. 59–87.
[26] S. Pan and K. Duraisamy, *On the structure of time-delay embedding in linear models of non-linear dynamical systems*, Chaos: An Interdisciplinary Journal of Nonlinear Science, 30 (2020), p. 073135.
[27] J. L. Proctor and P. A. Eckhoff, *Discovering dynamic patterns from infectious disease*

data using dynamic mode decomposition, International health, 7 (2015), pp. 139–145.
[28] C. W. Rowley, I. Mezić, S. Bagheri, P. Schlatter, and D. S. Henningson, *Spectral analysis of nonlinear flows*, Journal of Fluid Mechanics, 641 (2009), pp. 115–127.
[29] S. Sarmast, R. Dadfar, R. F. Mikkelsen, P. Schlatter, S. Ivanell, J. N. Sørensen, and D. S. Henningson, *Mutual inductance instability of the tip vortices behind a wind turbine*, Journal of Fluid Mechanics, 755 (2014), pp. 705–731.
[30] P. J. Schmid, *Dynamic mode decomposition of numerical and experimental data*, Journal of Fluid Mechanics, 656 (2010), pp. 5–28.
[31] P. J. Schmid, *Dynamic mode decomposition and its variants*, Annual Review of Fluid Mechanics, 54 (2022), pp. 225–254.
[32] A. Towne, O. T. Schmidt, and T. Colonius, *Spectral proper orthogonal decomposition and its relationship to dynamic mode decomposition and resolvent analysis*, Journal of Fluid Mechanics, 847 (2018), pp. 821–867.
[33] J. H. Tu, C. W. Rowley, D. M. Luchtenburg, S. L. Brunton, and J. N. Kutz, *On dynamic mode decomposition: Theory and applications*, arXiv preprint arXiv:1312.0041, (2013).
[34] M. T. Wanner, *Robust Approximation of the Stochastic Koopman Operator*, University of California, Santa Barbara, 2020.
[35] M. O. Williams, I. G. Kevrekidis, and C. W. Rowley, *A data–driven approximation of the koopman operator: Extending dynamic mode decomposition*, Journal of Nonlinear Science, 25 (2015), pp. 1307–1346.

Appendix A. Examining finite dimensional Koopman invariant subspaces.

A.1. Compact representation of Koopman mode expansion. Suppose the matrix $\mathbf{Z}$ is generated by observables that lie in a finite dimensional Koopman invariant subspace (3.15). Then, its row space is contained in the row space of the Vandermonde matrix whose nodes are the Koopman eigen-values.

We begin with the definition of $\mathbf{Z}$ in (3.5), making special note of the temporal ordering of its columns.

$$\mathbf{z}_{j+1} \;=\; \boldsymbol{\psi}(\boldsymbol{v}_{j+1}) \;=\; \boldsymbol{\psi}(\Gamma^j(\boldsymbol{v}_1)).$$

Using (3.15), if we write $\boldsymbol{\psi}$ in terms of the eigenfunctions $\boldsymbol{\phi}$, the Koopman operator can be used to replace the potentially nonlinear Γ^j with a matrix multiplication.

$$\mathbf{z}_{j+1} \;=\; \tilde{\mathbf{C}}\boldsymbol{\phi}(\Gamma^j(\boldsymbol{v}_1)) \;=\; \tilde{\mathbf{C}}U^j\boldsymbol{\phi}(\boldsymbol{v}_1) \;=\; \tilde{\mathbf{C}}\boldsymbol{\Lambda}^j\boldsymbol{\phi}(\boldsymbol{v}_1).$$

Using (3.16), we may replace $\tilde{\mathbf{C}}$ with $\mathbf{C}$.

$$\mathbf{z}_{j+1} \;=\; \mathbf{C}[\lambda_i^j]_{i=1}^r.$$

Compiling this expression for all columns of $\mathbf{Z}$, we obtain:

$$\mathbf{Z} \;=\; \mathbf{C}\boldsymbol{\Theta}.$$

A.2. Rank conditions for Vandermonde matrices. Vandermonde matrices $\boldsymbol{\Theta}$, $\boldsymbol{\Theta}_{\text{ms}}$ and their sub-matrices are ubiquitous in the forthcoming analysis. An important property of square Vandermonde matrices is that they are invertible if and only if their nodes are distinct [16]. This result forms the basis for two rank conditions that will be heavily used in the sequel.

1. A Vandermonde matrix has linearly independent rows if and only if it has at least as many columns as rows and its nodes are distinct.

   Lemma A.1. *[14] Consider the Vandermonde matrix* $\boldsymbol{\Theta}_1 \in \mathbb{C}^{r\times n}$.

   $$\forall\, i,j,\ \lambda_i \neq \lambda_j \,\&\, n \geq r \iff \boldsymbol{\Theta}_1 \text{ has full row rank.}$$

2. A Vandermonde matrix with distinct nodes has linearly independent columns if and only if the number of columns does not exceed the number of rows.

LEMMA A.2. *[16] Consider the Vandermonde matrix $\boldsymbol{\Theta}_1 \in \mathbb{C}^{r\times n}$. Suppose it has distinct nodes i.e. $\forall\, i, j,\ \lambda_i \neq \lambda_j$. Then, we have*

$$n \leq r \iff \boldsymbol{\Theta}_1 \text{ has full column rank.}$$

A.3. Connecting some characteristics of generalizability in DMD. We begin by showing that linear consistency is tantamount to Koopman invariance of $\boldsymbol{\psi}$ if DMD is well-posed.

Proof of Proposition 3.7. The forward implication starts with the linearly consistent pair $(\mathbf{X}, \mathbf{Y})$. By Definition 3.5, there is a matrix $\mathbf{A}$ such that $\mathbf{AX} = \mathbf{Y}$. We may expand the data matrices using (3.19) to obtain:

$$(\mathbf{AC})\boldsymbol{\Theta}_1 = (\mathbf{C}\boldsymbol{\Lambda})\boldsymbol{\Theta}_1.$$

The dependence on the initial condition $\boldsymbol{\upsilon}_1$ can be factored out using the definition of $\mathbf{C}$ in (3.16). As $\boldsymbol{\Lambda}$ and $\operatorname{diag}[\boldsymbol{\phi}(\boldsymbol{\upsilon}_1)]$ are diagonal matrices, they commute to produce the following expression:

$$\begin{aligned} & (\mathbf{A}\tilde{\mathbf{C}})\ \operatorname{diag}[\boldsymbol{\phi}(\boldsymbol{\upsilon}_1)]\boldsymbol{\Theta}_1 = (\tilde{\mathbf{C}}\boldsymbol{\Lambda})\ \operatorname{diag}[\boldsymbol{\phi}(\boldsymbol{\upsilon}_1)]\boldsymbol{\Theta}_1 \\ \iff\ & (\mathbf{A}\tilde{\mathbf{C}} - \tilde{\mathbf{C}}\boldsymbol{\Lambda})\ \operatorname{diag}[\boldsymbol{\phi}(\boldsymbol{\upsilon}_1)]\boldsymbol{\Theta}_1 = \mathbf{0}. \end{aligned} \tag{A.1}$$

Well-posedness, as defined in Definition 3.4, ensures that the product $\operatorname{diag}[\boldsymbol{\phi}(\boldsymbol{\upsilon}_1)]\boldsymbol{\Theta}_1$ has full row rank. Firstly, it explicitly states that $\operatorname{diag}[\boldsymbol{\phi}(\boldsymbol{\upsilon}_1)]$ is invertible. In addition, we have $n \geq r$. Since $\boldsymbol{\Theta}_1 \in \mathbb{C}^{r\times n}$ has distinct nodes, Lemma A.1 says it has linearly independent rows. The product of two matrices with full row rank will also have full row rank. Using this in (A.1), we get:

$$\mathbf{A}\tilde{\mathbf{C}} = \tilde{\mathbf{C}}\boldsymbol{\Lambda}. \tag{A.2}$$

We will now establish Koopman invariance by proving that $U \circ \boldsymbol{\psi} = \mathbf{A}\boldsymbol{\psi}$. First, we use (3.15) to express $\boldsymbol{\psi}$ in terms of the eigen-functions $\boldsymbol{\phi}$:

$$U \circ \boldsymbol{\psi} \ = \ U \circ (\tilde{\mathbf{C}}\boldsymbol{\phi}).$$

Linearity of the Koopman operator lets us bypass $\tilde{\mathbf{C}}$ and update $\boldsymbol{\phi}$. Specifically, we have:

$$U \circ (\tilde{\mathbf{C}}\boldsymbol{\phi}) \ = \ \tilde{\mathbf{C}}(U \circ \boldsymbol{\phi}) \ = \ \tilde{\mathbf{C}}\boldsymbol{\Lambda}\boldsymbol{\phi}.$$

Equation (A.2) lets us express $U \circ \boldsymbol{\psi}$ in terms of $\boldsymbol{\psi}$ itself.

$$(\tilde{\mathbf{C}}\boldsymbol{\Lambda})\boldsymbol{\phi} \ = \ \mathbf{A}(\tilde{\mathbf{C}}\boldsymbol{\phi}) \ = \ \mathbf{A}\boldsymbol{\psi}.$$

The backward implication is easier. By Definition 3.6, Koopman invariance of $\boldsymbol{\psi}$ means there is a matrix $\mathbf{A}$ such that $U \circ \boldsymbol{\psi} = \mathbf{A}\boldsymbol{\psi}$. If we evaluate this condition along the trajectory beginning at $\boldsymbol{\upsilon}_1$, we get $\mathbf{AX} = \mathbf{Y}$ which is the desired conclusion. ∎

Next, we show that the notion of Koopman invariant $\boldsymbol{\psi}$ is the same as the coincidence of spectral and spatial complexities.

Proof of Proposition 3.9. We prove the equivalence of these three statements in a cyclic fashion.

- $1 \implies 2$: Suppose spectral and spatial complexities match i.e. $\dim(\mathcal{R}(\tilde{\mathbf{C}})) = r$. Then, $\tilde{\mathbf{C}}$ has r linearly independent columns. However, we also know that $\tilde{\mathbf{C}} \in \mathbb{C}^{m\times r}$. Hence, it has full column rank.
- $2 \implies 3$: Consider the following $m \times m$ matrix:

$$\mathbf{A} \;:=\; \tilde{\mathbf{C}}\mathbf{\Lambda}\tilde{\mathbf{C}}^{\dagger}.$$

We claim that $U \circ \boldsymbol{\psi} \;=\; \mathbf{A}\boldsymbol{\psi}$. Consider its right-hand side and expand $\boldsymbol{\psi}$ using (3.15):

$$\mathbf{A}\boldsymbol{\psi} \;=\; \mathbf{A}\tilde{\mathbf{C}}\boldsymbol{\phi} \;=\; (\tilde{\mathbf{C}}\mathbf{\Lambda}\tilde{\mathbf{C}}^{\dagger})\tilde{\mathbf{C}}\boldsymbol{\phi}.$$

Since $\tilde{\mathbf{C}}$ has full column rank, $\tilde{\mathbf{C}}^{\dagger}\tilde{\mathbf{C}} = \mathbf{I}$. We can, then, bring in the Koopman operator U using equation (3.15):

$$\tilde{\mathbf{C}}\mathbf{\Lambda}(\tilde{\mathbf{C}}^{\dagger}\tilde{\mathbf{C}})\boldsymbol{\phi} \;=\; \tilde{\mathbf{C}}(\mathbf{\Lambda}\boldsymbol{\phi}) \;=\; \tilde{\mathbf{C}}\; U \circ \boldsymbol{\phi}.$$

The final step uses the linearity of U to link $\tilde{\mathbf{C}}$ and $\boldsymbol{\phi}$:

$$\tilde{\mathbf{C}}\; U \circ \boldsymbol{\phi} \;=\; U \circ (\tilde{\mathbf{C}}\boldsymbol{\phi}) \;=\; U \circ \boldsymbol{\psi}.$$

- $3 \implies 1$: A Koopman invariant $\boldsymbol{\psi}$ implies the existence of a matrix $\mathbf{A}$ such that

$$U \circ \boldsymbol{\psi} \;=\; \mathbf{A}\boldsymbol{\psi}.$$

If we expand ψ in terms of the eigen-functions $\boldsymbol{\phi}$ and use the linearity of U, we get:

$$U \circ (\tilde{\mathbf{C}}\boldsymbol{\phi}) \;=\; \tilde{\mathbf{C}}(U \circ \boldsymbol{\phi}) \;=\; \tilde{\mathbf{C}}\mathbf{\Lambda}\boldsymbol{\phi} \;=\; \mathbf{A}\tilde{\mathbf{C}}\boldsymbol{\phi}.$$

Since this relationship holds for all values of $\boldsymbol{\phi}$, we have:

$$\tilde{\mathbf{C}}\mathbf{\Lambda} \;=\; \mathbf{A}\tilde{\mathbf{C}}.$$

Observe that the columns of $\tilde{\mathbf{C}}$ are the eigen vectors of $\mathbf{A}$ corresponding to distinct eigen-values. Hence, they must be linearly independent. Since $\tilde{\mathbf{C}} \in \mathbb{C}^{m\times r}$, we have:

$$\dim(\mathcal{R}(\tilde{\mathbf{C}})) = r. \qquad \square$$

Appendix B. On DMD-DFT equivalence.

This section details the proofs for all of our major results on the equivalence of mean-subtracted DMD and DFT.

B.1. A necessary and sufficient condition.

Proof of Theorem 4.1. We begin by studying the following affine subspace which is the feasible set for the optimization routine in (3.13):

$$\{\mathbf{c} \mid \mathbf{X}_{\text{ms}}\mathbf{c} \;=\; \mathbf{z}_{n+1} - \boldsymbol{\mu}\}. \tag{B.1}$$

An affine subspace is simply a subspace with a constant offset. A representation of the affine subspace can use any of its elements as the offset. Since $-\mathbf{1}_n$ is an element of (B.1), the latter may be rewritten as follows:

$$\{\mathbf{c} \mid \exists\; \mathbf{d} \;\in\; \mathcal{N}(\mathbf{X}_{\text{ms}}) \text{ such that } \mathbf{c} = -\mathbf{1}_n + \mathbf{d}\}.$$

Since any element may serve as the offset, the nearest point in (B.1) to the origin, $-\mathcal{P}_{\mathcal{R}(\mathbf{X}_{\text{ms}}^H)}(\mathbf{1}_n)$, gives an alternate representation of the optimal set:

$$\{\mathbf{c} \mid \exists\ \tilde{\mathbf{d}}\ \in\ \mathcal{N}(\mathbf{X}_{\text{ms}}) \text{ such that } \mathbf{c} = -\mathcal{P}_{\mathcal{R}(\mathbf{X}_{\text{ms}}^H)}(\mathbf{1}_n) + \tilde{\mathbf{d}}\}.$$

The two terms that sum to $\mathbf{c}$ are orthogonal and so we get:

$$\|\mathbf{c}\|^2 = \left\|\mathcal{P}_{\mathcal{R}(\mathbf{X}_{\text{ms}}^H)}(\mathbf{1}_n)\right\|^2 + \left\|\tilde{\mathbf{d}}\right\|^2 \geq \left\|\mathcal{P}_{\mathcal{R}(\mathbf{X}_{\text{ms}}^H)}(\mathbf{1}_n)\right\|^2.$$

The vector $\mathbf{c}_{\text{ms}}[\mathbf{Z}]$ is the *minimum norm* solution and consequently has $\tilde{\mathbf{d}} = 0$. Thus,

$$\mathbf{c}_{\text{ms}}[\mathbf{Z}] = -\mathcal{P}_{\mathcal{R}(\mathbf{X}_{\text{ms}}^H)}(\mathbf{1}_n).$$

Using the identity $I = \mathcal{P}_{\mathcal{N}(\mathbf{X}_{\text{ms}})} + \mathcal{P}_{R(\mathbf{X}_{\text{ms}}^H)}$, we simultaneously obtain the forward and backward implications:

$$\mathbf{c}_{\text{ms}}[\mathbf{Z}] \ = \ -\mathbf{1}_n \implies \mathcal{P}_{\mathcal{N}(\mathbf{X}_{\text{ms}})}\mathbf{1}_n = 0 \implies \mathbf{c}_{\text{ms}}[\mathbf{Z}] \ = \ -\mathbf{1}_n. \qquad \square$$

Note that this characterization of DMD-DFT equivalence does not invoke the existence of a finite dimensional Koopman invariant subspace. However, beyond this point, the assumptions given in (3.20) will be in effect.

B.2. Equivalence when $\mathbf{X}_{\text{ms}}$ has linearly dependent columns. In order to prove Theorem 4.2, we establish the following algebraic result:

LEMMA B.1.

$$\mathbf{1}_r \ - \ \left(\frac{1}{n+1}\right)\mathbf{\Theta}\mathbf{1}_{n+1} \ = \ -\left(\frac{1}{n+1}\right)(\mathbf{\Lambda} - \mathbf{I})\mathbf{\Theta}_1 \begin{bmatrix} n \\ n-1 \\ \vdots \\ 1 \end{bmatrix}.$$

Proof. Consider the i-th component of the vector in question:

$$1 - \frac{1}{n+1}\ \mathbf{gp}_{n+1}[\lambda_i]^T\ \mathbf{1}_{n+1}.$$

Expanding the inner product and factoring out the denominator, we get:

$$\frac{1}{n+1}\left((n+1) - (1 + \lambda_i + \lambda_i^2 + \ldots + \lambda_i^n)\right).$$

The two sums in the numerator have $(n+1)$ terms each. By summing them in pairs, we obtain:

$$-\frac{1}{n+1}\left((\lambda_i - 1) + (\lambda_i^2 - 1) + \ldots + (\lambda_i^n - 1)\right).$$

By factoring out $(\lambda_i - 1)$ from each of the remaining n terms, we get the following:

$$-\frac{\lambda_i - 1}{n+1}\begin{bmatrix}1 & \lambda_i & \ldots & \lambda_i^{n-1}\end{bmatrix}\begin{bmatrix} n \\ n-1 \\ \vdots \\ 1 \end{bmatrix}.$$

Collect the components into a column vector, and group terms to reach the desired conclusion. $\square$

Proof of Theorem 4.2. We begin with a quick sanity check that our observables are indeed non-trivial. By Lemma A.2, $n \leq r$ ensures that $\mathbf{\Theta}_1 \in \mathbb{C}^{r\times n}$ has full column rank. In particular, $\mathbf{l}$, the last column of $\mathbf{\Theta}_1$, will not be in the span of the remaining columns. Hence, $\mathbf{l}^\perp \neq 0$ and our observables, represented by $\tilde{\mathbf{C}}$, are non-trivial.

Our objective is to show that $\mathbf{X}_{\text{ms}}$ has linearly dependent columns and also satisfies $\mathcal{P}_{\mathcal{N}(\mathbf{X}_{\text{ms}})}\mathbf{1}_n = \mathbf{0}$.

Rank defectiveness of $\mathbf{X}_{\text{ms}}$ follows directly from its shape. Since $\tilde{\mathbf{C}}$ is a row vector, so too is $\mathbf{X}_{\text{ms}}$. The condition $n \geq 2$ means $\mathbf{X}_{\text{ms}}$ has at least 2 columns which must be linearly dependent because it only has a single row.

We prove DMD-DFT equivalence by showing that the data matrix $\mathbf{X}_{\text{ms}}$ satisfies a sufficient condition. To this end, we construct a banded matrix $\mathbf{B} \in \mathbb{C}^{n\times(n-1)}$ as follows:

$$\mathbf{B} \;:=\; \begin{bmatrix} -1 & & \\ 1 & \ddots & \\ & \ddots & -1 \\ & & 1 \end{bmatrix}.$$

Evidently, $\mathbf{B}^H\mathbf{1}_n = \mathbf{0}$. Indeed, the columns of $\mathbf{B}$ form a basis for the orthogonal complement of the span of $\mathbf{1}_n$.

$$\mathcal{R}(\mathbf{B}) \;=\; \mathcal{N}(\mathbf{1}_n^H).$$

If we can show that $\mathcal{R}(\mathbf{B}) = \mathcal{N}(\mathbf{X}_{\text{ms}})$, then DMD-DFT equivalence is also true:

$$\mathcal{R}(\mathbf{B}) = \mathcal{N}(\mathbf{X}_{\text{ms}}) \implies \mathcal{P}_{\mathcal{N}(\mathbf{X}_{\text{ms}})}\mathbf{1}_n \;=\; \mathcal{P}_{\mathcal{R}(\mathbf{B})}\mathbf{1}_n \;=\; \mathcal{P}_{\mathcal{N}(\mathbf{1}_n^H)}\mathbf{1}_n \;=\; \mathbf{0}.$$

So, we have an alternative approach to proving DMD-DFT equivalence.

Before proceeding further, we perform some algebraic simplifications. By the definition of $\tilde{\mathbf{C}}$, we can simplify $\mathbf{Z}$ and $\boldsymbol{\mu}$:

$$\mathbf{Z} = \tilde{\mathbf{C}}_0\mathbf{\Theta} \implies \boldsymbol{\mu} = \tilde{\mathbf{C}}_0(\mathbf{\Theta}\mathbf{1}_{n+1})\left(\frac{1}{n+1}\right). \tag{B.2}$$

Consequently, $\mathbf{Z}_{\text{ms}}$ and $\mathbf{X}_{\text{ms}}$ may be factored as follows:

$$\mathbf{Z}_{\text{ms}} = \begin{bmatrix} -\boldsymbol{\mu} & \tilde{\mathbf{C}}_0 \end{bmatrix} \begin{bmatrix} \mathbf{1}_{n+1}^T \\ \mathbf{\Theta} \end{bmatrix}, \quad \mathbf{X}_{\text{ms}} = \begin{bmatrix} -\boldsymbol{\mu} & \tilde{\mathbf{C}}_0 \end{bmatrix} \begin{bmatrix} \mathbf{1}_n^T \\ \mathbf{\Theta}_1 \end{bmatrix}.$$

We will first show that $\mathcal{R}(\mathbf{B}) \subset \mathcal{N}(\mathbf{X}_{\text{ms}})$. Consider the product $\mathbf{X}_{\text{ms}}\mathbf{B}$ in light of the columns of $\mathbf{B}$ being orthogonal to $\mathbf{1}_n$.

$$\mathbf{X}_{\text{ms}}\mathbf{B} \;=\; \begin{bmatrix} -\boldsymbol{\mu} & \tilde{\mathbf{C}}_0 \end{bmatrix} \begin{bmatrix} \mathbf{1}_n^T \\ \mathbf{\Theta}_1 \end{bmatrix} \mathbf{B} \;=\; \tilde{\mathbf{C}}_0\mathbf{\Theta}_1\mathbf{B}.$$

The matrix product $\mathbf{\Theta}_1\mathbf{B}$ may be re-written as follows with a Vandermonde matrix

to the right.

$$\begin{aligned}\boldsymbol{\Theta}_1\mathbf{B} &= \begin{bmatrix}\lambda_1-1 & \lambda_1^2-\lambda_1 & \dots & \lambda_1^{n-1}-\lambda_1^{n-2}\\ \lambda_2-1 & \lambda_2^2-\lambda_2 & \dots & \lambda_2^{n-1}-\lambda_2^{n-2}\\ \vdots & \vdots & \ddots & \vdots \\ \lambda_r-1 & \lambda_r^2-\lambda_r & \dots & \lambda_r^{n-1}-\lambda_r^{n-2}\end{bmatrix}\\ &= \begin{bmatrix}\lambda_1-1 & & & \\ & \lambda_2-1 & & \\ & & \ddots & \\ & & & \lambda_r-1\end{bmatrix}\begin{bmatrix}1 & \lambda_1 & \dots & \lambda_1^{n-2}\\ 1 & \lambda_2 & \dots & \lambda_2^{n-2}\\ \vdots & \vdots & \ddots & \vdots \\ 1 & \lambda_r & \dots & \lambda_r^{n-2}\end{bmatrix}\\ &= (\boldsymbol{\Lambda}-\mathbf{I})\boldsymbol{\Theta}_2.\end{aligned}$$

This lets us bring in $\mathbf{l}^\perp$ into $\mathbf{X}_{\text{ms}}\mathbf{B}$:

$$\mathbf{X}_{\text{ms}}\mathbf{B} \;=\; \tilde{\mathbf{C}}_0\boldsymbol{\Theta}_1\mathbf{B} \;=\; \tilde{\mathbf{C}}_0(\boldsymbol{\Lambda}-\mathbf{I})\boldsymbol{\Theta}_2 \;=\; (\mathbf{l}^\perp)^H\boldsymbol{\Theta}_2 \;=\; \mathbf{0}.$$

Thus, $\mathcal{R}(\mathbf{B}) \subset \mathcal{N}(\mathbf{X}_{\text{ms}})$.

Observe that $\mathcal{R}(\mathbf{B})$ is a $n-1$ dimensional subspace of $\mathbb{C}^n$. So, if $\mathcal{R}(\mathbf{B})$ is a strict subset of $\mathcal{N}(\mathbf{X}_{\text{ms}})$, then, by the rank-nullity theorem, $\mathbf{X}_{\text{ms}} = \mathbf{0}$. Therefore, proving that $\mathbf{X}_{\text{ms}} \neq \mathbf{0}$ is enough to show that $\mathcal{R}(\mathbf{B}) = \mathcal{N}(\mathbf{X}_{\text{ms}})$. We examine the first column of $\mathbf{X}_{\text{ms}}$:

$$\mathbf{X}_{\text{ms}}\mathbf{e}_1 \;=\; \begin{bmatrix}-\boldsymbol{\mu} & \tilde{\mathbf{C}}_0\end{bmatrix}\begin{bmatrix}\mathbf{1}_n^T\\ \boldsymbol{\Theta}_1\end{bmatrix}\mathbf{e}_1 \;=\; -\boldsymbol{\mu} + \tilde{\mathbf{C}}_0\mathbf{1}_r.$$

If we expand $\boldsymbol{\mu}$ as in (B.2), it becomes amenable to Lemma B.1:

$$\mathbf{X}_{\text{ms}}\mathbf{e}_1 \;=\; \tilde{\mathbf{C}}_0\left[\mathbf{1}_r - (\boldsymbol{\Theta}\mathbf{1}_{n+1})\left(\frac{1}{n+1}\right)\right] \;=\; \tilde{\mathbf{C}}_0(\boldsymbol{\Lambda}-\mathbf{I})\boldsymbol{\Theta}_1\begin{bmatrix}n\\ n-1\\ \vdots\\ 1\end{bmatrix}\left(\frac{-1}{n+1}\right).$$

Once again, we introduce $\mathbf{l}^\perp$ and make note of its orthogonality to the first $n-1$ columns of $\boldsymbol{\Theta}_1$:

$$\mathbf{X}_{\text{ms}}\mathbf{e}_1 \;=\; (\mathbf{l}^\perp)^H\boldsymbol{\Theta}_1\begin{bmatrix}n\\ n-1\\ \vdots\\ 1\end{bmatrix}\left(\frac{-1}{n+1}\right) \;=\; (\mathbf{l}^\perp)^H\mathbf{l}\left(\frac{-1}{n+1}\right) \;=\; \|\mathbf{l}^\perp\|^2\left(\frac{-1}{n+1}\right).$$

Since we've already seen that $\mathbf{l}^\perp \neq \mathbf{0}$, the matrix-vector product $\mathbf{X}_{\text{ms}}\mathbf{e}_1 \neq \mathbf{0}$. ∎

B.3. A modal decomposition of mean-subtracted data. When the Koopman mode expansion possesses only a finite number of terms, we have seen, in Appendix A.1, that the time series $\mathbf{Z}$ can be written as the product $\mathbf{C}\boldsymbol{\Theta}$. Here, we derive an analogous factorization for the mean-removed data-set $\mathbf{Z}_{\text{ms}}$.

As a preliminary step, we partition the matrices $\mathbf{C}$ and $\boldsymbol{\Theta}$ when we have a Koopman eigenvalue at 1. Let $\mathbf{c}_1$ be the column of $\mathbf{C}$ that multiplies $\mathbf{1}_{n+1}^T$ in the product $\mathbf{C}\boldsymbol{\Theta}$. Also, let $\mathbf{C}_{\not\ni 1}$ be the sub-matrix of $\mathbf{C}$ obtained by excluding $\mathbf{c}_1$. Similarly, suppose $\boldsymbol{\Theta}_{\not\ni 1}$ is the sub-matrix of $\boldsymbol{\Theta}$ obtained by deleting the row corresponding to $\mathbf{1}_{n+1}^T$. Then, from (3.17), we have:

$$\mathbf{Z} \;=\; \mathbf{C}\boldsymbol{\Theta} \;=\; \mathbf{c}_1\mathbf{1}_{n+1}^T + \mathbf{C}_{\not\ni 1}\boldsymbol{\Theta}_{\not\ni 1}. \tag{B.3}$$

Now, we proceed to factorize $\mathbf{Z}_{\text{ms}}$ by re-writing its definition in (3.12) as the product of two matrices.

$$\mathbf{Z}_{\text{ms}} = \begin{bmatrix} \mathbf{C} & -\boldsymbol{\mu} \end{bmatrix} \begin{bmatrix} \boldsymbol{\Theta} \\ \mathbf{1}_{n+1}^T \end{bmatrix}. \tag{B.4}$$

Consider the two matrices $\mathbf{C}_{\text{ms}}$ and $\boldsymbol{\Theta}_{\text{ms}}$ defined as follows, over a mutually exclusive and exhaustive set of scenarios.

1. $\boldsymbol{\mu} \neq \mathbf{0}$ & $1 \notin \sigma(\boldsymbol{\Lambda})$:

$$\mathbf{C}_{\text{ms}} := \begin{bmatrix} \mathbf{C} & -\boldsymbol{\mu} \end{bmatrix}, \quad \boldsymbol{\Theta}_{\text{ms}} := \begin{bmatrix} \boldsymbol{\Theta} \\ \mathbf{1}_{n+1}^T \end{bmatrix}$$

2. $\boldsymbol{\mu} = \mathbf{0}$:

$$\mathbf{C}_{\text{ms}} := \mathbf{C}, \quad \boldsymbol{\Theta}_{\text{ms}} := \boldsymbol{\Theta}$$

3. $1 \in \sigma(\boldsymbol{\Lambda})$:
   (a) $\mathbf{c}_1 = \boldsymbol{\mu}$:

$$\mathbf{C}_{\text{ms}} := \mathbf{C}_{\not\ni 1}, \quad \boldsymbol{\Theta}_{\text{ms}} := \boldsymbol{\Theta}_{\not\ni 1}$$

   (b) $\mathbf{c}_1 \neq \boldsymbol{\mu}$:

$$\mathbf{C}_{\text{ms}} := \begin{bmatrix} \mathbf{c}_1 - \boldsymbol{\mu} & \mathbf{C}_{\not\ni 1} \end{bmatrix}, \quad \boldsymbol{\Theta}_{\text{ms}} := \boldsymbol{\Theta} = \begin{bmatrix} \mathbf{1}_{n+1}^T \\ \boldsymbol{\Theta}_{\not\ni 1} \end{bmatrix}$$

The fastidiousness above helps us ensure that every column of $\mathbf{C}_{\text{ms}}$ is non-zero, $\boldsymbol{\Theta}_{\text{ms}}$ has distinct nodes and more importantly:

$$\mathbf{Z}_{\text{ms}} = \mathbf{C}_{\text{ms}} \boldsymbol{\Theta}_{\text{ms}}. \tag{B.5}$$

In other words, every row of $\mathbf{Z}_{\text{ms}}$ lies in the row space of the Vandermonde matrix $\boldsymbol{\Theta}_{\text{ms}}$, which is related to but potentially different from $\boldsymbol{\Theta}$.

B.4. Over-sampling and linear consistency prevent equivalence. We define the following structures that are central to the forthcoming analysis:

1. $\sigma(\boldsymbol{\Lambda}_{\text{ms}})$:= Nodes of the Vandermonde matrix $\boldsymbol{\Theta}_{\text{ms}}$.
2. $\boldsymbol{\Lambda}_{\text{ms}}$:= Diagonal matrix constructed using $\sigma(\boldsymbol{\Lambda}_{\text{ms}})$.

The effect of mean subtraction may be systematically studied by classifying $\mathbf{Z}_{\text{ms}}$ into four non-intersecting categories. First, we check for the presence of 1 in the "mean-subtracted Koopman spectrum" $\sigma(\boldsymbol{\Lambda}_{\text{ms}})$. Then, we look for the presence of 1 in the Koopman spectrum $\sigma(\boldsymbol{\Lambda})$. Table B.1 elucidates this partition, and some simple algebraic consequences that can be readily verified.

TABLE B.1

Delineating the effect of mean subtraction: There are four possible outcomes associated with this pre-processing step. The column titled "Branch 1" splits them into two groups, while the next one further divides each group in two. The remaining columns describe the characteristics of each case.

Case #	Branch 1	Branch 2	$\sigma(\boldsymbol{\Lambda}_{\text{ms}})$	Rows in $\boldsymbol{\Theta}_{\text{ms}}$	$\mathbf{C}_{\text{ms}}$	$\boldsymbol{\Theta}_{\text{ms}}$
I	$1 \in \sigma(\boldsymbol{\Lambda}_{\text{ms}})$	$1 \notin \sigma(\boldsymbol{\Lambda})$	$\sigma(\boldsymbol{\Lambda}) \cup \{1\}$	$r+1$		
II		$1 \in \sigma(\boldsymbol{\Lambda})$	$\sigma(\boldsymbol{\Lambda})$	r		$\boldsymbol{\Theta}$
III	$1 \notin \sigma(\boldsymbol{\Lambda}_{\text{ms}})$	$1 \notin \sigma(\boldsymbol{\Lambda})$	$\sigma(\boldsymbol{\Lambda})$	r	$\mathbf{C}$	$\boldsymbol{\Theta}$
IV		$1 \in \sigma(\boldsymbol{\Lambda})$	$\sigma(\boldsymbol{\Lambda}) \cap \{1\}^c$	$r-1$	$\mathbf{C}_{\not\ni 1}$	

Understanding the over-sampled regime requires some auxillary results on the temporal mean and importantly $\mathbf{C}_{\text{ms}}$. Firstly, we show that $\boldsymbol{\mu} \neq \mathbf{0}$ unless we are in Case III. This is proven in three parts and begins by studying Cases II and IV:

PROPOSITION B.2. *If $\tilde{\mathbf{C}}$ has full column rank and 1 is a Koopman eigenvalue i.e. $1 \in \sigma(\mathbf{\Lambda})$, then the temporal mean $\boldsymbol{\mu} \neq 0$*

Proof. The condition $1 \in \sigma(\mathbf{\Lambda})$ ensures that $\mathbf{\Theta 1}_{n+1}$ has atleast one non-zero coefficient. Since $\tilde{\mathbf{C}}$ (and equivalently $\mathbf{C}$) has full column rank, $\boldsymbol{\mu} \neq 0$. ∎

Case I is tackled by finding a necessary condition for zero mean and taking the contrapositive.

PROPOSITION B.3. *If the temporal mean $\boldsymbol{\mu} = 0$ and $1 \in \sigma(\mathbf{\Lambda}_{\text{ms}})$, then $\tilde{\mathbf{C}}$ has linearly dependent columns.*

Proof. We claim that the vector $\mathbf{z} := \mathbf{\Theta 1}_{n+1}$ is a non-trivial element of $\mathcal{N}(\mathbf{C})$. First, zero mean implies that $\mathbf{C}_{\text{ms}} = \mathbf{C},\ \mathbf{\Theta}_{\text{ms}} = \mathbf{\Theta}$. As a result, $1 \in \sigma(\mathbf{\Lambda})$ which gives $\mathbf{\Theta 1}_{n+1} = \mathbf{z} \neq 0$. Finally, we note:

$$\mathbf{C}\mathbf{z}\frac{1}{n+1} = \mathbf{C}\mathbf{\Theta 1}_{n+1}\frac{1}{n+1} = \boldsymbol{\mu} = 0.$$ ∎

Compiling the above results and studying Case III, we find that it is the only scenario when the mean is $\mathbf{0}$.

LEMMA B.4. *If $\tilde{\mathbf{C}}$ has full column rank, then the mean $\boldsymbol{\mu}$ is zero only in Case III.*

$$\boldsymbol{\mu} = \mathbf{0} \iff \textit{Case III.}$$

Proof. We prove the forward implication by contraposition. Consider Cases I, II and IV in Table B.1. By Proposition B.2, the mean is non-zero for Cases II and IV. Case I has $1 \in \sigma(\mathbf{\Lambda}_{\text{ms}})$. Since $\tilde{\mathbf{C}}$ has linearly independent columns, we can apply the contrapositive of Proposition B.3 to show $\boldsymbol{\mu} \neq \mathbf{0}$.

The backward implication is proven by contradiction. Suppose we have Case III and $\boldsymbol{\mu} \neq \mathbf{0}$. Since $1 \notin \sigma(\mathbf{\Lambda})$, removing the non-zero mean from $\mathbf{Z}$ will simply cause $1 \in \sigma(\mathbf{\Lambda}_{\text{ms}})$ which is in contradiction with Case III. ∎

The definition of the matrix $\mathbf{C}_{\text{ms}}$ in (B.5) belies the intricacies of mean subtraction that are detailed in Table B.1. Starting with the matrix $\mathbf{C}$, it is possible to gain (Case I) or lose (Case IV) a column. An existing column may be modified (Case II) or there may no effect whatsoever (Case III). Fortunately, it is sufficient to only understand the relationship between the column spaces of $\mathbf{C}_{\text{ms}},\ \mathbf{C}$ and their sub-matrices in order to study the under and just sampled regimes.

PROPOSITION B.5. *Let $\mathbf{C}_{\not\ni 1}$ be the submatrix of $\mathbf{C}$ formed by excluding the column (if it exists) corresponding to the Koopman eigenvalue at 1. Then,*

$$\begin{aligned}\boldsymbol{\mu} = 0 &\implies \mathbf{C}_{\text{ms}} = \mathbf{C}.\\ \boldsymbol{\mu} \neq 0 &\implies \mathcal{R}(\mathbf{C}_{\text{ms}}) = \mathcal{R}(\mathbf{C}_{\not\ni 1}).\end{aligned}$$

In addition, let $(\mathbf{C}_{\text{ms}})_{\not\ni 1}$ be the matrix analogous to $\mathbf{C}_{\not\ni 1}$ for $\mathbf{C}_{\text{ms}}$. We have:

$$\mathcal{R}\left((\mathbf{C}_{\text{ms}})_{\not\ni 1}\right) = \mathcal{R}\left(\mathbf{C}_{\not\ni 1}\right).$$

Proof. Follows from definition with routine algebraic manipulations. ∎

Technically, we are now embarking on the proof of Theorem 4.3. However, the arguments involved are also useful in establishing Corollary 4.4. So, they have been organized into the two theorems below to facilitate their reuse. Both of these are proven by contradiction and we begin by studying Cases III and IV.

THEOREM B.6. *Suppose we have* $1 \notin \sigma(\mathbf{\Lambda}_{\text{ms}})$. *If* $n \geq r$, *then mean-subtracted DMD is not DFT for Case IV in Table* B.1. *If* $n \geq r+1$, *non-equivalence holds for Case III too.*

Proof. We prove by contradiction. First, using Theorem 4.1, we assume that $\mathcal{P}_{\mathcal{N}(\mathbf{X}_{\text{ms}})}\mathbf{1}_n = \mathbf{0}$. Since $\mathcal{N}(\mathbf{X}_{\text{ms}})^{\perp} = \mathcal{R}(\mathbf{X}_{\text{ms}}^H)$, an equivalent statement would be:

$$\exists\ \mathbf{d} \text{ such that } \mathbf{d}^H\mathbf{X}_{\text{ms}} = \mathbf{1}_n^H.$$

By equation (B.5), $\mathbf{X}_{\text{ms}} = \mathbf{C}_{\text{ms}}(\mathbf{\Theta}_{\text{ms}})_1$. Using this identity and shifting $\mathbf{1}_n^H$ to the left, we obtain an equivalent statement:

$$\exists\ \mathbf{d} \text{ such that } \begin{bmatrix}\mathbf{d}^H\mathbf{C}_{\text{ms}} & -1\end{bmatrix}\begin{bmatrix}(\mathbf{\Theta}_{\text{ms}})_1 \\ \mathbf{1}_n^H\end{bmatrix} = 0.$$

Hence, $\mathbf{\Theta}_{\text{aug}} := \begin{bmatrix}(\mathbf{\Theta}_{\text{ms}})_1 \\ \mathbf{1}_n^H\end{bmatrix}$ has linearly dependent rows.

But, the lower bounds on n mean that $\mathbf{\Theta}_{\text{aug}}$ has full row rank. Firstly, $1 \notin \sigma(\mathbf{\Lambda}_{\text{ms}})$ means $\mathbf{\Theta}_{\text{aug}}$ has distinct nodes. While it has n columns, the number of rows is case dependent. In Case III, $\mathbf{\Theta}_{\text{aug}}$ has $r+1$ rows and at least $r+1$ columns. Similarly, in Case IV, $\mathbf{\Theta}_{\text{aug}}$ has r rows and at least r columns. Hence, by Lemma A.1, $\mathbf{\Theta}_{\text{aug}}$ has full row rank which is a contradiction. ∎

Cases I and II have a similar proof strategy where Proposition B.5 plays a crucial role.

THEOREM B.7. *Suppose we have* $1 \in \sigma(\mathbf{\Lambda}_{\text{ms}})$ *and a full column rank* $\tilde{\mathbf{C}}$. *If* $n \geq r$, *then mean-subtracted DMD is not DFT for Case II in Table* B.1. *If* $n \geq r+1$, *non-equivalence also holds for Case I.*

Proof. As with Theorem B.6, we prove by contradiction. Using Theorem 4.1 in conjunction with the fact that $\mathcal{N}(\mathbf{X}_{\text{ms}})^{\perp} = \mathcal{R}(\mathbf{X}_{\text{ms}}^H)$, we have the following assertion:

$$\exists\ \mathbf{d} \text{ such that } \mathbf{d}^H\mathbf{X}_{\text{ms}} = \mathbf{1}_n^H.$$

Since $\mathbf{X}_{\text{ms}} = \mathbf{C}_{\text{ms}}(\mathbf{\Theta}_{\text{ms}})_1$, we get:

$$\exists\ \mathbf{d} \text{ such that } (\mathbf{d}^H\mathbf{C}_{\text{ms}})(\mathbf{\Theta}_{\text{ms}})_1 = \mathbf{1}_n^H. \tag{B.6}$$

Observe that the bounds on n endow $(\mathbf{\Theta}_{\text{ms}})_1$ with linearly independent rows. In Case I, $(\mathbf{\Theta}_{\text{ms}})_1 \in \mathbb{C}^{(r+1)\times n}$ and $n \geq r+1$. Case II has $(\mathbf{\Theta}_{\text{ms}})_1 \in \mathbb{C}^{r\times n}$ and $n \geq r$. Therefore, Lemma A.1 says $(\mathbf{\Theta}_{\text{ms}})_1$ has full row rank.

Consequently, $\mathbf{d}^H\mathbf{C}_{\text{ms}}$ is the unique representation of $\mathbf{1}_n^H$ in the row space of $(\mathbf{\Theta}_{\text{ms}})_1$. Additionally, $1 \in \sigma(\mathbf{\Lambda}_{\text{ms}})$ i.e. 1 is a node of $(\mathbf{\Theta}_{\text{ms}})_1$. So, $\mathbf{d}^H\mathbf{C}_{\text{ms}}$ must be zero at all indices except that corresponding to the node at 1. Hence,

$$\mathbf{d}^H(\mathbf{C}_{\text{ms}})_{\not\ni 1} = \mathbf{0}.$$

Proposition B.5 says $\mathcal{R}\left((\mathbf{C}_{\text{ms}})_{\not\ni 1}\right) = \mathcal{R}\left(\mathbf{C}_{\not\ni 1}\right)$. This gives:

$$\mathbf{d}^H\mathbf{C}_{\not\ni 1} = \mathbf{0}.$$

Since we are not dealing with Case III, Lemma B.4 gives $\boldsymbol{\mu} \neq \mathbf{0}$, Proposition B.5 also says that $\mathcal{R}(\mathbf{C}_{\text{ms}}) = \mathcal{R}(\mathbf{C}_{\not\ni 1})$. Thus, we get:

$$\mathbf{d}^H\mathbf{C}_{\text{ms}} = \mathbf{0}.$$

This is in contradiction with (B.6). ∎

Consequently, we have a deceptively short proof for non-equivalence in the over-sampled regime.

Proof of Theorem 4.3. We begin by acknowledging that the DMD problem is well-posed. This means that linear consistency of $(\mathbf{X}, \mathbf{Y})$ is tantamount to $\tilde{\mathbf{C}}$ having full column rank (Propositions 3.7 and 3.9).

The proof consists of two branches:

1. $1 \in \sigma(\mathbf{\Lambda}_{\text{ms}})$: Since all the conditions for Theorem B.7 are met, there is no DMD-DFT equivalence.
2. $1 \notin \sigma(\mathbf{\Lambda}_{\text{ms}})$: Since $n \geq r+1$, by Theorem B.6, there is no DMD-DFT equivalence. ∎

B.5. Exploring the under and just-sampled regimes. Lemma 3.2 explains the under-sampled regime. Alas, there is no simple explanation for the just-sampled regime. To see these, we formalize an intermediary of import:

PROPOSITION B.8. *If $\tilde{\mathbf{C}}$ has full column rank and $1 \in \sigma(\mathbf{\Lambda}_{\text{ms}})$, then $\mathcal{N}(\mathbf{C}_{\text{ms}})$ is the one dimensional subspace spanned by $\mathbf{\Theta}_{\text{ms}}\mathbf{1}_{n+1}$.*

Proof. We need to prove the following statement:

$$\mathcal{N}(\mathbf{C}_{\text{ms}}) \;=\; \mathcal{R}(\mathbf{\Theta}_{\text{ms}}\mathbf{1}_{n+1}).$$

We begin by showing that $\mathcal{N}(\mathbf{C}_{\text{ms}}) \;\supset\; \mathcal{R}(\mathbf{\Theta}_{\text{ms}}\mathbf{1}_{n+1})$. Consider $\mathbf{Z}_{\text{ms}}$ as defined in (B.5). Since it is constructed as a mean-subtracted matrix, it has zero temporal mean:

$$\mathbf{Z}_{\text{ms}}\frac{\mathbf{1}_{n+1}}{n+1} = \mathbf{0} \iff \mathbf{C}_{\text{ms}}\mathbf{\Theta}_{\text{ms}}\mathbf{1}_{n+1} = \mathbf{0} \implies \mathcal{N}(\mathbf{C}_{\text{ms}}) \supset \mathcal{R}(\mathbf{\Theta}_{\text{ms}}\mathbf{1}_{n+1}).$$

We will show that the set containment proceeds both ways, and the condition $1 \in \sigma(\mathbf{\Lambda}_{\text{ms}})$ helps simplify this process.

Firstly, $1 \in \sigma(\mathbf{\Lambda}_{\text{ms}})$ means $\mathbf{\Theta}_{\text{ms}}\mathbf{1}_{n+1} \;\neq\; \mathbf{0}$. Therefore, $\mathcal{R}(\mathbf{\Theta}_{\text{ms}}\mathbf{1}_{n+1})$ is a non-trivial subspace of dimension 1. Secondly, it ensures that $\boldsymbol{\mu} \neq \mathbf{0}$. To see this, consider the exhaustive set of possibilities described in Table B.1 when $1 \in \sigma(\mathbf{\Lambda}_{\text{ms}})$:

- $1 \notin \sigma(\mathbf{\Lambda})$ & $\boldsymbol{\mu} \neq \mathbf{0}$ (Case I): The second condition explicitly states that the temporal mean is non-zero.
- $1 \in \sigma(\mathbf{\Lambda})$ & $1 \in \sigma(\mathbf{\Lambda}_{\text{ms}})$ (Case II): Since $\tilde{\mathbf{C}}$ has full column rank and $1 \in \sigma(\mathbf{\Lambda})$, we get $\boldsymbol{\mu} \neq \mathbf{0}$ from Proposition B.2.

Consequently, we apply Proposition B.5 to get $\mathcal{R}(\mathbf{C}_{\text{ms}}) = \mathcal{R}(\mathbf{C}_{\not\ni 1})$. By the rank-nullity theorem, we then obtain:

$$\dim(\mathcal{N}(\mathbf{C}_{\text{ms}})) \;=\; \text{Number of columns in } \mathbf{C}_{\text{ms}} \;-\; \dim(\mathcal{R}(\mathbf{C}_{\not\ni 1})).$$

Table B.1 gives us the inputs needed to compute $\dim(\mathcal{N}(\mathbf{C}_{\text{ms}}))$, and the analysis splits once again into two branches:

1. $1 \notin \sigma(\mathbf{\Lambda})$ & $\boldsymbol{\mu} \neq \mathbf{0}$ (Case I): The Vandermonde matrix $\mathbf{\Theta}_{\text{ms}}$ has $r+1$ rows. So, by (B.5), $\mathbf{C}_{\text{ms}}$ has $r+1$ columns. Since $1 \notin \sigma(\mathbf{\Lambda})$, $\mathbf{C}_{\not\ni 1} = \mathbf{C}$ which has full column rank of r. Hence,
$$\dim(\mathcal{N}(\mathbf{C}_{\text{ms}})) \;=\; (r+1) - (r) \;=\; 1.$$
2. $1 \in \sigma(\mathbf{\Lambda})$ & $1 \in \sigma(\mathbf{\Lambda}_{\text{ms}})$ (Case II): The matrix $\mathbf{C}_{\text{ms}}$ has r columns as $\mathbf{\Theta}_{\text{ms}}$ has r rows. Since $1 \in \sigma(\mathbf{\Lambda})$ and $\tilde{\mathbf{C}}$ has full column rank, $\mathbf{C}_{\not\ni 1}$ has $r-1$ linearly independent columns. Therefore, we have:
$$\dim(\mathcal{N}(\mathbf{C}_{\text{ms}})) \;=\; (r) - (r-1) \;=\; 1.$$

Since we already know that this null space contains the span of $\boldsymbol{\Theta}_{\text{ms}}\mathbf{1}_{n+1}$, we get:

$$\mathcal{N}(\mathbf{C}_{\text{ms}}) = \mathcal{R}(\boldsymbol{\Theta}_{\text{ms}}\mathbf{1}_{n+1}). \qquad \square$$

Corollary 4.4 is now amenable to reasoning:

Proof of Corollary 4.4. There are two distinct segments to this proof, corresponding to the under-sampled ($n < r$) and the just-sampled ($n = r$) regimes. As a preliminary step, we use Proposition 3.9 to rewrite the condition of Koopman invariant $\boldsymbol{\psi}$ as $\tilde{\mathbf{C}}$ having full column rank. By equations (3.16) and (3.20), $\mathbf{C}$ also possesses linearly independent columns.

- $n < r$:
  The primary focus of this part will be to show that $\mathbf{X}_{\text{ms}}$ has full column rank. DMD-DFT equivalence follows as a consequence of Lemma 3.2.
  1. $1 \notin \sigma(\boldsymbol{\Lambda}_{\text{ms}})$: The matrix $\mathbf{C}_{\text{ms}}$ is either $\mathbf{C}$ or $\mathbf{C}_{\not\ni 1}$, both of which have full column rank. So, $(\boldsymbol{\Theta}_{\text{ms}})_1$ has at least $r-1$ rows. Since it has n columns, for $n \leq r-1$, it will have full column rank according to Lemma A.2. Therefore, $\mathbf{X}_{\text{ms}} = \mathbf{C}_{\text{ms}}(\boldsymbol{\Theta}_{\text{ms}})_1$ will have linearly independent columns.
  2. $1 \in \sigma(\boldsymbol{\Lambda}_{\text{ms}})$: Suppose $\mathbf{X}_{\text{ms}}\mathbf{z} = \mathbf{0}$ for some $\mathbf{z} \neq \mathbf{0}$. By Proposition B.8, we know $\mathcal{N}(\mathbf{C}_{\text{ms}}) = \mathcal{R}(\boldsymbol{\Theta}_{\text{ms}}\mathbf{1}_{n+1})$. Hence, there exists a scalar β such that:
  $$(\boldsymbol{\Theta}_{\text{ms}})_1\mathbf{z} = \beta\boldsymbol{\Theta}_{\text{ms}}\mathbf{1}_{n+1} \iff \boldsymbol{\Theta}_{\text{ms}}\begin{bmatrix}\mathbf{z}-\beta\mathbf{1}_n\\ -\beta\end{bmatrix} = \mathbf{0}.$$
  Note that $\boldsymbol{\Theta}_{\text{ms}}$ has $n+1$ columns and at least r rows. Since $n+1 \leq r$, $\boldsymbol{\Theta}_{\text{ms}}$ has full column rank by Lemma A.2. Using this in the above expression, we have $\beta = 0$ and $\mathbf{z} = \mathbf{0}$, which contradicts our assumption that $\mathbf{z} \neq \mathbf{0}$. Hence, $\mathbf{X}_{\text{ms}}$ has full column rank.
- $n = r$: Just-sampling necessitates a case-by-case handling of the scenarios described in Table B.1.
  1. Case I: The arguments are very similar to the proof for $n < r$. Suppose there exists $\mathbf{z} \neq \mathbf{0}$ satisfying $\mathbf{X}_{\text{ms}}\mathbf{z} = \mathbf{0}$. As with $n < r$, Proposition B.8 says that there exists a β such that
  $$\boldsymbol{\Theta}_{\text{ms}}\begin{bmatrix}\mathbf{z}-\beta\mathbf{1}_n\\ -\beta\end{bmatrix} = \mathbf{0}.$$
  In Case I, $\boldsymbol{\Theta}_{\text{ms}}$ has dimensions $r+1 \times r+1$. By Lemma A.1, we find that $\boldsymbol{\Theta}_{\text{ms}}$ is invertible. Thus, $\beta = 0$ and $\mathbf{z} = \mathbf{0}$ which is a contradiction. Hence, $\mathbf{X}_{\text{ms}}$ is full column rank which ensures DMD-DFT equivalence.
  2. Case II: We have $n = r$ and $1 \in \sigma(\boldsymbol{\Lambda}_{\text{ms}})$ along with a full column rank $\tilde{\mathbf{C}}$. Hence, by Theorem B.7, there is no DMD-DFT equivalence.
  3. Case III: According to Lemma B.4, $\boldsymbol{\mu} = \mathbf{0}$, which makes $\mathbf{X}_{\text{ms}} = \mathbf{X} = \mathbf{C}\boldsymbol{\Theta}_1$. The matrix $\boldsymbol{\Theta}_1 \in \mathbb{C}^{r\times r}$ has full column rank by Lemma A.2. Hence, $\mathbf{X}_{\text{ms}}$ has full column rank and therefore we have DMD-DFT equivalence by Lemma 3.2.
  4. Case IV: The columns of the matrix $\mathbf{Z}_{\text{ms}} = \mathbf{C}_{\text{ms}}\boldsymbol{\Theta}_{\text{ms}}$ can be viewed as snapshots of the same dynamical system generated using a different set of observables. The new functions lie in a $r-1$ dimensional Koopman invariant subspace with Koopman spectrum $\sigma(\boldsymbol{\Lambda}_{\text{ms}}) = \sigma(\boldsymbol{\Lambda}) \cap \{1\}^c$. Further, note that
     - The matrix $\mathbf{C}_{\text{ms}} = \mathbf{C}_{\not\ni 1}$ has full column rank.

– The mean-subtracted time series $\mathbf{Z}_{\text{ms}}$ has zero temporal mean.
– The number of columns in $\mathbf{X}_{\text{ms}}$ (r) is at least 1 more than the the dimension of the underlying Koopman invariant subspace ($r-1$).

Applying Theorem 4.3, we see that $\mathbf{c}^*[\mathbf{Z}_{\text{ms}}] = \mathbf{c}_{\text{ms}}[\mathbf{Z}] \neq -\mathbf{1}_n$. Hence, we don't have DMD-DFT equivalence. ∎

Appendix C. From Generalizability of DMD to mode-norm based pruning .

Our emphasis on capturing the Koopman eigen-values within the DMD spectrum can be explained from a generalizability perspective, as detailed in Lemma 5.2. Our claim is that these phenomena, namely spectral confinement and generalizability, go hand-in-hand. Here, we present a formal proof of this assertion:

Proof of Lemma 5.2. We begin with the backward implication. First, we factor $\mathbf{X}({\boldsymbol{v_1}}^{\text{test}})$ using (3.16) to obtain an analogous decomposition to $\mathbf{X}$ in (3.19).

$$\mathbf{X}({\boldsymbol{v_1}}^{\text{test}}) \;=\; \tilde{\mathbf{C}}\ \text{diag}(\boldsymbol{\phi}({\boldsymbol{v_1}}^{\text{test}}))\boldsymbol{\Theta}_1. \tag{C.1}$$

If $\sigma(\mathbf{T}^*) \supset \sigma(\boldsymbol{\Lambda})$, then by equation (3.8), the rows of the Vandermonde matrix $\boldsymbol{\Theta}_1$ are left eigen-vectors of $\mathbf{T}^*$ i.e. $\boldsymbol{\Theta}_1\mathbf{T}^* \;=\; \boldsymbol{\Lambda}\boldsymbol{\Theta}_1$. Therefore, we have:

$$\mathbf{X}({\boldsymbol{v_1}}^{\text{test}})\mathbf{T}^* \;=\; \tilde{\mathbf{C}}\ \text{diag}(\boldsymbol{\phi}({\boldsymbol{v_1}}^{\text{test}}))(\boldsymbol{\Theta}_1\mathbf{T}^*) \;=\; \tilde{\mathbf{C}}\ \text{diag}(\boldsymbol{\phi}({\boldsymbol{v_1}}^{\text{test}}))\boldsymbol{\Lambda}\boldsymbol{\Theta}_1.$$

The equation corresponding to the last column reads $\mathbf{X}({\boldsymbol{v_1}}^{\text{test}})\ \mathbf{c}^* = \mathbf{y}({\boldsymbol{v_1}}^{\text{test}})$ which is the desired conclusion.

We prove the forward implication by contraposition. Suppose the Koopman eigenvalue λ is not a DMD eigenvalue. Then, we may pick the initial condition ${\boldsymbol{v_1}}^{\text{test}}$ such that it has a non-zero projection only onto the eigen-space corresponding to λ. Without loss of generality, we ask that this projection take the value 1. If $\tilde{\mathbf{c}}_\lambda$ is the column of $\tilde{\mathbf{C}}$ that multiplies the row $\mathbf{gp}_n[\lambda]^T$ of $\boldsymbol{\Theta}_1$ to produce $\mathbf{X}({\boldsymbol{v_1}}^{\text{test}})$ in (C.1), then we have:

$$\mathbf{X}({\boldsymbol{v_1}}^{\text{test}}) \;=\; \tilde{\mathbf{c}}_\lambda\mathbf{gp}_n[\lambda]^T, \quad \mathbf{y}({\boldsymbol{v_1}}^{\text{test}}) \;=\; \tilde{\mathbf{c}}_\lambda\lambda^n.$$

Since $\lambda \notin \sigma(\mathbf{T}^*)$, equation (3.8) says that the vector $\mathbf{gp}_n[\lambda]$ is not a left eigen-vector of $\mathbf{T}^*$ corresponding to λ. Specifically, we have:

$$\mathbf{gp}_n[\lambda]^T\ \mathbf{T}^* \neq \lambda\ \mathbf{gp}_n[\lambda]^T.$$

Note that the equation corresponding to the last coefficient reads $\mathbf{gp}_n[\lambda]^T\mathbf{c}^* \neq \lambda^n$. Since every column of $\tilde{\mathbf{C}}$ is non-zero, we have $\tilde{\mathbf{c}}_\lambda \neq \mathbf{0}$. Hence, the prediction error is non-zero:

$$\mathbf{X}({\boldsymbol{v_1}}^{\text{test}})\ \mathbf{c}^* - \mathbf{y}({\boldsymbol{v_1}}^{\text{test}}) \;=\; \tilde{\mathbf{c}}_\lambda(\mathbf{gp}_n[\lambda]^T\mathbf{c}^* - \lambda^n) \;\neq\; \mathbf{0}.$$ ∎

Now, we proceed to justifying the practice of using the DMD mode norm to identify Koopman eigen-values from the DMD spectrum.

Proof of Theorem 5.4. Let $\check{\mathbf{X}}$ and $\check{\mathbf{Y}}$ denote the first n and last n columns of $\check{\mathbf{Z}}$ respectively.

$$\check{\mathbf{X}} \;=\; \check{\mathbf{C}}\boldsymbol{\Theta}_1,\ \check{\mathbf{Y}} \;=\; \check{\mathbf{C}}\boldsymbol{\Lambda}\boldsymbol{\Theta}_1. \tag{C.2}$$

Suppose $\mathbf{v}_\mu$ is the eigenvector of $\check{\mathbf{T}}^*$ corresponding to eigenvalue μ[14]. Then, the statement to be proved may be rephrased as follows:

$$\mu \;\in\; \sigma(\check{\mathbf{T}}^*)\ \&\ \check{\mathbf{X}}\mathbf{v}_\mu \;\neq\; \mathbf{0} \iff \mu \;\in\; \sigma(\boldsymbol{\Lambda}). \tag{C.3}$$

[14] μ is a scalar quantity and is not to be confused with the vectorial quantity $\boldsymbol{\mu}$ which is the temporal mean.

We begin by observing that Proposition 5.3 guarantees the existence of a solution to the minimization in (3.6) with zero residue, when $n \geq r$.

$$\exists\ \mathbf{c} \text{ such that } \check{\mathbf{Y}} \ = \ \check{\mathbf{X}}\mathbf{T}[\mathbf{c}].$$

According to (C.2), both $\check{\mathbf{X}}$ and $\check{\mathbf{Y}}$ contain $\check{\mathbf{C}}$. The latter can be simply discarded as it has full column rank, and this gives:

$$\exists\ \mathbf{c} \text{ such that } \mathbf{\Lambda}\mathbf{\Theta}_1 \ = \ \mathbf{\Theta}_1\mathbf{T}[\mathbf{c}].$$

By virtue of its optimality, $\check{\mathbf{c}}^*$ can replace $\mathbf{c}$.

$$\mathbf{\Lambda}\mathbf{\Theta}_1 \ = \ \mathbf{\Theta}_1\check{\mathbf{T}}^*. \tag{C.4}$$

Since $\mathbf{\Lambda}$ is a diagonal matrix, (C.4) is an eigenvector-eigenvalue equation. The rows of $\mathbf{\Theta}_1$ are the left eigen-vectors of $\check{\mathbf{T}}^*$ with the corresponding eigen-values on the diagonal of $\mathbf{\Lambda}$. Hence, we have:

$$\sigma(\mathbf{\Lambda}) \ \subset \ \sigma(\check{\mathbf{T}}^*). \tag{C.5}$$

We now proceed to prove (C.3).

To show the forward implication, we begin with the definition of $\mathbf{v}_\mu$.

$$\check{\mathbf{T}}^*\mathbf{v}_\mu \ = \ \mu\ \mathbf{v}_\mu.$$

If we pre-multiply both sides with $\mathbf{\Theta}_1$, it is possible to apply (C.4):

$$\mathbf{\Theta}_1\ \check{\mathbf{T}}^*\mathbf{v}_\mu \ = \ \mu\ \mathbf{\Theta}_1\ \mathbf{v}_\mu \implies \mathbf{\Lambda}(\mathbf{\Theta}_1\mathbf{v}_\mu) \ = \ \mu\ (\mathbf{\Theta}_1\mathbf{v}_\mu).$$

Now, we only need to show that $\mathbf{\Theta}_1\mathbf{v}_\mu \ \neq \ \mathbf{0}$. This is possible using $\check{\mathbf{X}}\mathbf{v}_\mu \ \neq \ \mathbf{0}$ since $\check{\mathbf{C}}$ has full column rank.

$$\check{\mathbf{X}}\mathbf{v}_\mu \ \neq \ \mathbf{0} \iff \mathbf{\Theta}_1\mathbf{v}_\mu \ \neq \ \mathbf{0}.$$

For the backward implication, we note that (C.5) gives $\mu \ \in \ \sigma(\check{\mathbf{T}}^*)$. The corresponding DMD mode is seen to be non-zero using the duality of left and right eigen-vectors. Let $\mathbf{w}_\mu$ be the left eigenvector of $\check{\mathbf{T}}^*$ corresponding to the eigenvalue μ. We say "the" and not "a" because companion matrices can only have a single eigenvector for an eigenvalue, regardless of its multiplicity [16]. Thus, by duality, we have

$$\mathbf{w}_\mu^T\mathbf{v}_\mu \ \neq \ 0. \tag{C.6}$$

Since we have shown $\mu \in \sigma(\check{\mathbf{T}}^*) \ \cap \ \sigma(\mathbf{\Lambda})$, by (C.4), there is a row of $\mathbf{\Theta}_1$ that is a scaled version of $\mathbf{w}_\mu$. Hence, according to (C.6), we have:

$$\mathbf{\Theta}_1\mathbf{v}_\mu \ \neq \ \mathbf{0}.$$

Pre-multiplying both sides with $\check{\mathbf{C}}$ shows that the DMD mode corresponding to μ, $\check{\mathbf{X}}\mathbf{v}_\mu$, has non-zero norm. ∎

Appendix D. Efficacy of mean subtraction for Koopman invariant observables.

This section details the proofs for Theorem 5.9 and Theorem 5.10. These two theorems encapsulate necessary and sufficient conditions for the success of mean subtraction (Definition 5.8), under the assumption of Koopman invariant observables (Definition 3.6). We begin with an equivalent characterization of the success of mean subtraction using the mean $\boldsymbol{\mu}$ and the presence or absence of 1 in the Koopman spectrum.

PROPOSITION D.1. *Mean subtraction succeeds if and only if any one of the following holds:*

1. $1 \notin \sigma(\mathbf{\Lambda})$ *and* $\boldsymbol{\mu} = 0$.
2. $1 \in \sigma(\mathbf{\Lambda})$ *and* $\boldsymbol{\mu}$ *is precisely the column of* $\mathbf{C}$ *that is multiplied by the row* $\mathbf{1}_{n+1}^T$ *of* $\mathbf{\Theta}$ *in the product* $\mathbf{Z} = \mathbf{C\Theta}$.

Thus, mean subtraction succeeds if and only if 1 is not a Koopman eigenvalue and $\boldsymbol{\mu} = \mathbf{0}$ or if 1 is a Koopman eigenvalue and $\boldsymbol{\mu}$ is the corresponding Koopman mode. We note that the presence or absence of 1 in the Koopman spectrum organizes Proposition D.1. Since the proofs for Theorem 5.9 and Theorem 5.10 are built around the above proposition, they too inherit the same organization.

Proof of Theorem 5.9. We first prove the above assertion in the special case where 1 is not a Koopman eigenvalue, and then extend it to the scenario where 1 lies in the Koopman spectrum.

When $1 \notin \sigma(\mathbf{\Lambda})$, Proposition D.1 says:

$$\text{Mean subtraction succeeds} \iff \boldsymbol{\mu} = \mathbf{0}.$$

Recall, from equation (3.11), that $\boldsymbol{\mu} = \mathbf{C\Theta}\frac{\mathbf{1}_{n+1}}{n+1}$. In addition, Proposition 3.9 says that $\mathbf{C}$ has linearly independent columns due to the Koopman invariance of the dictionary $\boldsymbol{\psi}$. Combining these two facts, we have:

$$\boldsymbol{\mu} = \mathbf{0} \iff \mathbf{\Theta 1}_{n+1} = \mathbf{0}.$$

The condition on the right can be rephrased component-wise as follows:

$$\mathbf{\Theta 1}_{n+1} = \mathbf{0}. \iff \forall\ \lambda \in \sigma(\mathbf{\Lambda}),\ \mathbf{gp}_{n+1}[\lambda]^T \mathbf{1}_{n+1} = 0.$$

We simplify the expression on the right in two steps. Firstly, we recognize that $\mathbf{gp}_{n+1}[\lambda]^T \mathbf{1}_{n+1}$ is a geometric sum and use the relevant formula:

$$\mathbf{gp}_{n+1}[\lambda]^T \mathbf{1}_{n+1} \ = \ 1 + \lambda + \cdots + \lambda^n \ = \ \frac{\lambda^{n+1} - 1}{\lambda - 1}.$$

Secondly, if we let

$$q_1 \ := \ (n+1) \mod p^*, \tag{D.1}$$

we can use the fact that the Koopman eigen-values are p^*-th roots of unity to write:

$$\lambda^{n+1} \ = \ \lambda^{q_1}.$$

Using $1 \notin \sigma(\mathbf{\Lambda})$ together with the two simplifications above, we have the following statement:

$$\forall\ \lambda \in \sigma(\mathbf{\Lambda}),\ \mathbf{gp}_{n+1}[\lambda]^T \mathbf{1}_{n+1} = 0 \iff \forall\ \lambda \in \sigma(\mathbf{\Lambda}),\ \lambda^{q_1} \ = \ 1.$$

Following the chain of equivalences backward, we find that mean subtraction succeeds if and only if every Koopman eigenvalue is a q_1-th root of unity. Hence, in the absence of a Koopman eigenvalue at 1, we only need to prove the following:

$$\forall\ \lambda \in \sigma(\mathbf{\Lambda}),\ \lambda^{q_1} \ = \ 1 \iff q_1 \ = \ 0. \tag{D.2}$$

The backward implication is trivial. To prove the forward implication, we note that q_1 is, by definition (D.1), a whole number strictly less that p^*. If $q_1 \neq 0$, it would contradict the definition of p^* as the *smallest* natural number such that every Koopman eigenvalue is a p^*-th root of unity. Therefore, q_1 must be 0.

At this juncture, we have proven the following statement:

(D.3) If $1 \notin \sigma(\mathbf{\Lambda})$ & $\boldsymbol{\psi}$ is Koopman invariant, $\quad \boldsymbol{\mu} = \mathbf{0} \iff (n+1) \mod p^* = 0.$

We now tackle the case where 1 is a Koopman eigenvalue. First, we recall the matrix partitioning that is developed in (B.3) to emphasize the contribution of the Koopman mode at 1.

$$\mathbf{Z} = \mathbf{c}_1 \mathbf{1}_{n+1}^T + \mathbf{C}_{\not\ni 1} \mathbf{\Theta}_{\not\ni 1}. \tag{D.4}$$

In this setting, the temporal mean reads thus:

$$\boldsymbol{\mu} = \mathbf{c}_1 + \mathbf{C}_{\not\ni 1} \mathbf{\Theta}_{\not\ni 1} \frac{\mathbf{1}_{n+1}}{n+1}.$$

By making the definition

$$\boldsymbol{\mu}_{\not\ni 1} := \mathbf{C}_{\not\ni 1} \mathbf{\Theta}_{\not\ni 1} \frac{\mathbf{1}_{n+1}}{n+1},$$

we may write

$$\boldsymbol{\mu} = \mathbf{c}_1 + \boldsymbol{\mu}_{\not\ni 1}.$$

Using the above expression in conjunction with Proposition D.1, we obtain:

$$\text{Mean subtraction succeeds} \iff \boldsymbol{\mu} = \mathbf{c}_1 \iff \boldsymbol{\mu}_{\not\ni 1} = \mathbf{0}.$$

The remainder of this proof will use (D.3), in an approach similar to the proof of Corollary 4.4 in the just-sampled regime, for Case IV. Let $\mathbf{Z}_{\not\ni 1}$ denote the product $\mathbf{C}_{\not\ni 1} \mathbf{\Theta}_{\not\ni 1}$. Firstly, $\mathbf{Z}_{\not\ni 1}$ can be seen as $(n+1)$ sequential observations of the dynamical system (3.1), using observables that have no projection onto the eigen-space at 1. In addition, this dictionary is Koopman invariant as it is represented by the full column rank matrix $\mathbf{C}_{\not\ni 1}$[15]. Moreover, the temporal mean of $\mathbf{Z}_{\not\ni 1}$ is $\boldsymbol{\mu}_{\not\ni 1}$. Finally, p^* continues to be the smallest natural number such that every node of $\mathbf{\Theta}_{\not\ni 1}$ is a p^*-th root of unity. Hence, we use (D.3) to get

$$\boldsymbol{\mu}_{\not\ni 1} = \mathbf{0} \iff (n+1) \mod p^* = 0,$$

which is the desired conclusion. ∎

We preface the formal proof of Theorem 5.10 with an informal version. At a fundamental level, Theorem 5.10 may be seen as a corollary of Theorem 5.9. If the Koopman eigen-values are not roots of unity for some common power, then $p^*$is effectively $+\infty$. Consequently, $(n+1) \mod p^* \neq 0$ for any natural number n and so mean subtraction always fails. In light of this argument, it is not surprising that the formal justification of Theorem 5.10 closely shadows that of Theorem 5.9.

[15] The columns of $\mathbf{C}_{\not\ni 1}$ are linearly independent because they are a subset of the full column rank matrix $\mathbf{C}$

Proof of Theorem 5.10. This proof mirrors the one for Theorem 5.9, and reuses many of the simplifications developed there. Hence, we strongly recommend reading the aforementioned proof to fully grasp the reasoning ahead.

We first establish the result when 1 is not a Koopman eigenvalue. Here, we have:

$$\text{Mean subtraction succeeds} \iff \forall\, \lambda \in \sigma(\mathbf{\Lambda}),\ \lambda^{n+1} = 1.$$

The given spectral constraint on the Koopman eigen-values,

$$\forall\, q \in \mathbb{N},\ \exists\, \lambda \in \sigma(\mathbf{\Lambda}) \text{ such that } \lambda^q \neq 1,$$

ensures that the right hand side is never true for any value of n. Therefore, mean subtraction always fails.

At this juncture, we have proven the following statement:

$$\text{If } 1 \notin \sigma(\mathbf{\Lambda}) \;\&\; \boldsymbol{\psi} \text{ is Koopman invariant}, \quad \boldsymbol{\mu} \neq \mathbf{0}. \tag{D.5}$$

When 1 is a Koopman eigenvalue, we have seen that

$$\text{Mean subtraction succeeds} \iff \boldsymbol{\mu}_{\not\equiv 1} = \mathbf{0}.$$

By the same arguments used in the proof of Theorem 5.9, we can draw upon (D.5) to say that $\boldsymbol{\mu}_{\not\equiv 1}$ is never zero. Therefore, mean subtraction always fails even when 1 lies in the Koopman spectrum. ∎

Appendix E. Justifying the numerical checks associated with equation (6.4).

Numerical verification of equation (6.4) requires two theoretically sound but computationally absurd operations. At the highest level, we have a set equality while the search for non-zero DMD mode ensues one level below. Our performance measure, KMD-Quality, depends on two non-negative indicators, ρ_{subset} and δ_{trivial}, whose equality to 0 is necessary and sufficient for (6.4). More precisely, for every mode-extraction theorem, the following holds:

$$\rho_{\text{subset}} = 0 \;\&\; \delta_{\text{trivial}} = 0 \iff \text{Equation (6.4) holds.}$$

Thus, low values of both indicators, under the specified conditions, would numerically vindicate the theorem being scrutinized. KMD-Quality is an attempt to check for the above requirement:

$$\text{KMD-Quality}[\tilde{\mathbf{Z}}, B, \mathbf{c}] := 1 - \max\left[1 - 10^{-\rho_{\text{subset}}[B, \sigma(\mathbf{T}[\mathbf{c}])]}, \delta_{\text{trivial}}[\tilde{\mathbf{Z}}, B, \mathbf{c}]\right]. \tag{E.1}$$

The two properties of "spectral containment" and "index of non-triviality" follow directly from ρ_{subset} and δ_{trivial} respectively.

E.1. An indicator of set containment. We start with the following observation:

$$(6.4) \implies \sigma(\mathbf{T}[\mathbf{c}]) \supset B.$$

This can be numerically checked with the following indicator of set inclusion:

$$\rho_{\text{subset}}[B_1, B_2] := \max_{b_1 \in B_1} \min_{b_2 \in B_2} |b_1 - b_2|. \tag{E.2}$$

Note that $\rho_{\text{subset}}[B_1, B_2]$ is a non-negative quantity. Moreover, $\rho_{\text{subset}}[B_1, B_2] = 0$ if and only if $B_1 \subset B_2$. Hence, $\rho_{\text{subset}}(B, \sigma(\mathbf{T}[\mathbf{c}])) << 1$ is equivalent to $\sigma(\mathbf{T}[\mathbf{c}])$ effectively containing B.

E.2. A quantification of mode truncation.

E.2.1. Notation. Let $\text{poly}_{\boldsymbol{\alpha}}$ denote the polynomial represented by $\boldsymbol{\alpha}$, i.e.

$$\text{poly}_{\boldsymbol{\alpha}}[z] = \sum_{i=0}^{\#[\boldsymbol{\alpha}]-1} \alpha_{i+1} z^i.$$

For example,

$$\begin{aligned} \boldsymbol{\alpha}_1 &:= \begin{bmatrix} 1 & -2 & 1 \end{bmatrix}^H && \implies \text{poly}_{\boldsymbol{\alpha}_1}[z] = 1 - 2z + z^2. \\ \boldsymbol{\alpha}_2 &:= \begin{bmatrix} 0 & -3 & 0 & 3 \end{bmatrix}^H && \implies \text{poly}_{\boldsymbol{\alpha}_2}[z] = -3z + 3z^3. \end{aligned}$$

E.2.2. Leveraging the closest consistent companion matrix. Suppose the value of $\rho_{\text{subset}}(B, \sigma(\mathbf{T}[\mathbf{c}]))$ is negligible i.e. every element of B is nearby *some* eigenvalue of $\mathbf{T}[\mathbf{c}]$. Then, we need to identify elements of $\sigma(\mathbf{T}[\mathbf{c}])$ with B to compute the relevant σ_{nontriv}. In lieu of a matching problem, we find the "closest" companion matrix that contains B up to machine precision. Let $\boldsymbol{\beta}^*$ be the unique vector such that $B =$ roots of $\text{poly}\begin{bmatrix} \boldsymbol{\beta}^* \\ -1 \end{bmatrix}$.

$$\mathbf{c}^*_{\text{Superset}}[B, \mathbf{c}] := \begin{cases} \arg\min_{\boldsymbol{\gamma}} \|\mathbf{c} - \boldsymbol{\gamma}\|_2^2 & \#[\mathbf{c}] > \#[B] \\ \text{subject to} & \\ \quad \sigma(\mathbf{T}[\boldsymbol{\gamma}]) \supset B & \\ & \\ \boldsymbol{\beta}^* & \text{Otherwise.} \end{cases} \tag{E.3}$$

$$\sigma^*_{\text{Superset}}[B, \mathbf{c}] := \sigma(\mathbf{T}[\mathbf{c}^*_{\text{Superset}}[B, \mathbf{c}]]).$$

In other words, we find the monic polynomial closest to $\text{poly}\begin{bmatrix} -\mathbf{c} \\ 1 \end{bmatrix}$ whose roots subsume B. Since polynomial multiplication is a convolution in coefficient space, the above minimization can be cast as a least squares regression (Refer Section 3 in [15]). For $p := \#[B]$, we have:

$$\sigma(\mathbf{T}[\boldsymbol{\gamma}]) \supset B \iff \exists\, \boldsymbol{\alpha} \text{ such that } \begin{bmatrix} \boldsymbol{\gamma} \\ -1 \end{bmatrix} = \begin{bmatrix} \beta_1^* & & & \\ \vdots & \beta_1^* & & \\ \beta_p^* & \vdots & \ddots & \\ -1 & \beta_p^* & \ddots & \beta_1^* \\ & -1 & \ddots & \vdots \\ & & \ddots & \beta_p^* \\ & & & -1 \end{bmatrix} \begin{bmatrix} \boldsymbol{\alpha} \\ -1 \end{bmatrix}.$$

Now, we compute the relative contribution of DMD eigen-values excluded from B using δ_{trivial}:

$$\delta_{\text{trivial}}[\tilde{\mathbf{Z}}, B, \mathbf{c}] := 1 - \left(\frac{\sum_{\lambda \in B} \|\tilde{\mathbf{X}}\mathbf{v}_\lambda\|^2}{\sum_{\lambda \in \sigma^*_{\text{Superset}}[B,\mathbf{c}]} \|\tilde{\mathbf{X}}\mathbf{v}_\lambda\|^2} \right). \tag{E.4}$$

where $\mathbf{v}_\lambda$ is the eigenvector of $\mathbf{T}[\mathbf{c}^*_{\text{Superset}}[B, \mathbf{c}]]$ with eigenvalue λ and $\tilde{\mathbf{X}}$ is the submatrix of $\tilde{\mathbf{Z}}$ obtained by dropping the last column. Hence, whenever (6.4) holds, δ_{trivial} will be 0.